MINISTERUL EDUCAŢIEI ŞI CERCETĂRII

ANALELE UNIVERSITĂŢII "DUNĂREA DE JOS" DIN GALAŢI

Fascicula IX

FACULTATEA DE METALURGIE ŞI ŞTIINŢA MATERIALELOR

ANUL XXIII (XXVIII), nov. 2005, nr.2

ISSN 1453-083X

MINISTRY OF EDUCATION AND RESEARCH

THE ANNALS OF "DUNAREA DE JOS" UNIVERSITY OF GALATI

Fascicle IX

FACULTY OF METALLURGY AND MATERIALS SCIENCE

YEAR XXIII (XXVIII), Nov. 2005, no.2

ISSN 1453-083X

Table of Content

LASER SURFACE HARDENING OF 51CrV4 STEEL

Sanda Maria Levcovici[1], Dan Teodor Levcovici[2]

[1]University "Dunarea de Jos" of Galați,
[2]S.C. Uzinsider Engineering S.A. Galați,
e-mail: dan.levcovici@uzineng.ro,

ABSTRACT

The work presents the surface changes in microstructure and properties by quenching the 51CrV4 steel from liquid and solid phase, using a CO_2 continue laser wave with 900W power. In order to determine the hardening conditions, processing parameters on the geometry of the hardened layer and surface hardness were analyzed. Microhardness profile of heat affected zone was traced and correlated with structural changes. The effect of subsequent tempering was investigated.

KEYWORDS: laser hardening, steel, tempering, microstructure, microhardness.

1. Introduction

Laser beam superficial quenching is known as unconventional method of efficient local thermal treatment for cutting, cold deforming and trimming tools [1], [2], [3], [4], [5].

Laser beam gives an ultrarapidly heating speed of superficial layer (over10^3 °C/s) that provides getting of fine inhomogeneous austenite or superficial melting Relative small volume cooling lately, by thermal conductivity within mass of metal makes the cooling speed very rapidly to be, in order to allow an ultrarapidly solidification [6], followed by martensitic quenching with formation of ultrafine martensitic structure with high hardness, tenacity and wear resistance, [7], [8].

Hereby paper was originated by request of increasing the durability of knife blade from guillotine shares for paper cutting, made of 51CrV4 steel. It was intended to find the optimal laser quenching of this steel and thermal stability of the structure resulted in order to enlarge the use of steel to other tools for hot deforming or cutting.

2. Experimental conditions

Lab experiments were made on 12 mm thickness samples made of 51CrV4 grade steel as per SR EN 10083-1:1994 with 0,48%C; 0,33%Si; 0,97%Mn; 0,012%P; 0,020%S; 0,90%Cr; 0,10%Ni; 0,12%V; 0,04%Al; 0,13%Cu in its chemical composition. Taking into consideration the use of material for cold cutting tools, samples were originally quenched in oil at 850°C and annealed at 150°C at 6550 MPa Vickers hardness (49N load).

Laser hardening was made in a CO_2 continuous wave laser installation as GT type of 1400W (Romania), endowed by x-y-z coordinate table. Single strips were drawn using a ZnSe laser beam focusing lens with 125 mm focal distance and a 900W power beam, defocused by 20 mm, that lead to a 1.8 mm laser beam equivalent diameter. In order to trace the radiating running influence upon hardening depth and level, surface scanning speed within 12,5…24,5 mm/s range were experimented. To increase laser radiation energy absorption it was used a zinc oxide absorbent cover on the surface to be worked. Ultrarapidly thermal cycle made by laser beam does not provide the chemical homogenization of austenite and when martensitic quenching a large quantity of residual austenite remains. In order to decrease the residual austenite quantity, after quenching by laser, samples were quenched in liquid nitrogen at negative temperatures [9].

To see the possibility of using the steel hardened by laser for hot cutting tools also, it was studied the structure thermal stability resulted on laser hardened samples, during this running, and tempered at 200, 300 and 400°C, for 45 minutes.

Structure and properties changes when laser quenching and tempering as well as their enlargement in depth were studied in laser strips cross section by micro structural and dimensional analysis and $HV_{0,98}$ Vickers microhardness profile drawing (100g load) in thermal influenced layer depth. As global hardening index the

HV_{49} Vickers (49N load) was determined on laser processed surface.

3. Results and Discussion

3.1 Microstructure analysis

Microstructure analysis in cross section of laser quenched strip pointed out that experimental running made the quenching since liquid phase. From surface into depth the following layers may be seen (figure 1 and figure 2-I):

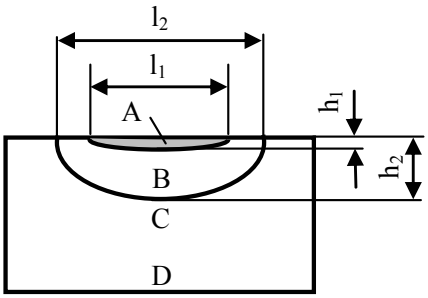

Figure 1. *Scheme of layers in laser quenched strip cross section*

A – quenched layer from liquid phase, got by heating over alloy liquidus point, rapidly solidifying and martensitic quenching; microstructure contains martensite columnar grains as finest as increasing the scanning speed;

B – quenched layer from solid phase by heating between Ac_3 and alloy solidus point. In layer bottom side it may be seen fine martensite needles and VN precipitates. At the top side, at higher temperatures, fine VN precipitates dissolving in austenite took place, austenite grains growing, martensite needles respectively. The layer is bottom limited by an intercritical quenching strip with troostite - martensite structure;

C – the tempered layer, by heating the Ac_1 subcritical basic material, where the tempering martensite is decomposed in a fine ferrite - carbide mixture;

D – thermal nonaffected basic material, by heating under its tempering temperature.

Microstructural analysis of tempered layers at different temperatures in the range of 200-400°C (figure 2 - IV) emphases the beginning of laser quenching martensite decomposing in ferrite - carbide mixture, more enhanced by tempering temperature growth.

In table no.1 are given the results from layers dimensional analysis of experimental running laser quenched layers and in figure no.3 is shown the scanning speed influence upon them, where h_1, l_1 mean the depth and width of quenched layer from liquid phase and h_2, l_2 those of quenched layer from solid phase. Quenched layer dimensions decrease by scanning speed, more visible in quenched layer width from liquid phase.

Table 1 *Dimensional analysis results*

Sample code	Scanning speed [mm/s]	Laser quenched layers depth [mm]		Laser quenched layers width [mm]	
		h_1	h_2	l_1	l_2
1	26	0.037	0.46	0.81	2.41
2	24.5	0.062	0.46	0.95	2.42
3	23	0.074	0.56	1.12	2.63
4	21.5	0.086	0.59	1.23	2.65
5	20	0.104	0.59	1.36	2.68
6	18.5	0.128	0.63	1.57	2.63
7	17	0.148	0.67	1.67	2.65
8	15.5	0.170	0.69	1.75	2.70
9	14	0.185	0.70	1.86	2.73
10	12.5	0.202	0.77	1.79	2.99

3.2 Microhardness analysis

In figures no. 4 and 5 the $HV_{0,98}$ microhardness variation in laser hardened layer from samples with code 4 and 8 is given.

Laser quenched layer from liquid and solid phase shows a higher microhardness of basic material processed in volume quenching and tempering at 150^0C. Hardening is stronger when processing by high scanning speeds, in which quicker heating cycle provides more enhanced microstructure finishing as well as increased density of structural defects.

Liquid phase quenched layer microhardness is more reduced than that one of the layer quenched from solid phase, more enhanced at slower scanning speeds, in which the absorbed energy density gives larger size quenched layers in liquid phase with rougher dendrite structure. Later tempering reduces both layer hardness quenched by laser and that one of basic material, more enhanced when

tempering temperature increases. The tempered underlayer has a lower microhardness than basic material.

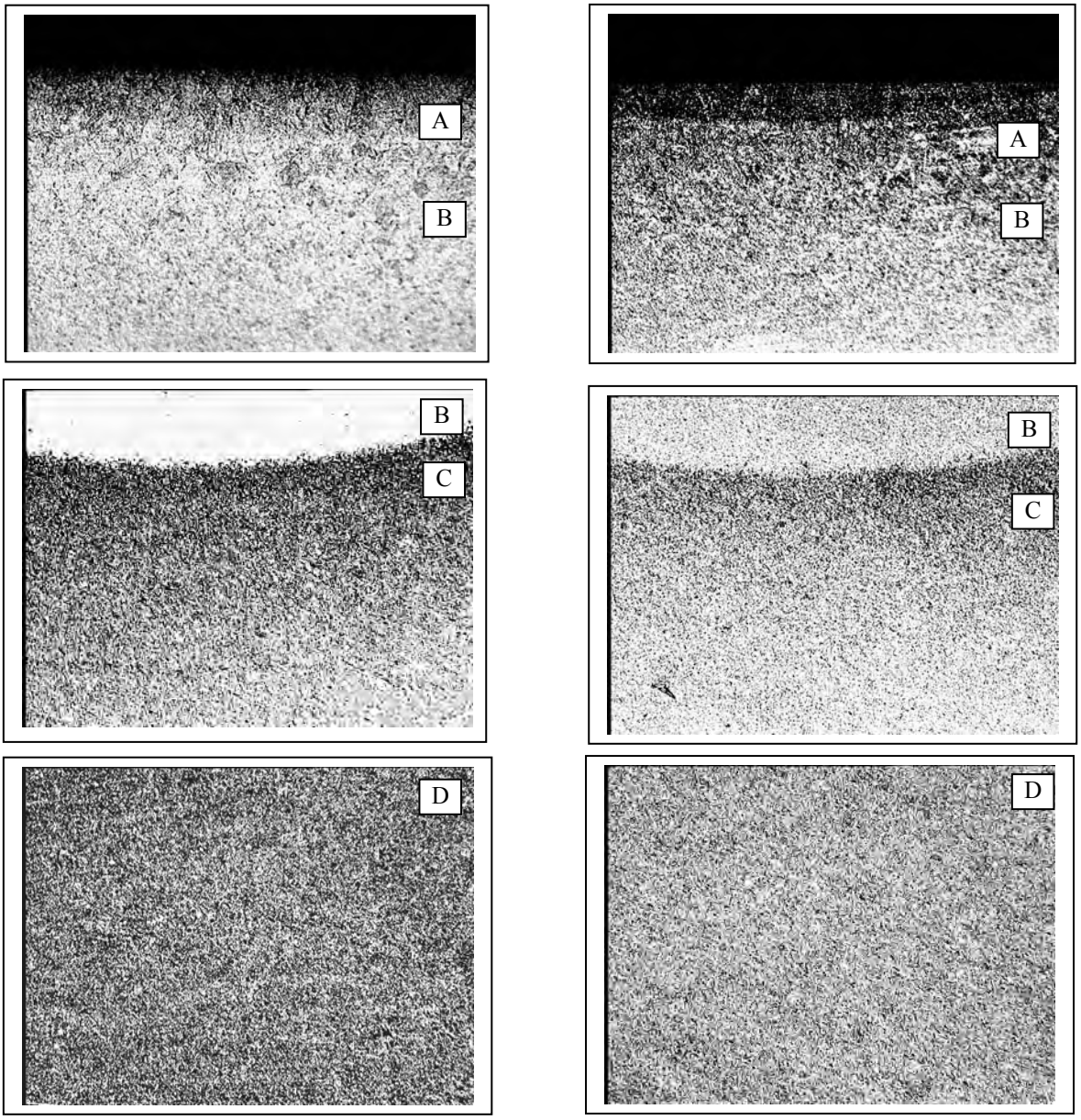

Figure 2. *Microstructure of thermal influenced area (A,B,C) and of basic material (D): I – after laser quenching in P=900W, v=15,5mm/s running ; IV – after tempering at 400°C; 2% Nital Attach; x 200*

.

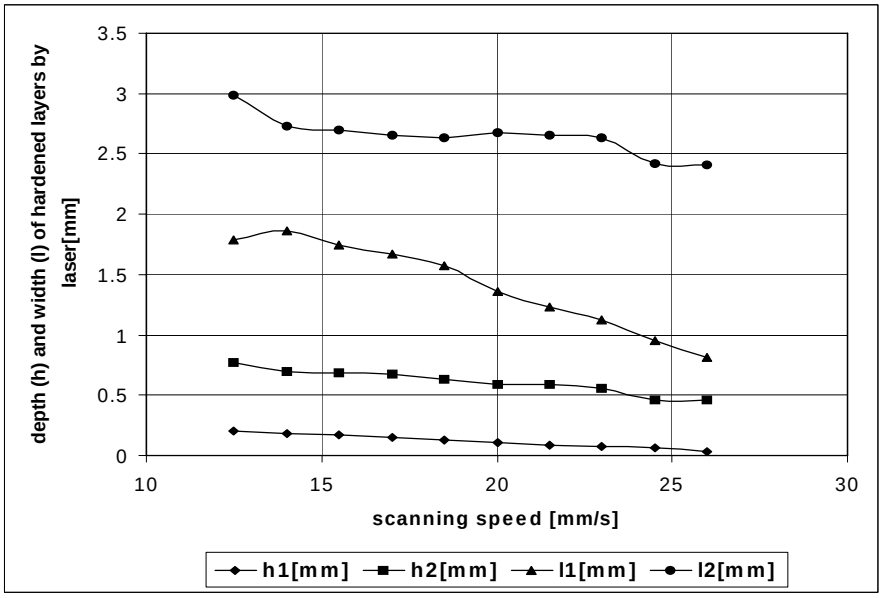

Figure 3. *Variation of depth and width quenched by laser from liquid phase (h_1, l_1) and solid phase (h_2, l_2) with surface scanning speed.*

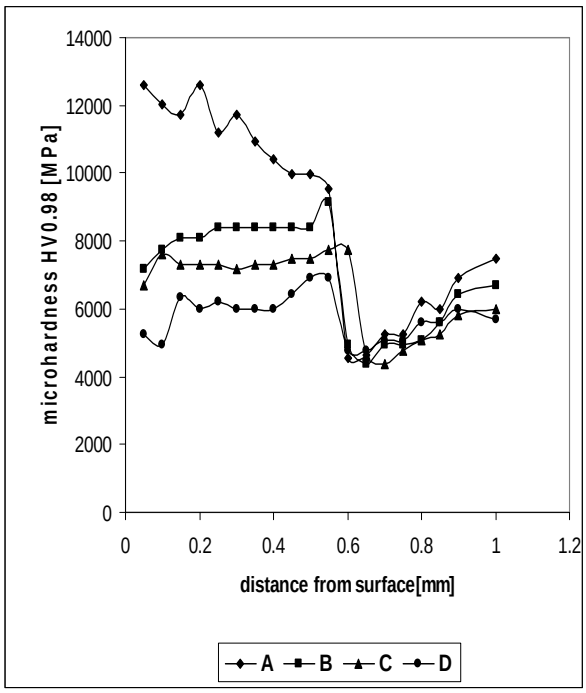

Figure 4. *$HV_{0,98}$ microhardness variation in laser quenched layer at sample with code 4, quenched by laser in P=900W and v=21,5mm/s running*

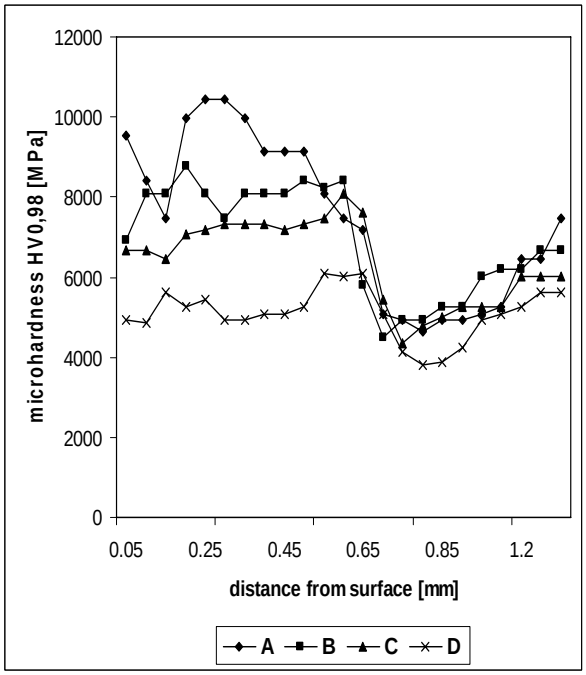

Figure 5. *$HV_{0,98}$ microhardness variation in laser quenched layer depth at sample with code 8, quenched by laser in P=900W; v=15,5mm/s running;*

1.3 Surface hardness analysis

Hardening analysis on the processed surface integrates the microhardening effect and layers thickness. Hardness finding was performed on laser processed surface after superficial irregularities removed by grinding in 0.1 mm in depth since the surface. As a result, in running that made quenched layers from liquid state under 0.1 mm in thickness, they were removed.

In figure no.6 is given HV_{49} hardness variation on the processed surface by scanning speed compared to basic material hardness (0 scanning speed). Maximum hardening is equivalent to laser quenched layers from solid phase with scanning speeds ≥ 21.5 mm/s. At lower speeds the
liquid phase quenched layer and rougher granulation decrease the superficial hardness. Laser quenched layer hardness decreases in the same time with tempering temperature increasing. Solid phase quenched layers hardness stays higher compared to those quenched from liquid phase. At 300^0C solid phase quenched layers only keep higher the basic material hardness. At 400°C, their hardness is equal to basic material hardness.

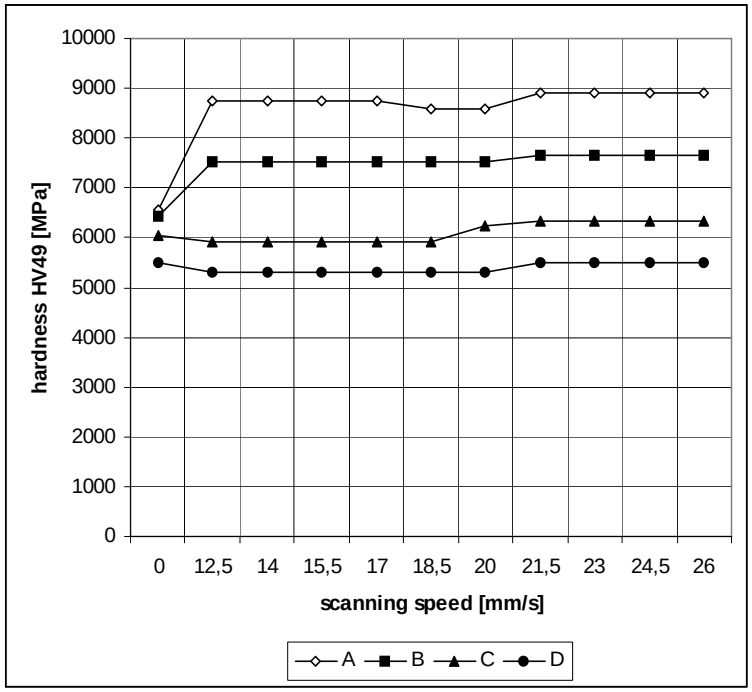

Figure 6. *HV_{49} superficial microhardness variation compared to scavenging speed after laser quenching (A), tempering at 200°C(B), 300°C(C) and 400°C (D)*

2. Conclusions

Study made on 51CrV4 steel superficial laser quenching capacity pointed out that solid phase quenching is efficiently. In order to get the maximum quenching depth associated to 8910 MPa maximum superficial hardness, it is recommended laser quenching in P=900W; d=1,8mm; v=21.5mm running that provides a solid phase quenched layer of 0.5 mm in depth after surface grinding.

Studying of laser quenching thermal stability showed that solid phase quenched layer hardness, in recommended running, decreases the tempering temperature so that at 400°C volume quenched material hardness is reached.

Laser quenching is recommended for cutting and cold or hot deforming tools that works up to maximum 300°C.

References

[1.CHABROL C., MERRIEN P. - *Durcissement superficiel des aciers par faisceau lase*r, Revue de Métallurgie - CIT, 1989, page 491;

[2].DIACENKO V.S. - *Osobenisti stroenia i svoistva bâstrorejuişcih stalei posle lazernoi obrabotke*. MITOM nr. 8/1985, page 50;

[3].KRIANINA M.N., BERNSTEIN A.M., CIUPROVA T.P. - *Termiceskaia obrabotka bistro-rejuişcei stali s primeneniem neprerâvnogo lazernogo izlucenia* MITOM nr. 10/1989, page 7;

[4].LEVCOVICI S.M., MUNTEANU V, LEVCOVICI D.T.,- *The Influence of the Several Quenching Conditions on the Working Life on High-Speed Steels Hardened by Laser Processing*, Proceedings of the ASM International Conference on Quenching and Control of Distortion, 1999, Prague, Czech Republic, page 522-526;

[5].LEVCOVICI S.M., LEVCOVICI D.T., *Surface Hardening of Rp5 Steel by Continuous Wave CO_2 Laser,* The Annals of University of Galati, fascicle IX, 1996, page 95-100;

[6].BREINEN E. M., KEAR B.H - *Rapid Solidification Laser Processing at High Power Density,* Laser Materials Processing, North Holland Pub. Comp. 1983, page 235;

[7].LEVCOVICI S.M., CRUDU I. etc., *Elasto-Plastic Transition of Carbon Tool Steel Superficially Treated with Laser, Proceedings of 4th International Conference on "Low Cycle Fatigue and Elasto-Plastic Behavior of Materials"*, Garmish-Partenkirken, Germany, 1998, pag.417-422;

[8].LEVCOVICI D.T., PARASCHIV M.M., LEVCOVICI S.M., *Contributions in Describing the Wear Behavior of Mosaic-Shaped Surface by Laser Hardening,* Proceedings of EUROMAT'97, Maastricht, Netherlands, Surface Engineering and Functional Materials, pag.135-138.

[9].LEVCOVICI S.M., LEVCOVICI D.T., *The Influence of Refrigeration on the High-Speed Steel Hardened by Laser Processing*, Proceedings of the ASM International Conference on Quenching and Control of Distortion, 1999, Prague, Czech Republic, page 527-529;

INFLUENCE OF ATMOSPHERIC CONDITIONS ON THE MECHANICAL PROPERTIES OF PET RUBBER COMPOSITES

Cristina VLADUTA, Anca DUTA

"Transilvania" University of Braşov, Centre for Sustainable Energy,
e-mail: c.vladuta@unitbv.ro, a.duta@unitbv.ro

ABSTRACT

The aim of paper is to study the influence of environmental open air conditions on the PET-rubber composites. Two set of samples (Type I, Type II) were obtained with the same composition, but the composites of Type I are random mixed while Type II are layered. These samples were obtained by compression molding for 45 minutes, working in a temperature domain of 180°C-260°C. The samples were left free in atmospheric conditions (at temperature between 3°C- 30°C, under sun light and rain) for two months. These samples were mechanicaly tested and aging was evaluated.

KEYWORDS**:** recycling, PET-rubber composites, compression molding.

1. Introduction

Recycling plastic materials and rubber offers a solution which is satisfactory in terms of preventing environmental pollution.

The recycling of polymeric materials has been in substantial progress during the past few years. Particularly noteworthy has been the development of the Plastic Container Code System used by consumers and community groups to identify, separate, and recycle thermoplastic materials. Plastic recycling is complicated by the presence of fillers that were added to modify the original properties. The recycled plastic is less costly than the original material, and quality and appearance are degraded with each recycle. The recycling of thermoset resin (such as vulcanized rubber) is much more difficult since these materials are not easily remolded or reshaped due to their crosslinked or network structures. Some thermosets are ground up and added to the virgin molding material prior to processing; as such, they are recycled as filler materials. As a result, other methods to recycle the rubber must be found. Grinding is one method to recycle a thermoset. The ground rubber can be used alone or mixed with thermoplastics to achieve the desired properties, such as impact modification, [1-4].

Scrap tire rubber has many excellent mechanical properties in comparison to other materials. These include impact resistance, flexibility, abrasion resistance, and resistance to degradation. Therefore, the concept of using crumb rubber as an engineering material is justified. The structure of the rubber polymer itself makes recycling difficult. Tire rubber is a thermoset, meaning the polymer is crosslinked into a network. These crosslinks are usually covalent bonds between polymer chains, which are difficult to break by simple means. Once the polymer chains have been crosslinked, it is no longer possible to reform the material simply by heating the polymer, as it is done with thermoplastics like polyethylene terephthalate (PET). Crosslinking can be introduced into the polymer by heat and/or chemical means. In rubber, crosslinking is more commonly known as vulcanization, which uses heat and sulfur, [3-5].

The production of plastic materials, especially PET, is nowadays increasing, which will lead to an increasing quantity of plastic wastes. The polyethylenterephthalate is a sophisticated material with great resistance which is most effectively used for beverage containers: and it is one of the most important engineering thermal plastics used for fibers, films and bottles. The advantage of recycling the PET containers is huge, taking into account the impressive number of containers that can be used at acceptable cost. Many studies have been carried out in order to investigate the possibilities of recycling PET bottles for the production of injection-moldable, extrudable, and thermoformable PET resins. That could be used to make structural parts of vehicles, automotive textiles, bottles, food containers, and raw materials for polyurethane [6-10].

The objective of this paper is to develop new composites with the following materials: PET, rubber and HDPE as additive. Attempts are made, to quantify

important molecular structure/physical properties relationships in the various blends, as well as critical rheological and processing parameters.

2. Experimental

2.1. Blending

The HDPE and PET bottles were first washed out of impurities and then cut in small pieces in order to obtain flakes and the recycled rubber was granulated using a milling machine; the rubber was granulated using a milling machine. Then materials were mixed and put into the die for obtained samples. Two set of samples (Type I, Type II) were obtained with the same composition (rubber: HDPE: PET = 85:5:10, wt. %), in the same working conditions. The composites of Type I are random mixed and of Type II are layered. Type II of samples is obtained as follows: the first layer HDPE + rubber, the second layer PET + rubber, and the third are similar with the first layer, [11, 12].

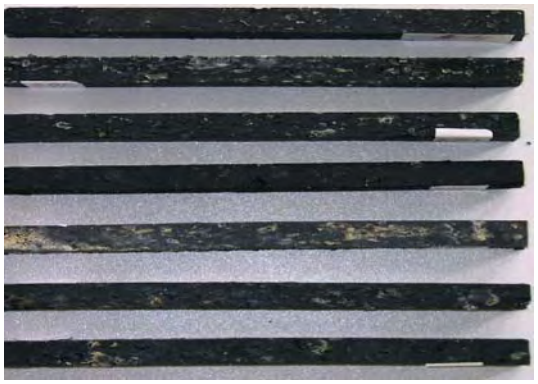

***Fig. 1** Samples with random mixed, Type I*

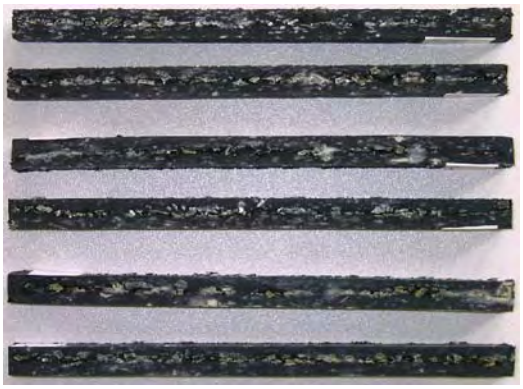

***Fig.2.** Samples with layerd mixed, Type II*

2.2. Compression molding

Compression molding was performed in a heated press. The samples were obtained at high temperature (180^0C…260^0C, Table 1) using a thermostated heater, type ECv 200-300, with strict temperature control (± 5^0C). During molding, materials were heated for 45 minutes.

Table 1. Temperature preparation of samples

Sample No.	I1 II1	I2 II2	I3 II3	I4 II4	I5 II5	I6 II6	I7 II7	I8 II8	I9 II9
Temp. T(°C)	180	190	200	210	220	230	240	250	260

2.3. Testing

The samples were prepared using our prototype and these were tested. Compression testing were performed using a mechanical stand type MTS (Multi Tester System) with attached computer operating system. Some samples were left free in atmospheric conditions, at temperatures between 3°C-30°C, under sun light and rain, for two months. Other samples were left at room temperature for the same time.

3. Results and discussions

The mechanical properties of samples depend on temperature processing period, manufacturing conditions, composition, and environmental open air conditions. During compounding at an elevated temperature, a chemical reaction occurs at the interfaces, leading to increased adhesion between thermoplastic (HDPE, PET) and rubber phases.

The mechanical tests have been applied more samples, some were used for testing compression, making two measurements for each temperature. Compression force dependence on time is presented in Fig. 1, 2, 3, 4, which shows curves of the same shape. Under lower compression forces, the samples at temperature lower then 200°C still conserve a porous structure. At higher temperature samples prove to have the most compact structure.

As we have noticed virgin rubber is solid and glassy at a temperature of -195°C while at temperatures between 0°C and 10°C it is frail, and at temperatures over 30°C rubber becomes liquid. These features are no longer sustained when rubber is mixed with other materials such as PET and HDPE. In contact with the oxygen in the air, rubber is subject to aging. This is due to the fact that oxygen influences the double bonds in the virgin rubber. Recycled rubber contains small quantities of sulphur which make it elastic.

The absence of polar functional groups capable of forming hydrogen bonds with molecules of water and the high packing density of the macromolecules on the supermolecular level (there is

marked ordering even in amorphous regions) create steric and kinetic hindrances for penetration of molecules of low-molecular-weight substances in PET. This results in low energy of the surface reaction with water and the poor capacity of polyester fibres to sorbs low-molecular-weight substances, primarily moisture.

Another distinctive feature of PET is the higher rigidity in comparison with rubber and HDPE. The equilibrium moisture content in sorption-desorption of moisture from air is low for PET. In the domain temperature 3°C - 30°C at which the samples were exhibited, and relative humidity, equilibrium sorption of moisture is relative lower.

However, the absorbed water from the atmosphere produces changes of the matrix and interfaces. Through this, the humidity can affect the mechanical properties of composites.

The orientation of PET pellets in composite influence meaningful the resistance on humidity and temperature.

If we compare the layered and random mixed samples let in indoor conditions, it is observe that the layered samples are more resistant at compression test, Fig. 3, 4.

The results are not the same in atmospheric conditions. In this case, the layered samples have a lower resistance than random mixed samples, Fig. 1, 2. Between layers, the water molecules sorptions produce the delaminating of composite.

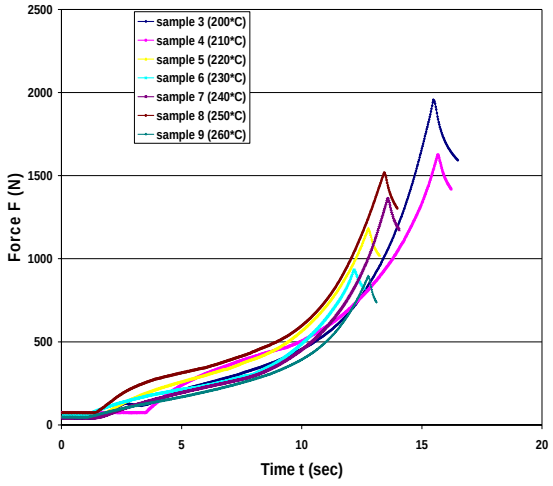

Fig. 1. *Compression graphical representation for the layers samples let in atmospheric conditions*

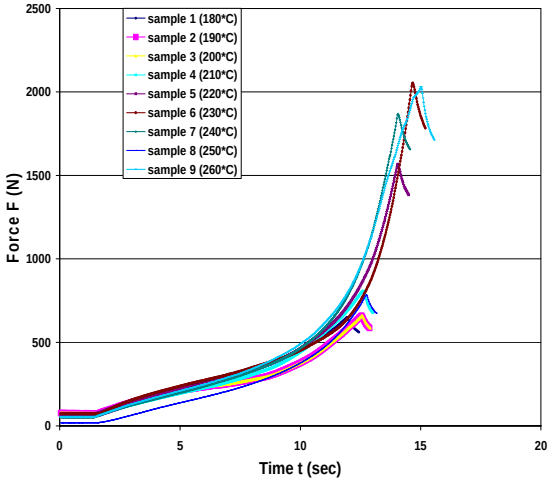

Fig. 2. *Compression graphical representation for the random mixed samples let in atmospheric conditions*

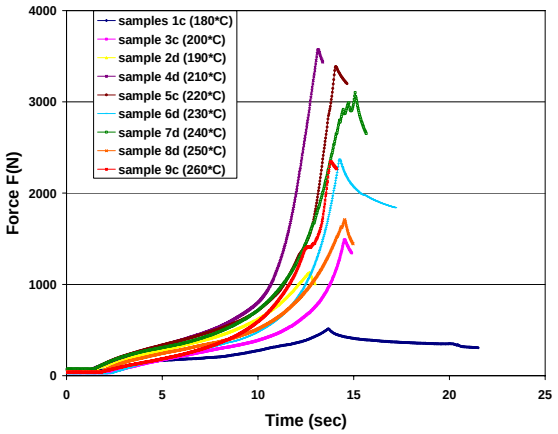

Fig. 3*. Compression graphical representation for the layers samples let in indoor conditions*

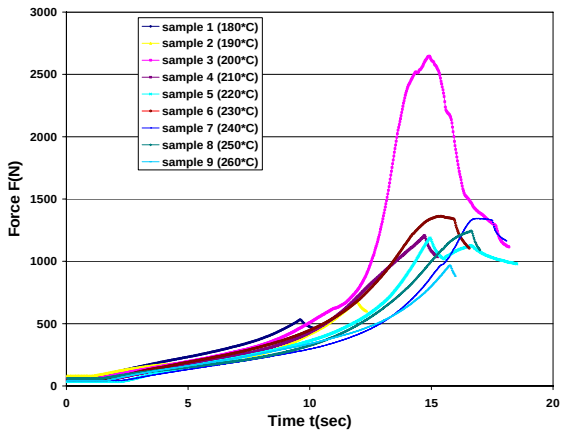

Fig. 4. *Compression graphical representation for the random mixed samples let in indoor conditions*

4. Conclusions

This work has evaluated methods of using recycled scrap rubber and PET in the development of new materials on a laboratory scale. Specifically, the recycled ground rubber was blended with PET and HDPE to form a thermoplastic elastomer appropriate for use in paving the yards, playgrounds in parks; also in construction industry as thermal and phonic insulators, successfully replacing different types of floor. In addition, this work has converted a thermoset material into a thermoplastic elastomer, which can be reused and converted into new products.

The study on the mechanical properties of layered composites and random composites indicates that:

- PET-rubber composites can be used with a small amount of HDPE without the use of supplementary additives;
- The mechanical properties of the composites strongly depend on the moulding temperature and environmental open air conditions;
- In the range of medium to high deformation forces and at increasing temperature, also during longer load time, a viscous deformation overlays the elastic deformation;
- The layered samples can be used for paving inside, but the samples with random mixture for paving outside.

References

[1] M. Pittolo and R.P. Burford, *Rubber Chem. Technol.* 58, p.97 (1985).

[2] Myhre, M. J. and MacKillop, D. A., *Rubber World*, 111:5, p.42 (1996).

[3] Stotsky, S., *"Innovation in the development and use of recycled rubber"*, (paper #42) presented at a meeting of the Rubber Division, Amer. Chem. Soc., May 1997.

[4] Gunnigle, J. R., *"Recycled rubber based compounds – an unusual opportunity to cut cost"*, (paper No. 68), presented at a meeting of the Rubber Division, Amer. Chem. Soc., Pittsburgh, PA, October, 1994.

[5] Ismail H., Nordin R., Noor A.M., *Polymer Testing* 21 (2002) 565-569.

[6] S. Birch, J. Yamaguchi, A. Demmler, K.Jost, Aui mot.m., 101, (1993), p.109.

[7] Wellman International. Nat. Reklam Week. 163, 6 (1994).

[8] New methods of using post-consumer PET in food contact containers, Reuse Recycle, 24, 57 (1%).

[9] Society of the Plastics Industry, Polyurethane News, 3, 3 (1990)

[10] C. Vlăduță, E. B. Fazakaş, A. Duță, I. Vişa, V. Pop, *Influence of interfaces matrix rubber on properties of rubber plastic materials composites,* 20-21 May 2005, Ecological Chemistry, ISBN 9975-62-134-1, Chisinau, Moldova, p.579-583.

[11] C. Vlăduță, A. Duță, E. B. Fazakaş, I. Vişa, *Influence of temperature on the mechanical properties of PET and HDPE with rubber layered composites,* 22-24 September 2005, The 14th Romanian International Conference on Chemistry and Chemical Engineering.

CHEMICAL AND STRUCTURAL CHANGES FOR BIMETALLIC MATERIALS OBTAINED BY THE WELDING PROCESS

Anişoara Ciocan, Felicia Bratu

„Dunărea de Jos" University of Galaţi
email: aciocan@email.ro

ABSTRACT

This paper presents the transformations which take place during the obtaining process of bimetallic materials. As a plating process was used the welding. The added material was a bronze with aluminum complex alloyed with iron, nickel. The based material was the steel. EDAX analyses and microstructures analyses were done in order to explain the metallurgical processes which take place during the facing by melting.

KEYWORDS: bimetal, plating by welding, steel, bronze with aluminium complex alloyed

1. Introduction

In many industrial applications, the working surfaces of the cast or plastic deformed bench-mark are simultaneously exposed to a very different kind of stresses. In these types of working regime, plated metallic materials can be used. These materials are obtained using the depositing process of one material, as layers with different thicknesses, on top of another material considered as a base. The plated metallic materials, also named bimetallic can satisfy some requests of the working conditions impossible to be obtained using one single metallic material. The covered steels with non-ferrous alloys layers are an example. The bimetallic pieces were obtained by the welding process. The idea was to produce some steel machine parts covered with antifriction non-ferrous alloys layers. These are characterized by a high hardness necessary for special working conditions: a good wear resistance at a specific contact pressure of min. 200 daN/mm^2 and a working speed of 60 m/min, high corrosion and abrasion resistance, a minimum wear loss after the end of working time. As added materials bronzes with aluminium complex allied with iron, nickel and manganese were used. These materials posses a good tenacity combined with a suitable bursting resistance, low coefficient of friction, good behaviour during the wear tests, a high capacity of shock damping, and a good fatigue resistance (Table 1).

The structure of CuAlNi alloys. The Cu-Al alloys with aluminium content higher than 9.4 % solidify by forming the β phase which is transformed gradually, during a slow cooling, in a $\alpha+\gamma$ phase through a eutectoid reaction at ≈ 570 ^{o}C. The γ phase can be corroded preferentially due to the presence of high aluminium content. This presence deteriorates the material (Figure 1). The addition of nickel and iron in Cu-Al alloys leads with an increase of stability domain for α phase and a decreased formation of β phase. The addition ok Ni and Fe increase significantly the mechanical properties of CuAlNiFe alloys due to the formation of both α and β phases by the *k* intermetallics compounds. Thus, the CuAlNiFe alloys become quaternary copper based alloys. Accordingly the literature, casting alloys solidify by forming one single phase, β solid solution. This one is stable to the cooling process until $\approx$ 1000 ^{o}C [1-4]. Under this temperature, the α phase precipitates from β phase with Widmannstatten morphology, followed by a nucleation process of the globular k constituent. This constituent is identified as Fe3Al (named k_{II} for the elements content from table 1 and k_{I} at a Fe content $\geq 5\%$ when its morphology is dendritic).

Tabel 1. *Chemical composition of CuAlNiFe alloys, Wt %*

Element	Al	Ni	Fe	Mn	Cu
Limits of concentration	11,0-12,0	4,0-5,0	4,0-5,0	0,8-1,2	rest

At ≈ 850 °C, the iron solubility in the α phase decreases and it starts to precipitate a fine k constituent (Fe_3Al), named k_{IV}. At the end, at ≈ 850 °C, it appears a k phase rich in Ni, k_{III}, with a globular morphology. The morphology is formed by a eutectoid reaction when $\alpha + k_{III}$ is obtained (Figure 2).

The mechanical properties of bronzes with aluminium depend by the aluminium content and substantially vary with the secondary allegation elements contents. The iron refines the structure, increases the resistance and the hardness and decreases the fluidity of the alloy; every Fe percentage in a bronze with aluminium leads with an increase of the mechanical resistance of the alloys with 2.8 daN/mm^2. The nickel is the most efficient addition in the bronze with aluminium. The addition of nickel increases the mechanical characteristics, the antifriction and anticorrosion properties. The nickel addition also increases the compactness and the high temperature resistance. The manganese increases resistance, plasticity and the antifriction properties, but significantly decreases the fluidity. Comparing with iron, the manganese behaves as a stabilizer. It is dissolved in the solid solution and it doesn't provoke structural changes [5]. The bimetallic pieces are obtained using the welding process [6]. This process must provide a perfect adhesion of the plated layer on the based material. In the same time, the welding process parameters must create the most reasonable conditions in order to not affect the physical, chemical and mechanical properties of the compounds.

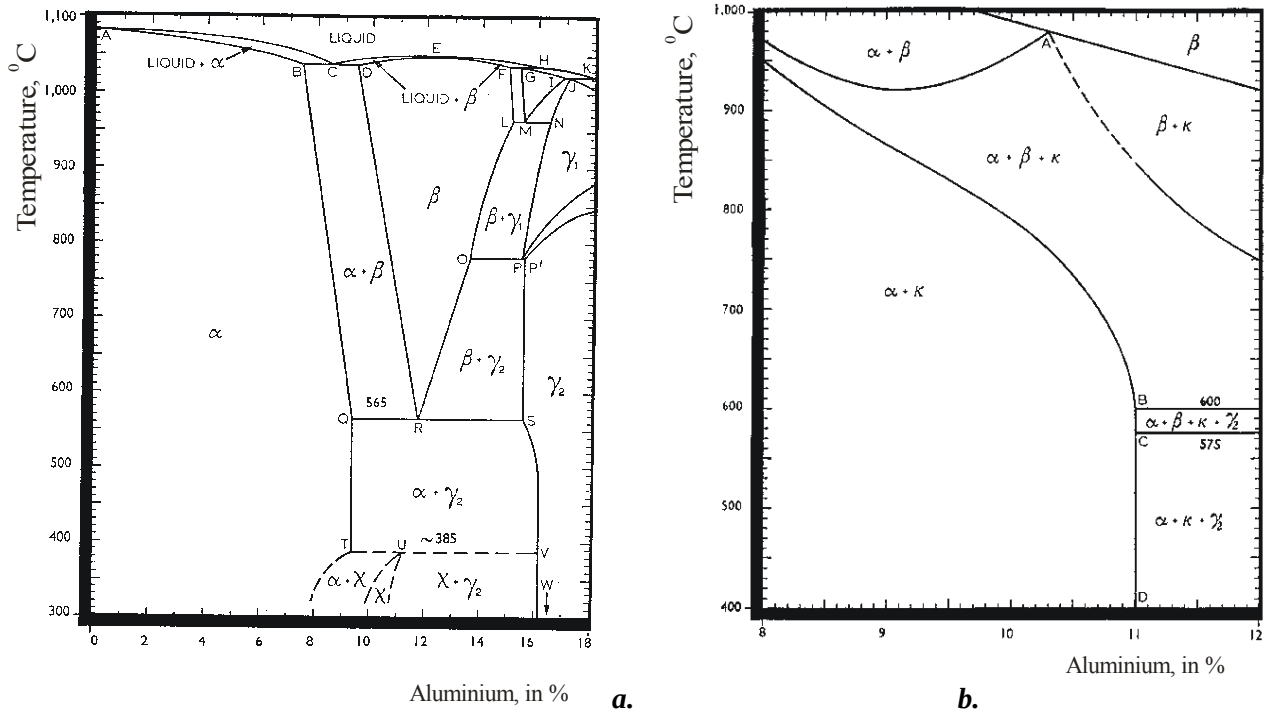

a. ***b.***

Fig.1. *The equilibrium diagram of Cu-Al system (a) and a cross section of CuAlFeNiMn diagram at 5% Fe and 5% Ni (b).*

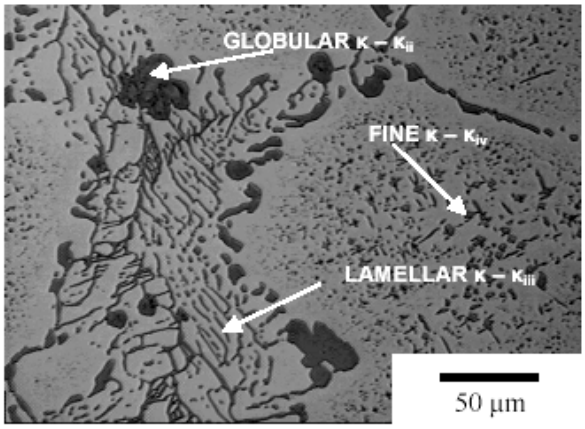

Fig.2. *The microstructure of CuAlFeNiMn casted-on alloy*

I

The compounds participate to the mechanical stress of the plated pieces. The welding process provides a good junction of the layers specific to the interatomic junction at the grains boundaries of a polycrystalline material.The junction is favoured by the diffusion phenomenons which take place in the contact zones of the two materials. It is necessary to take place a reciprocally diffusion process between the added material and the based one. The mechanism and the characteristics of the junction is determinate by the metallic material nature, by the temperature, the damping properties of the solid based material with the welted added material, by the welding conditions, etc.

2. Experimental

The plating process of the steel was done with antifriction alloys using a welding process with an electric arc in a protected argon environment, type WIG. The deposited material was cast-on as wires with 4 mm diameters and 400 mm length. The optimized welding parameters were:

- preheating temperature of 150-200 ^{o}C;
- an alternative current or a direct current with an inverse polarization (DC^{+});
- an welding current, I=120…150 mA;
- a protecting gas volume of 20…30 l/min.

Due to the big differences between the chemical compositions of the based and addition materials, the deposition process was done in many layers in order to reduce the effects of elements dissolution and diffusion phenomenon. The obtained thickness of the layers was enough to provide the chemical composition in order to obtain their required properties (figure 3).

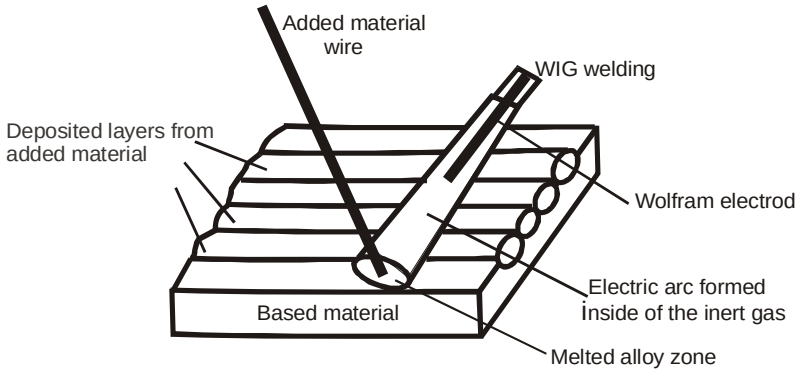

Fig. 3. *The multilayers deposition diagram of the antifriction alloy*

3. Results and discussions

On the border of the based material and the addition material it is formed a transition zone where take place structural and composition changes. This is due to the melting of non-ferrous alloy which behaves as a metallic bath. In this metallic bath take place the same processes as those specific for the non-ferrous alloys making: gases adsorption, elements loss by oxidation, etc (figure 4). The presence in the based material of some very strongly thermal influenced zones determinates diffusion and dissolution of the elements of both metallic materials. Figure 5 shows the microstructure of the obtained bimetallic material on the border of deposited non-ferrous alloy and the steel. It can be observed that the transition zone is very uniform, with a constant thickness about 0.010 mm, as consequences of a very well controlled deposition process. In the vicinity of the interfaces, the structure of the deposited material is dendriform with axes perpendicular oriented on the interface of the two materials (figure 6).

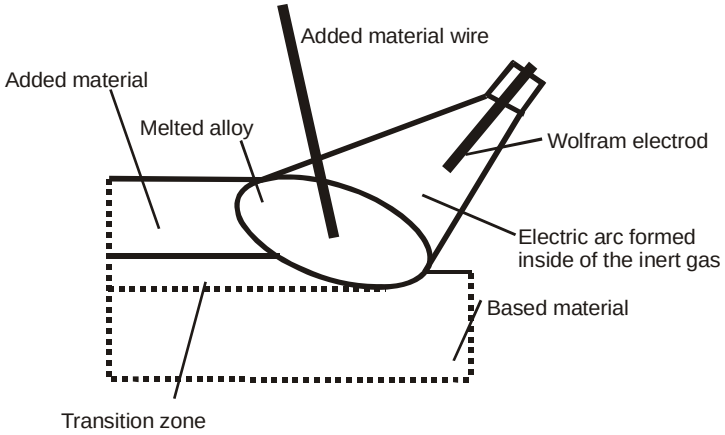

Fig. 4. *The processes which take place in the deposition zone*

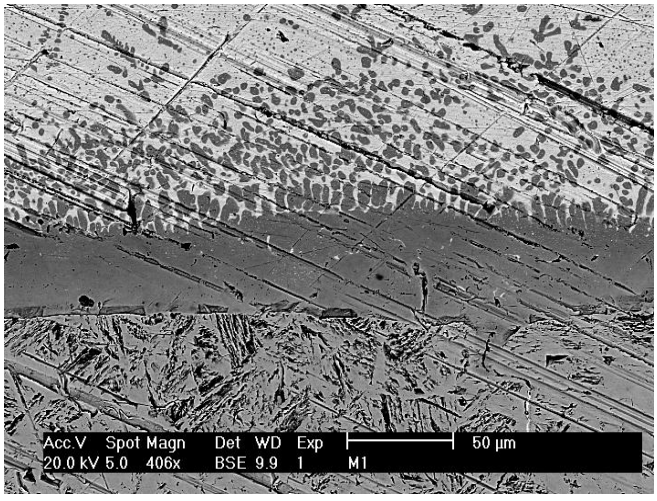

Fig. 5: *The transition zone; x 400, 20 kV, BSE (back scattering electrons).*

Fig. 6: *The dendriform structure of the deposited material in the vicinity of the transition zone.*

The chemical analyses made in different points of the transition zone show that the diffusion processes take place in two directions: from the steel to the non-ferrous alloy and reversed. Therefore, in the transition zone can be find chemical elements of the both materials (Table 2, figure 7).

Tabel 2. *The elements concentration in different points of the transition zone, Wt %*

Element	Location in the transition zone		
	Point close by the non-ferrous alloy	Point in the centre	Point close by the steel
Al	8,09	6,04	3,35
Si	0,40	0,48	0,45
Mn	1,55	1,05	0,75
Fe	80,12	85,18	90,37
Ni	4,86	3,62	2,84
Cu	4,98	3,64	2,23

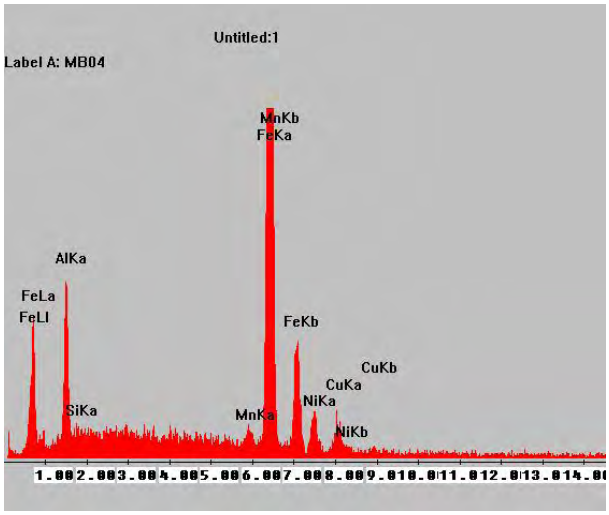

a. Point close by the non-ferrous alloy

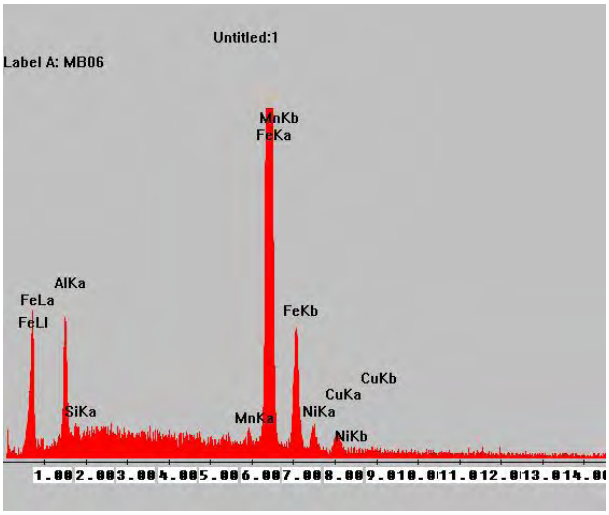

b. Point in the center

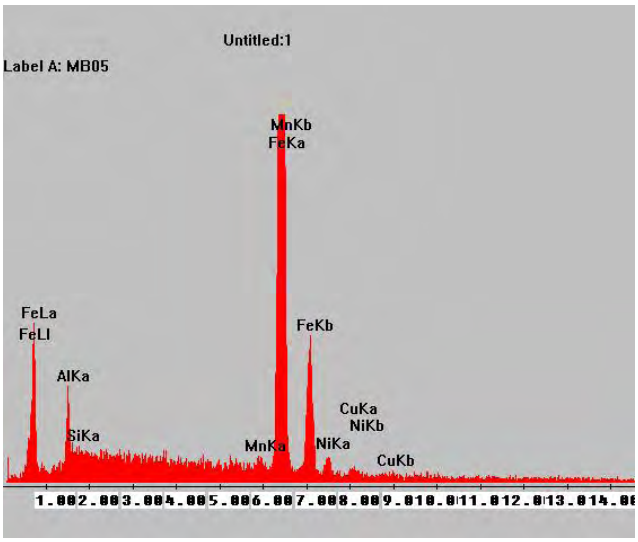

c. Point close by the steel

Fig. 7: *EDAX analyses in different points of the transition zone.*

The cross section analyses of the bimetallic material shows that the deposited layers surface has not defect as oxide films, others inclusions or porosities. The obtained bimetal material is a compact mass, without spiels, inclusions or cracks. In the based metallic material, at some depth from the deposition surface, it was noticed a thermal influenced zone where take place only the changes in the solid state. In this zone, the material was practically under uncontrolled thermal treatment. The effects of this treatment consist in a recristalisation and a presence of some grains with small dimensions, very close by the deposition zone. This caused an increase of the mechanical resistance of the bimetallic material (figure 8). Anyway, in order to reduce the effects of these thermal superheating some suitable thermal treatments are performed. As a consequence the required properties are obtained.

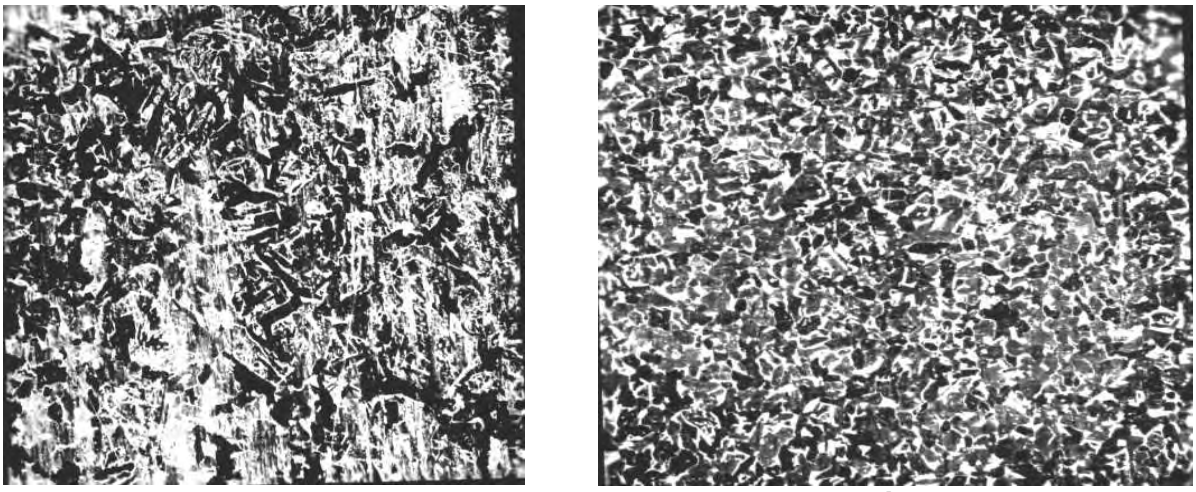

a. *b.*

Fig. 8. *Microstructure analyses on the based material:*
a – the steel microstructure used as based material, b – the superheating zone

4. Conclusions

The processes which take place when the steel is plated with a non-ferrous alloy using the welding are similar with the processes specific for a metallic bath formed through a metal melting in the welding zone with the contribution of both involved materials. The solidification mechanism of added material which caused the formation of a transition structure characterized by variable composition and properties can be different. If the welding process is well done, the transition zone of the melted added material and the superheating based material is formed.

This leads with an avoiding of unexpected variations in the chemical composition and properties from one material to the other one. The diffusion process, which takes place in both directions leads with formation of globular, or punctiform constituents. These constituents increase the hardness of material but do not affect its fragility.

There are not material defects and acicular constituents, which should affect the material quality.

Bibliografie

[1]. Meigh, H.,– "Cast and Wrought Aluminum Bronzes Properties, Processes and Structure", B 697 ISBN 1861250622 Hardbook

[2]. Oh-ishi, K.,Cuevas, A.M., Swisher, D.L., McNelley, T.R.,"The influence of Friction Stir Processing on Microstructure and Properties of a Cast Nickel Aluminium Bronze Material" , Metallurgical and Materials Transactions A., vol.35A, sept.2004

[3]. Culpan, E.A., Rose, G., British Corrosion J, vol.14,1979, p.160

4. **Hasan, F.,** Metallurgical Transactions A, Vol. 13 A, aug. 1982

[5]. *** - "Know How Welding Repair for New Propeller, Nakashima Propeller Co. Ltd.

[6]. Popovits David, Subu Teofil - "Bimetals, Editura Facla, Timisoara, 1982

RESEARCHES REGARDING STRUCTURAL CHANGES DUE TO NICKEL MICROLALLOYING OF HOT GALVANIZING BATHS

Radu BOICIUC[1], Adriana PREDA[1], Simona BOICIUC[2]

[1] S.C. Uzinsider Engineering S.A. Galați,
[2]"Dunărea de Jos" Galați University
e-mail: boiciuc.simona@ugal.ro

ABSTRACT

This work offers a synthesis of researches performed in laboratory and regards the nickel microalloying of hot galvanizing baths. Experiments followed the structural changes of both hot galvanizing bath and deposed layer with effect on layer properties.

Characterization of deposed layer and nickel microalloying of galvanizing bath performed by spectral chemical analysis, optical microscopy and X ray diffraction emphasized the structural constituents nature as well as changes shown up depending on nickel concentration of galvanizing bath. Correlation diagrams between deposed layer thickness and structural constituents were also made.

Experimental results emphasized a close interdependence between nickel concentration and microstructure. This allowed to settle the optimal nickel concentration required by galvanizing bath microalloying with maximum effect upon hot galvanizing coating properties.

1. Generals

Experiments performed on a pilot plant used A5K steel strip (as per STAS 10.318) or A35 – 401 type (according to ZE French standard) and included coating by hot galvanizing of several samples (P_1-P_7 code) suitable for the following nickel concentrations in galvanizing bath: 0%; 0,02%; 0,06%; 0,09%; 0,11%; 0,16% and 0,20%.

Galvanizing technology used is the classical one. Samples were degreased, pickled, preheated for 30 seconds, immersed in galvanizing bath for 60 seconds and then freely cooled in air.

2. Spectral chemical composition of deposed layer

Spectral chemical analysis on coating layer performed by Baird DV 6 optical emission spectrometer got the results included in table no.1.

Table no.1 *– Spectral chemical composition (%) of samples galvanized and microalloyed by nickel*

Sample code	Ni	Fe	Cu	Pb	Sn	Cd
P_1	0	**4.651**	0.000	0.001	0.004	0
P_2	0.02	**1.599**	0.001	0.001	0.008	0.001
P_3	0.06	**0.412**	0.001	0.001	0.005	0.001
P_4	0.09	**0.264**	0.001	0.001	0.005	0.001
P_5	0.11	**0.177**	0.001	0.001	0.003	0.001
P_6	0.16	**0.168**	0.001	0.001	0.002	0.001
P_7	0.20	**0.163**	0.001	0.001	0.002	0.001

It may be seen an important decrease of Fe content in the coating layer in the same time with increasing the degree of bath microalloying up to 11% nickel content.

Over this value the Fe content will stay approximate constantly.

3. Structural methallographic determinations

Methallographic analysis performed by Olympus microscope, endowed by data acquisition automatic system, on specimens sampled from galvanized steel sheets and galvanizing bath.

Measurements results are given in table no.2.

Table no. 2. *Thickness of zinc layer and intermetallic layers*

Sample code	Zn layer thickness (eta) [μm]						Intermetalllic composes layer thickness [μm]					
	g_1	g_2	g_3	g_4	g_5	$G_{m\ Zn}$	g_6	g_7	g_8	g_9	g_{10}	$g_{m\ Cmet}$
P_1	31.64	32.52	30.77	29.10	29.84	30.77	48.35	49.77	48.52	50.25	50.11	49.40
P_2	46.61	42.19	48.41	48.34	46.59	43.43	37.55	34.89	37.07	35.16	36.93	36.32
P_3	58.89	57.16	56.87	58.02	58.89	57.96	15.85	15.82	15.81	15.26	15.82	15.71
P_4	61.73	60.68	60.65	60.65	61.54	61.05	14.85	15.59	15.49	15.94	15.77	15.53
P_5	71.19	71.24	71.22	71.19	70.95	71.16	15.70	15.33	15.78	15.43	15.20	15.48
P_6	69.25	69.34	70.11	70.08	69.53	69.66	15.82	15.27	15.84	15.83	15.83	15.72
P_7	70.34	70.86	70.64	71.48	71.20	70.84	20.21	19.13	20.23	20.21	20.19	19.99

Note: g_m – the average value of deposed layer

Analyzing the results it may be remarked that changes of deposed layers thickness took place depending on Ni percentage added in the bath.

Up to 11% Ni content inside bath the Zn layer thickness increase and intermetallic compounds layer thickness decrease are recorded. Over this value the deposed layers thickness is kept approximately steady and it is a relevant aspect on diagrams in figures no.1 and 2.

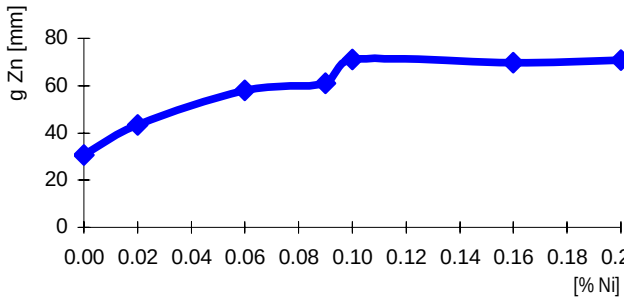

Fig. no.1. *Variation of Zn layer thickness depending on Ni content of metallic bath*

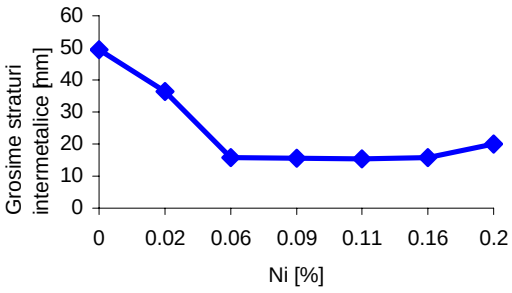

Fig. no.2. *Variation of intermetallic compounds layer thickness depending on Ni content of metallic bath*

Gradually by increasing the nickel microalloying degree of galvanizing bath, metallographic analysis emphasized (figures no. 3÷6) important changes in deposed layer structure:

- Finishing of Zn grains and apparition of Ni-Zn intermetallic compound disperse particles in eta layer;
- Decreasing and finishing the layer in "palisade";
- Coalescence of Ni-Zn intermetallic compound particles precipitated in eta layer.

Metallic bath microalloying by nickel, even in very small concentrations, made essential changes of its microstructure (Fig. no. 7÷12).

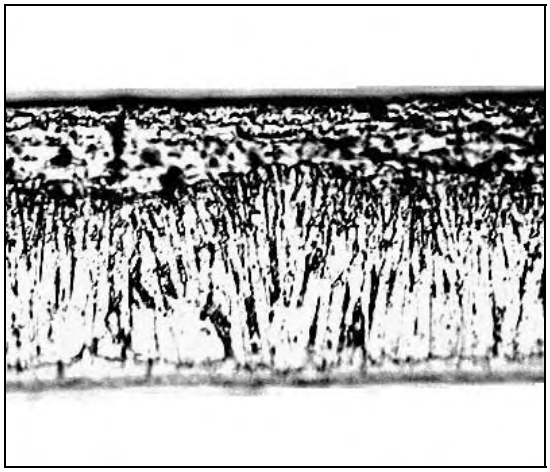

Fig. no. 3 *Microstructure of deposed layer, 0 % Ni. (x 500). 1% nital attach.*

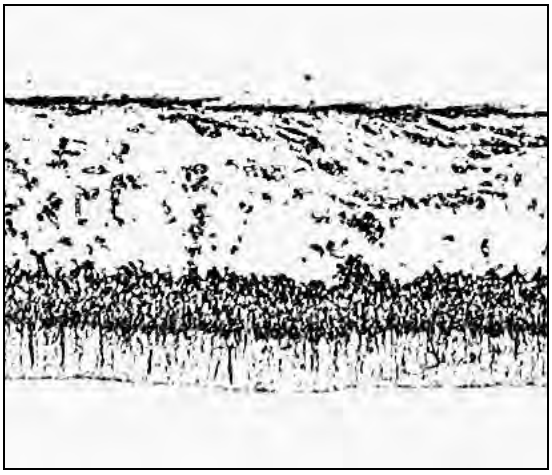

Fig. no. 4 *Microstructure of deposed layer, 0.06 % Ni. (x 500). 1% nital attach.*

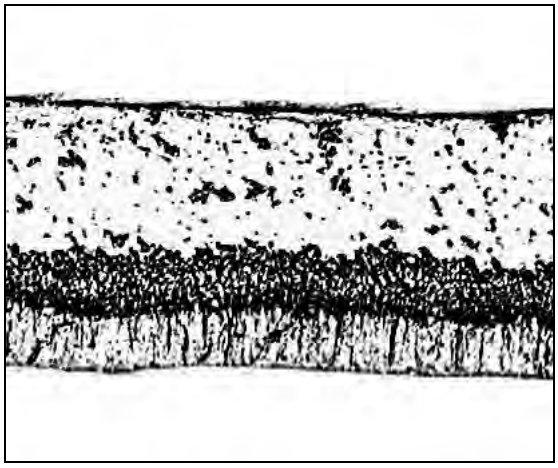

Fig. no. *5 Microstructure of deposed layer, 0.11 % Ni. (x 500). 1% nital attach.*

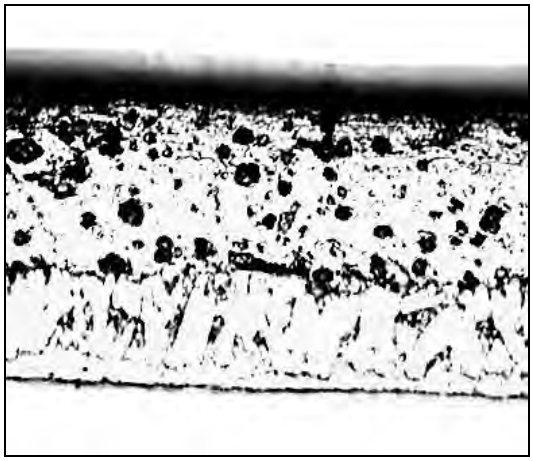

Fig. no. 6 *Microstructure of deposed layer, 0.20 % Ni. (x 500). 1% nital attach.*

Fig. no. 7 *Microstructure of the bath 0 % Ni. (x 100). 1% nital attach. Zn large crystals with macles.*

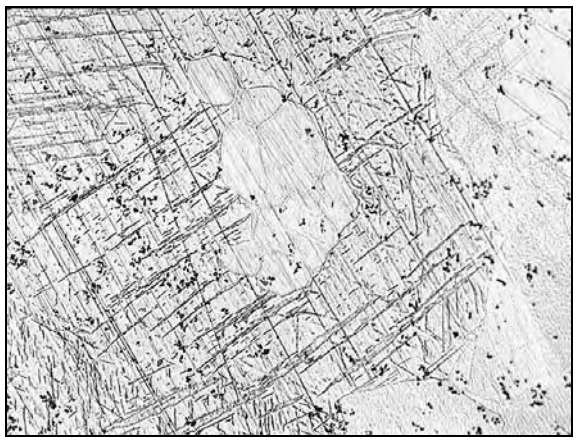

Fig. no. 8 *Microstructure of the bath 0,02 % Ni. (x 100). 1% nital attach. Zn large crystals with tendency to form Zn-Ni eutectic.*

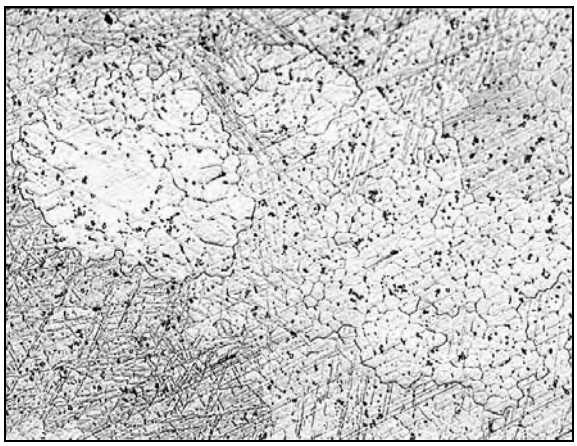

Fig. no. 9. *Microstructure of the bath 0,06 % Ni (x 100). 1% nital attach. Inhomogeneous eutectic structure in which very fine dispersed particles of Ni-Zn intermettalic compound show up.*

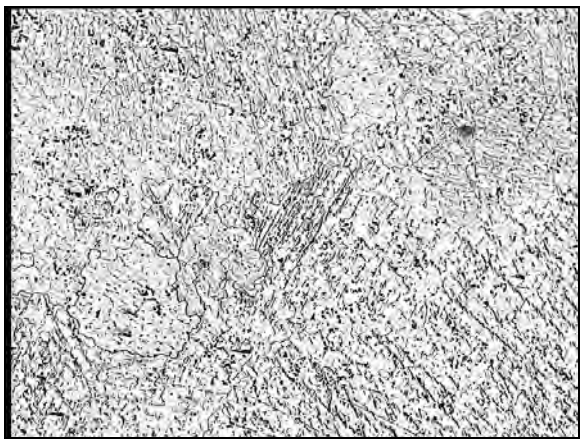

Fig. no. 10*. Microstructure of the bath 0,09 % Ni. (x 100). 1% nital attach. Eutectic structure in which fine dispersed particles of Ni-Zn intermettalic compound show up.*

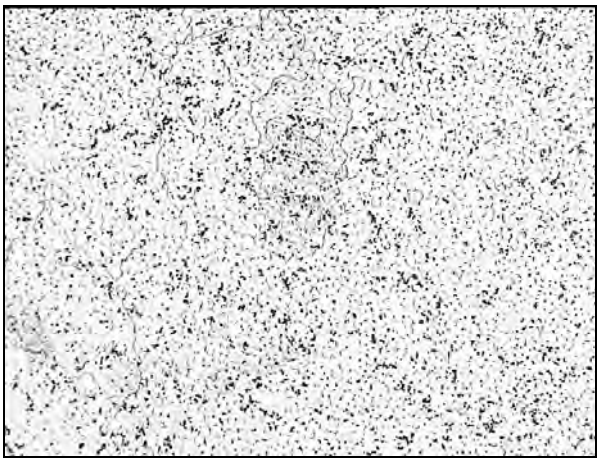

Fig. no. 11. *Microstructure of the bath 0,11 % Ni. (x 100). 1% nital attach. Fine eutectic structure in which fine particle agglomeration of Ni-Zn intermettalic compound show up dispesed.*

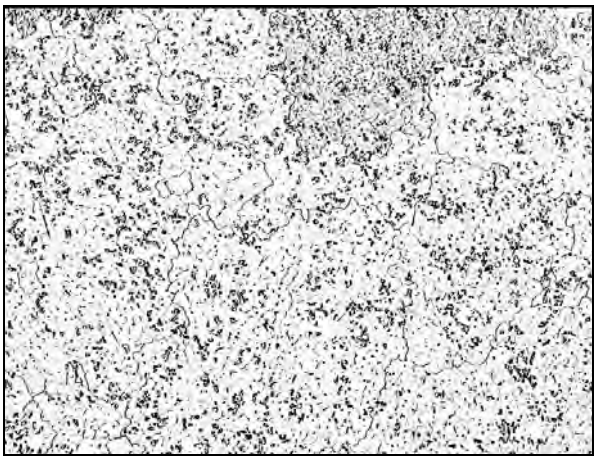

Fig. no. 12. *Microstructure of the bath 0,20 % Ni. (x 100). 1% nital attach. Fine eutectic structure in which globular particle agglomeration of Ni-Zn intermetallic compound show up.*

Large Zn crystals grained in the same time with Ni content increasing up to a very fine eutectic structure where the Ni-Zn intermetallic compound particles precipitated. Coalescence and crowding of these particles made in the same time with alloying percentage increasing.X ray diffractometric analysis confirmed the results got by both spectral chemical and metallographical analysis .

Phases identified in metallic layer were

- (γ) gamma adherence layer : Fe_5Zn_{21};
- (δ) delta frail layer in "palisade" : $FeZn_7$;
- (ξ) zeta intermediary layer - Fe_3Zn_{10};
- (η) eta layer or pure Zn;
- $NiZn_3$ intermetallic compound.

Quantitative ratio of the first four phases varies depending on Ni content up to Fe_3Zn_{10} intermediary phase vanishing.

$NiZn_3$ intermetallic compound apparition was signaled in the same time with feeding the Ni in metallic bath, its quantitative ratio increasing direct proportional by this element content recording a level inside 0.11÷0.16% Ni range (fig. no. 13).

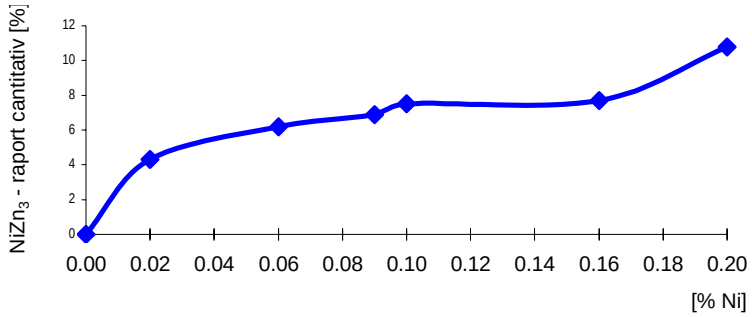

Fig. no. 13. *Variation of $NiZn_3$ phase quantitative ratio depending on Ni content of metalic bath*

Fine structure additionally hardened by $NiZn_3$ intermetallic compound, dispersed in pure zinc in quantitative ratio up to 10.8%, confers special resistance and corrosion properties.

4. Conclusions

Nickel microalloying of hot galvanizing bath determines essential changes of both bath and deposed layer microstructures.

Fe content decreases by Ni content increasing up to 0.11 % as a result of Fe_xZn_y type layers decreasing and apparition of $NiZn_3$ compound.

Eta zinc layer thickness increases by 131% and that one of intermetallic layers decreases by 69% Ni in galvanizing bath. Over this value thickness stays steadily.

Deposed layer structure records the following changes:

- Decreasing and finishing the layer in "palisade";
- Finishing of Zn grains and apparition of disperse particles of Ni-Zn intermetallic compound in eta layer;
- Coalescence of Ni-Zn intermetallic compound particles precipitated in eta layer.

Large Zn crystals grained in the same time with Ni content increasing up to a very fine eutectic.

$NiZn_3$ intermetallic compound presence in deposed layer, in a quantitative ratio of up to 7.5% suitable for 0.11% Ni content determines both structure finishing and additional hardening of coating with maximum effects on coating quality.

References

[1]. G. Reumont, P. Perrot, J. Foct - *Thermodynamic study of the galvanizing process in a Zn – 0,1 % Ni bath*, Journal of Materials Science 33, pg. 4759-4768, 1998.

[2]. G. P. Lewis, J. Pederson - *Optimizing the Ni-Zn process for hot dip galvanizing*, Cominco LTD., 1998

[3]. C. Alonso, J. Sanchez, J. Fullea, C. Andrade, P. Tierra, M. Bernal - *The addition of nickel to improve the corrosion resistance of galvanized reinforcement*, 1995

[4]. D. Stroud - *Galvanizing with Zn-Ni alloy*, Proceedings first Asian-Pacific General Galvanizing Conference, Taiwan, 1992

MATHEMATICAL MODEL OF THE STRIP ROLLING MADE OF THE SINTERIZED METALLIC POWDERS

Ionel PETREA, Sorin Miltiade ISTRATE

"Dunarea de Jos" University of Galati
e-mail: petrea.ionel@ugal.ro

ABSTRACT

The minimum-power method has been used to investigate the final ratio soft-layer thickness to tough-layer thickness in bimetals with porous layer rolling. The velocity fields has been determined and the total deformation power has been calculated: the rolling force and roll torque have alsobeen estimated, using the energy method.

KEYWORDS: reduction per pass, the power for internal deformation

1.Introduction

A prime objective of the mahematical analysis of rolling processes is to predict rolling force, roll torque and power, as well as strain distribution in the deformation zone.The problem is especially important in bimetal plate rolling, when the reduction of the tough layer is less than that of the reduction of the soft layer ($\varepsilon_M>\varepsilon>\varepsilon_T$). The reductions of the layers are depedent on the initial soft layer thickness to tough layer thickness (H_M/H_T), the ratio of the yield stresses (Y_M/Y_T), the mean thickness-to-length ratio of the plastic zone (Δ), the friction coefficient (f) and the reduction per pass (ε).

2.Velocity field in bimetal plate rolling

In order to determinate the velocity field the following assumptions have been made:
- a state of plane strain exists in the deformation zone;
- the arc of contact can be replaced by a chord;
- the function $v_x=v_x(y)$ is linear;
- the friction force is constant along the arc of contact;

Figure 1 shows the geometrical configuration of the rolls and the bimetal plate with an infinitesimal element in the deformation zone.

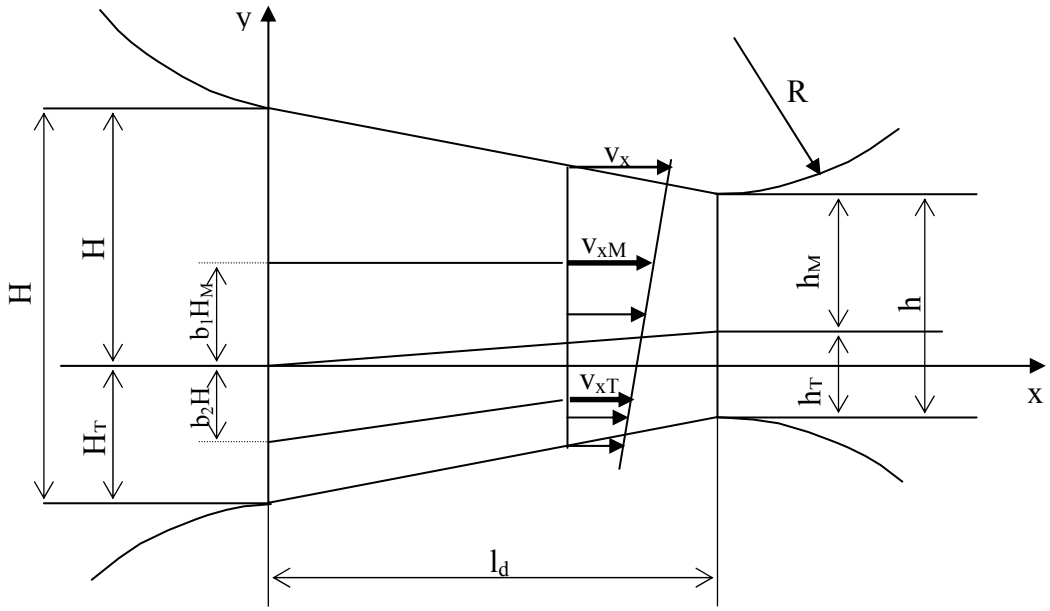

Fig. 1. *Geometry of the rolls and bimetal plate, showing the infinitesimal element.*

Notation:
a – variational parameter = h_M/h_T
H, h – initial and final thickness of the plate
H_M, h_M – initial and final thickness of the soft layer (the porous strate)
H_T,h_T – initial and final thickness of the hard layer (the steel strip support)
l_d – length of the deformation zone
R – roll radius
v_o – initial plate velocity
v_{oM}, v_{oT} – initial velocity in the soft and hard layer
v_r – peripheral roll velocity
v_{xM}, v_{xT} – metal velocity in the soft and hard layer
α - angle between a chord of the arc of the contact and the x axis
β - angle between an infinitesimal element and the x axis
Δ - the mean thickness –to-length ratio of the plastic zone
$\Delta y0$, $\Delta y1$ – initial and final thickness of infinitesimal element
ε – reduction per pass
ε_M,ε_T – reduction in the in the soft and hard layer
λ_M, λ_T – elongation coefficient in the soft and hard layer

If the layers should not be bonded, their elongation coefficients would be:

$$\lambda_M = H_M / h_M ; \quad \lambda_T = H_T / h_T; \tag{1}$$

For a given pass geometry, the velocities are determined from the continuity condition for an infinitezimal element by the following relationships:

$$v_{xM} = \frac{v_0}{1-(1-1/\lambda_m)(x/l_d)} = \frac{v_0}{1-z_M(x/l_d)}$$
$$v_{xT} = \frac{v_0}{1-(1-1/\lambda_T)(x/l_d)} = \frac{v_0}{1-z_T(x/l_d)} \tag{2}$$

where:

$$z_M = 1-a\frac{(1-\varepsilon)H}{(1+a)H_M} \quad , z_T = 1-a\frac{(1-\varepsilon)H}{(1+a)H_T} \tag{3}$$

Bonding of layers involves changes of velocity in the y direction, and the function $v_x=v_x(y)$ is assumed to be linear. The coordinates of the infinitesimal elements in which velocities are $v_x=v_{xM}$ and $v_x=v_{xT}$ are, respectively: $y = b_1H_M$ and $y = -b_2H_T$ (b_1 şi b_2 are coefficients, $0 \le b1 \le 1$; $0 \le b2 \le 1$). This results in the following relationship from (2):

$$v_x = \frac{v_{xM}-v_{xT}}{b_1H_M+b_2H_T}(y-b_1H_M)+v_{xM}$$

$$\frac{1}{A}\ln\frac{AH_M(1-b_1)+1/(1-z_M)}{1/(1-z_M)-Ab_1H_M}-\frac{ah}{1+a}=0$$
$$\frac{1}{A}\ln\frac{1/(1-z_M)-b_1AH_M}{1/(1-z_M)-A(H_T+b_1H_M)}-\frac{1}{1+a}=0 \tag{5}$$

where:

$$A=\frac{1/(1-z_M)-1/(1-z_T)}{b_1H_M+b_2H_T} \tag{6}$$

The non-linear equations (5) are solved by Newton-Raphson iterative method, enabling determination of coefficients b_1 and b_2.

By differentiation of the velocity field the strain-rate components are obtained in the form:

$$\dot{\varepsilon}_x = \frac{v_0}{l_d}\left\{\frac{y-b_1H_M}{b_1H_M+b_2H_T}\left[\frac{z_M}{(1-z_M(x/l_d))^2}-\frac{z_T}{(1-z_T(x/l_d))^2}\right]+\frac{z_M}{(1-z_M(x/l_d))^2}\right\}$$

$$\dot{\varepsilon}_x = \frac{v_0}{l_d}\left\{\frac{y - b_1 H_M}{b_1 H_M + b_2 H_T}\left[\frac{z_M}{(1 - z_M(x/l_d))^2} - \frac{z_T}{(1 - z_T(x/l_d))^2}\right] + \frac{z_M}{(1 - z_M(x/l_d))^2}\right\}$$

$$\dot{\varepsilon}_{xy} = v_0\left\{\frac{1}{1 - z_M(x/l_d)} - \frac{1}{1 - z_T(x/l_d)}\right\}\frac{1}{b_1 H_M + b_2 H_T} + \varepsilon_x tg\beta$$

where angle β is defined by:

$$tg\beta = \frac{1}{l_d}\left[y + H_T - \frac{1}{2}H\varepsilon - \frac{1}{A}\ln\frac{A(y - b_1 H_M) + 1(1 - z_M)}{1(1 - z_M) - A(H_T + b_1 H_M)}\right]$$

3. Mathematical model of rolling (the power balance equation)

The purpose is the obtaining of a dynamic function (F – rolling force, M – roll torque) in correlation with the initial plate velocity, with the reduction per pass, with the friction in the deformation process, with the behavior at deformation of the material. The mathematical model is obtained from the virtual power principle (the power balance equation):

$$P_D + P_S = P_M + P_F \qquad (9)$$

where:

P_D – the power for internal deformation

P_S – shear power over surfaces of velocity discontinuity

P_M – the driving power of the rolls

P_S – the power dissipated with the friction

4.Calculation of the process parameters of the rolling of bimetal plate

On the basis of equations shown in Section 3, computations of power for internal deformation, power for friction losses and power over the surfaces of velocity discontinuity have been carried out. The results of these computations are exemplified in Fig. 2., in terms of change of the power components as functions of the variational parameter $a = h_M/h_T$.

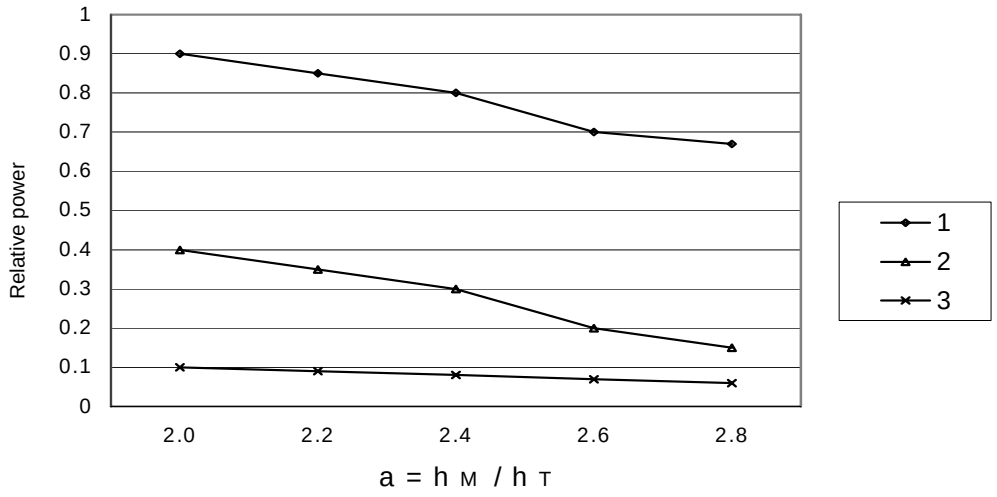

Fig.2. *The relationship of the power components to the h_M/h_T.ratio (H_M/H_T =3, ε = 0.3)*
1 – relative power for internal deformation; 2 –power for friction losses; 3 - power over the surfaces of velocity discontinuity.

5.Conclusions

The method described in the present paper enables the determination of the total power in the rolling of bimetal with porous layer. For any given set of rolling conditions, variational parameter (a)can be computed using the minimum power method, and rolling force and roll torque can be computed using the energy method. A range of computations has been carried out to illustrate the effect of variation of the different rolling parameters on the h_M /h_T ratio, as well as on the rolling force and the roll torque. The accuracy of the present method has been confirmed experimentally.

References

[1]. Dyja, H. , On the theory of the process of hot rolling of bimetal plate and sheet, *Journal of Mechanical Working Technology*, 1983, 309

[2]. Petrea, I., Researches regarding the rolling modelation of bimetal with porous layer, *National Conference of Metallurgy and Materials Science*, 2001, 442-444.

MODELLING OF THE FLOW AND DEFORMATION FIELDS AT THE PROFILES ROLLING BY FIELD LINES METHOD

Nicolae CANANAU, Ionel PETREA, Gheorghe COROBETE

Universitatea „Dunarea de Jos" Galati
e-mail: nicolae.cananau@ugal.ro

ABSTRACT

This paper presents a method for modeling of the rolling process based at the deformable continuous medium mechanics, the theory of field lines. The rolling of the profiles and plates may be evaluated as the plane strain state process. Using the equations of the continuous medium and the initial conditions and the limits conditions we solved the speed field, the strain rate field, the strain field. Applying an adequate computation program we obtained the values of the field factors of modeling process. The results are showed into this paper.

KEYWORDS: rolling process, field lines, continuous medium

1. Introduction

At the rolling of plates and profiles the deformation in a direction may be neglected, respectively in the lateral direction (Figure 1).

The lateral dimension of body (h_{i-1}) is appropriated of the dimension b_i of the deformation form of the rolls. Thus, the strain in this direction may be neglected [2].

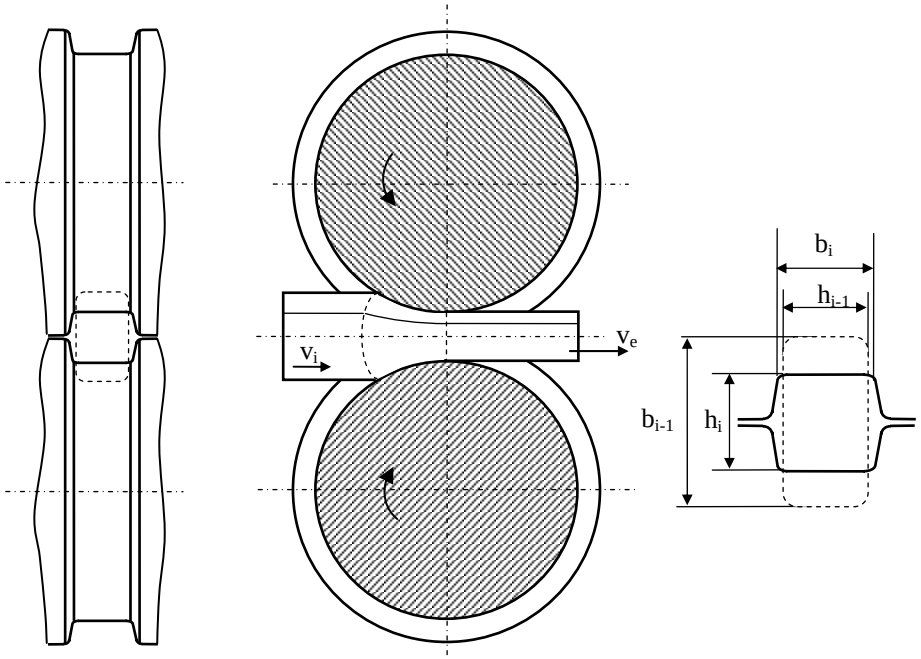

Fig. 1 *Scheme of profile rolling process and deformation conditions*

We consider the rolled body as a deformable continuous medium. The volume occupied by the continuous medium, at the really moment is divided in three domains (Figure 2) [2,4,6]:

- the domain D_1 before the entrance of medium between the rolls (rigid plastic medium),

- the domain D_2, deformation domain, the medium is between the rolls. In this domain is developed the deformation process,
- the domain D_3 at the exit of material between the rolls (rigid plastic, too).

2. Defining of the field line equation

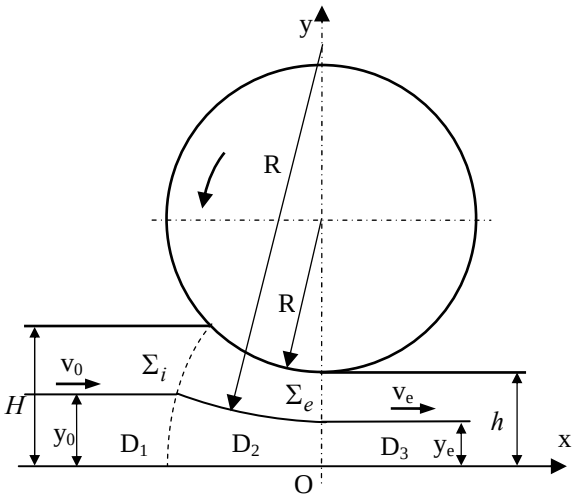

Fig. 2 *The deformation domain and field line*

In the conditions of a stationary regime of the continuous medium flow the field lines coincide to the movement trajectories of the material particles. In the Figure 2 we represent the field line of the material particles that are situated to y_0 of the axe Ox, the symmetry axe of the body.

The equations of the current line of parameter y_0 are so defined:

$$\begin{array}{l} y = y_0 \text{ , in } D_1 \\ \text{respectively,} \\ y = y_e \text{ , in } D_3 \end{array} \qquad (1)$$

In the deformation domain D_2 the field line may be expressed by circle arch what satisfy the following conditions:

- circle center is on the axe Oy, the axe of the rolling cylinder centers,
- the circle radius respects the conditions:

$$R(y) = R = \begin{cases} R_0 & \text{for} \quad y = H \\ \infty & \text{for} \quad y = 0 \end{cases} \qquad (2)$$

H is the initial semi-thickness of the body.

The conditions (2) are accomplished by the equation [2]:

$$R(y) = \frac{H}{y_0} \cdot R_0 \qquad (3)$$

Consequently the field line equation is:

$$x^2 + \left(y - \frac{H}{y_0} R_0 - y_e \right)^2 = R^2 \qquad (4)$$

We admit the hypothesis of the proportional repartitions of the deformation to the thickness of body. In this condition we have:

$$y_e = y_0 \cdot \frac{h}{H}$$

and (4) becomes [6]:

$$x^2 + \left(y - \frac{H}{y_0} R_0 - y_0 \frac{h}{H} \right)^2 - \left(\frac{H}{y_0} \cdot R_0 \right)^2 = 0 \qquad (5)$$

The surface Σ_i is defined by the points of coordinates:

$$\begin{array}{l} y = y_0 \\ x = x_0 = -\sqrt{\left(\frac{H}{y_0} \cdot R_0 \right)^2 - \left(y_0 - \frac{H}{y_0} R_0 - y_0 \frac{h}{H} \right)^2} \end{array} \qquad (6)$$

3. Defining of the speed field

In the D_1 and D_3 domains we have:

$$\begin{array}{ll} v_x = v_i & v_x = v_e \\ v_y = 0 & v_y = 0 \end{array} \text{ and , respectively}$$

In the domain D_2 we have the following conditions [1,3,5]:

- the continuity equation to incompressible medium $\quad y = y_0 \text{ , in } D_1$

$$div(\vec{v}) = 0$$

For plain strain state we have:

$$\frac{\partial v_x}{\partial x} + \frac{\partial v_y}{\partial y} = 0 \qquad (7)$$

- the field line equation:

$$\frac{dx}{v_x} = \frac{dy}{v_y} \qquad (8)$$

From (5), (7) and (8) we obtain:

$$\frac{v_x}{v_y} = -\frac{y - a}{x} \qquad (9)$$

We denote

$$a = \frac{H}{y_0} R_0 + y_0 \frac{h}{H}$$

Then we have:

$$\frac{v_x}{v_y} = -\frac{y-a}{x} \tag{10}$$

and

$$v = v_x\sqrt{1+\left(\frac{x}{y-a}\right)^2} \tag{11}$$

The continuity condition is defined by the constant material flux in the long of the field line.

We consider the elementary volume in the long of the field line (fig.3) [4,6].

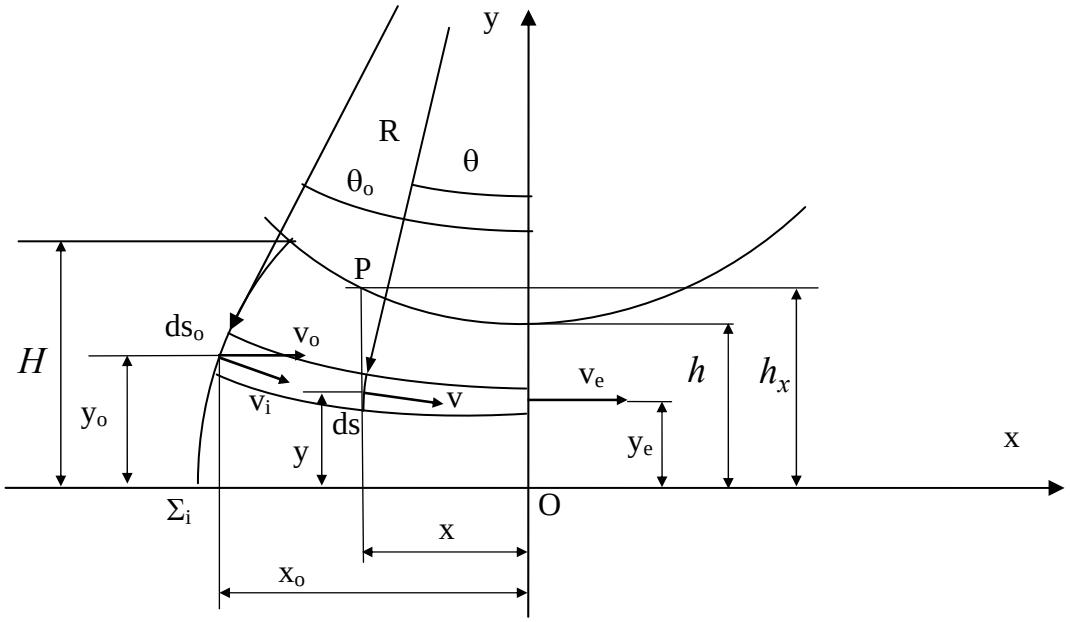

Fig. 3 *Scheme for establishing of continuity equation*

At the elementary surface $b \times ds_o$ of the surface Σ_i a discontinuity of material particle speed is appeared. Thus, we have:

$$\begin{aligned} v_i &= v_o \cdot \cos\theta_o \\ \Delta v &= v_t = v_o \cdot \sin\theta_o \end{aligned} \tag{12}$$

where

$$\theta_o = \arcsin\left(\frac{x_o}{R}\right) = \arcsin\left(\frac{x_o \cdot y_o}{H \cdot R_o}\right) \tag{13}$$

Applying the hypothesis of the plane strain state we may write:

$$v_i \cdot ds_o = v \cdot ds = v_e \cdot ds_e$$

At the same time having the hypothesis of uniform repartition of the deformation on the thickness of the body we have:

$$v = v_e \cdot \frac{h}{h_x} \tag{14}$$

In this relation we have h_x the thickness of the body according to coordinate x of the point of the field line and v_e is the speed of material particle at the exit from the deformation domain.

We have:

$$h_x = R_o + h - \sqrt{R_o^2 - x^2} \tag{15}$$

and

$$v_e = v_i \cdot \frac{H}{h} \tag{16}$$

Using the relations (10), (11), (14 and (15) we obtain:

$$v_x = v_e \cdot \frac{h}{a_o - \sqrt{R_o^2 - x^2}} \cdot \frac{1}{\sqrt{1+\left(\frac{x}{y-a}\right)^2}}$$

$$v_y = v_e \cdot \frac{h}{a_o - \sqrt{R_o^2 - x^2}} \cdot \frac{1}{\sqrt{1+\left(\frac{x}{y-a}\right)^2}} \cdot \frac{x}{y-a} \qquad (17)$$

4. Defined of the strain rate field

The components of the strain rate tensor are defined by equations:

$$\dot{\varepsilon}_{xx} = \frac{\partial v_x}{\partial x}; \quad \dot{\varepsilon}_{yy} = \frac{\partial v_y}{\partial y}; \quad \dot{\varepsilon}_{xy} = \frac{1}{2}\left(\frac{\partial v_x}{\partial y} + \frac{\partial v_y}{\partial x}\right)$$

Using the function (17) for the speed components we obtain:

$$\dot{\varepsilon}_{xx} = -\dot{\varepsilon}_{yy} = -\frac{v_e \cdot h \cdot x}{(a_o - \sqrt{R_o^2 - x^2})\sqrt{1+\left(\frac{x}{y-a}\right)^2}}\left[\frac{1}{(y-a)^2 \cdot \left[1+\left(\frac{x}{y-a}\right)^2\right]} + \frac{1}{(a_o - \sqrt{R_o^2 - x^2}) \cdot \sqrt{R_o^2 - x^2}}\right] \qquad (18)$$

$$\dot{\varepsilon}_{xy} = \frac{v_e \cdot h}{2(a_o - \sqrt{R_o^2 - x^2})(y-a)\sqrt{1+\left(\frac{x}{y-a}\right)^2}}\left[\frac{2x^2}{(y-a)^2 \cdot \left[1+\left(\frac{x}{y-a}\right)^2\right]} + \frac{x^2}{\sqrt{R_o^2 - x^2}} + 1\right] \qquad (19)$$

The strain rate intensity is defined by the relation [1]:

$$\bar{\dot{\varepsilon}} = \frac{2}{3}\sqrt{\dot{\varepsilon}_{xx}^2 + \dot{\varepsilon}_{yy}^2 + 2\dot{\varepsilon}_{xy}^2} \qquad (20)$$

For the numerical calculus we use the following normalized coordinates:

$$\eta = \frac{x}{x_o} \quad \text{respectively,} \quad \varphi = \frac{y_o}{H} \qquad (21)$$

and obtain:

$$v_x = v_e \cdot \frac{h}{a_o - \sqrt{R_o^2 - (\eta x_o)^2}} \cdot \frac{1}{\sqrt{1+\left(\frac{\eta x_o}{y(\eta)-a}\right)^2}}$$

$$v_y = v_e \cdot \frac{h}{a_o - \sqrt{R_o^2 - (\eta x_o)^2}} \cdot \frac{1}{\sqrt{1+\left(\frac{\eta x_o}{y(\eta)-a}\right)^2}} \cdot \frac{\eta x_o}{y(\eta)-a} \qquad (22)$$

$$\dot{\varepsilon}_{xx} = -\dot{\varepsilon}_{yy} = -\frac{v_e \cdot h \cdot \eta \cdot x}{(a_o - \sqrt{R_o^2 - (\eta x)^2})\sqrt{1+\left(\frac{\eta x}{y-a}\right)^2}}\left[\frac{1}{(y-a)^2 \cdot \left[1+\left(\frac{\eta x}{y-a}\right)^2\right]} + \right.$$
$$\left. + \frac{1}{(a_o - \sqrt{R_o^2 - (\eta x)^2}) \cdot \sqrt{R_o^2 - (\eta x)^2}}\right] \quad (23)$$

$$\dot{\varepsilon}_{xy} = \frac{v_e \cdot h}{2(a_o - \sqrt{R_o^2 - (\eta x)^2})(y-a)\sqrt{1+\left(\frac{\eta x}{y-a}\right)^2}}\left[\frac{2(\eta x)^2}{(y-a)^2 \cdot \left[1+\left(\frac{\eta x}{y-a}\right)^2\right]} + \right.$$
$$\left. + \frac{(\eta x)^2}{\sqrt{R_o^2 - (\eta x)^2}} + 1\right] \quad (24)$$

The field of strain intensity is defined by the expression [4]:

$$\bar{\varepsilon} = \int_0^t \bar{\dot{\varepsilon}} \cdot dt \quad (25)$$

For the numerical solve we will use the following principle (fig.4):

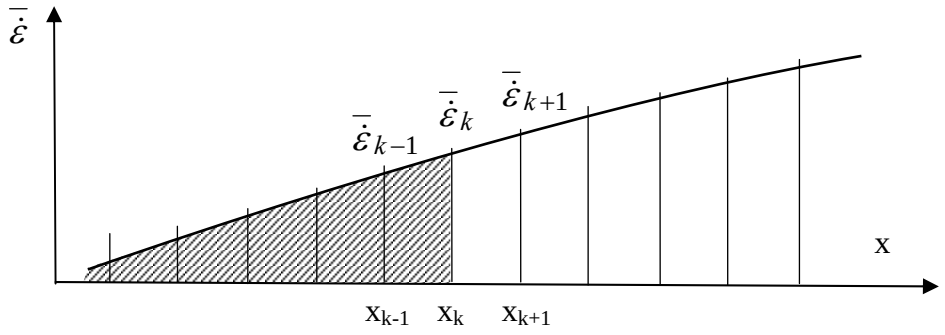

Fig. 4 *The calculus scheme of the strain intensity*

We defined the time differential as:

$$dt = \frac{dx}{v_x}$$

The numerical expression of the equation (25) is:

$$\bar{\varepsilon}_k = \bar{\varepsilon}_{k-1} + \left(\bar{\dot{\varepsilon}}_{k-1} + \bar{\dot{\varepsilon}}_k\right) \cdot \frac{x_k - x_{k-1}}{v_{x_k} + v_{x_{k-1}}} \quad (26)$$

In this expression the index k is defined in function of the index i as $k=n-i$, where i is the division operator in the long of the field line ($i=1,2,...,n$).

For initialization of the values of $\bar{\varepsilon}$ we consider what at the $k=0$, respectively, $i=n$, that is in the point of surface Σ_i the deformation is defined by the rotation of speed vector of angle θ_o.

Thus the initial strain is:

$$\bar{\varepsilon}_0 = \mathrm{tg}\,\theta_0 \quad (27)$$

Using the calculus algorithm described above we developed a computation program. The results of the calculus program we will present in the future paper.

5. Conclusions

The solving of the deformation process is possible using various methods. The field (or flow) line is one of these.

First we must defined clearly the domain that, at the real moment, is occupied of the body and the initial and limit conditions. The body is considered as deformable continuous medium. Then, we must define the equation of the flow line.

Using the equations of the mechanics of the deformable continuous medium, applying the initial conditions and the conditions at the limits we obtained, in the analytical form, the expressions of the components of the speed, and, derived by these, the components of the strain rate tensor.

If the components of strain rate tensor are defined, that is the field of strain rate tensor is defined, we can calculate the strain rate intensity, and finally, the strain intensity. Thus the analyze of cinematic process is solved.

From this level we can develop the analyze of process dynamic for establishing the data of the evaluation of the rolling process. The solving of this action we will show in the next paper.

References

[1] Moussy F., Franciosi P. *Physique et mecanique de la mise en forme des meteaux. Presses du CNRS,* Paris, 1990, ISBN 2-87682-023-4

[2] Dumitrescu A.T. *Contributii la modelarea laminarii in calibre.* Teza de doctorat, Institutul Politehnic Bucuresti, 1986.

[3] Adrian M., Badea S. *Bazele teoretice ale proceselor de deformare plastica*. Editura tehnica, Bucuresti, 1983.

[4] Cananau N. *Teoria deformarii plastice.* Universitatea Dunarea de Jos din Galati, vol.2, 1995.

[5] Dragan I. T*ehnologia deformarii plastice*. Editura Didactica si Pedagogica, Bucuresti, 1976.

[6] Corobete G. C*ontributii la cercetarea procesului de laminare a sarmelor din otel cu caracteristici mecanice superioare*. Referat de doctorat, Universitatea Dunarea de Jos din Galati, 2006.

THE ACTIONNARY SYSTEM OF THE CONTINNOUS DISCHARGE FURNACE FROM L.T.G -1. MITTAL STEEL

Stefan DRAGOMIR, Beatrice TUDOR, Marian BORDEI

"Dunarea de Jos"University of Galati,
email: doromir@email.ro

ABSTRACT

In this study the authors made a systematically research about the actionnary system at the continuous discharge heating furnace. It take in account the possibility to use a new material, with most good wear resistance, for the knuckles of this system. An anti-friction alloy containing 87% Sn, 15% Sl and Cu is proposed for the inner surface of the knuckle is used.

This material increase about 30% wear resistance while the friction coefficient decreases).

KEYWORDS: knuckle, heating furnace, hydraulic installation.

1. Introduction

The actionnary mechanism has two beams with independence moving, who determine the deplacement of slabs with constant speed.

The constant speed is necessary to realized a good heating treatment of thick iron plates.

The cyclogrames of moving into the heating furnace are realized with hydraulic rotary or linear engines.

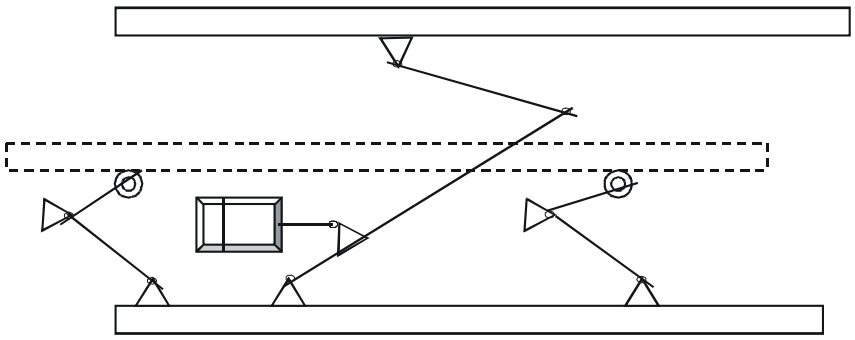

Fig.1. *The actionnary sistem of continnous discharge heating furnace*

The research of ondulatory phenomena are based wave method who study the transitory processes into the pipes.

We note with:

l – the length of pipe between the pressure source and cylinder;

F- piston force; $p_p(t)$ – the pressure on the piston;

V(l.t) – the flow speed at the pipe end, near cylinder;

The continuity equation in the connection point between cylinder and pipe is :

$$v(l,t) = \Omega\, v_p(t)$$

The condition for the stationary piston :

$$v(x,0) = 0 \; ; \; v_p(0) = 0$$

$$p(x,0) = p_0 ; p_p(0) = p_0$$

When the weaves are moving into the pipe by similitude we can describe the facts by partials derivations (N.E. Jukovsky) :

$$\frac{\partial p}{\partial x} = -\rho_0 \frac{\partial v}{\partial t} \qquad (1)$$

$$E \frac{\partial v}{\partial x} = -\frac{\partial p}{\partial t}$$

The sign "-" is considered in opposed moving direction for piston. After the integration of wave equations result :

$$p(x,t) - p_0 = \omega[\varphi(x - ct) + \psi(x + ct)] \qquad (2)$$

$$v(x,t) = \varphi(x,ct) - \psi(x + ct)$$

p_0 is the initially pressure into the pipe.

$$\omega = \sqrt{\rho_0 \cdot E} \qquad (3)$$

ω is a proportionally coefficient between the grow up the pressure and the grow up of flow.

$$c = \sqrt{E / \rho_0} \qquad (4)$$

c is the proportion speed of elastic wave disturbation
E is Young modules
ρ_0= flow density

$\varphi(x - ct)$- describe the propagation of direct wave process because of perturbatory element
$\psi(x + ct)$- describe the propagation precise of inverse wave.

The values of pressure and flow speed at the end of pipe for x=e are :

$$p(l,t) - p_0 = \omega[\varphi(l = ct) + (l + ct)] \qquad (5)$$

$$v(l,t) = \varphi(l - ct) - \psi(l + ct)$$

but:

$$v(l,t) = \Omega \cdot v_p(t)$$

result :

$$\psi(l + ct) = \varphi(l - ct) - \Omega \cdot v_p(t) \quad (6)$$

$$p(l,t) - p_0 = \omega[2\varphi(l - ct) - \Omega \cdot v_p(t)] \qquad (7)$$

$$\varphi(l - ct) = \frac{p_d(l,t) - p_0}{\omega} \qquad (8)$$

p_d is direct pressure in the piston.
From (7) and (8) result :

$$p(l,t) - p_0 = 2[p_d(l,t) - p_0] - \omega\Omega v_p(t) \qquad (9)$$

We consider that the pressure at the end of pipe is equal with cylinder pressure :

$$p(l,t) = p_p(t) \qquad (10)$$

We replace that relation in (9) and we obtain the law of changer pressure into the cylinder :

$$p_p(t) - p_0 = 2[p_d(l,t) - p_0] - \omega \cdot \Omega \cdot v_p(t) \qquad (11)$$

We can say : that the piston is nearly the direct wave and the grow up of the pressure in the cylinder is equal with double value of grow up for the direct wave pressure.

With the grow up of speed piston upper a precisian value, we see that the really piston pressure ,is less that initially pressure.

If the piston speed is in continuous grow up the pressure into the cylinder can decrease at atmospheric pressure value.

At the grow up of "Ω", the pressure nearly piston decrease very quick.

After the end of displacement effect, the pressure into the cylinder, decrease like a sinusoidal low.

The modification of the pressure and flow speed into the length of the pipe can be simulate with the relation presented in this work.

The increased pressure of contact, superior to limit mentioned above, determines the creation of plastically deformed zone . This zone becomes larger along with the increase of contact. The plastic deformation are integrated in an elastically deformed volume. This state of deformation is called elastoplastic.

The continuous increase of the contact pressure will determine an increase of the plastic zone and advancing toward surface.

The contact with or without sliding foes not significantly alter the above observation in case of single movement of the knuckle body over a contact spot. In the next step of passing , even a first step movement the elasticity is unlimited, the rezidual stress that are generated , will make possible the increase of the contact pressure.

This will lead to elastic deformation as well / a phenomenon called shakedown. The contact pressure should not be surpassed if we expected to continue having elastic deformations.

The elastic deformations in the surface of the contact parts cause modifications of the hertzian distribution of the pressure and provoke, under certain circumstances, among other, fissures that can lead to failure by pitting.

For the knuckles of the sustaining cylinders (chart1)-for which the maximum pressure in the knuckle is about $500x10^5 N/m^2$ = the energy losses caused by friction amount to 40-50% of the total amount of energy consumed. In the case of hydrodynamic knuckles with friction the oil supply is done by an overpressure of 0,1-0,25 MPa correlated with a minimal rotation velocity of the axle which should be higher than the critical rotation velocity which will ensure the oil flux.

The thickness of the oil stratum in the knuckle varies due to the rotation velocity and the charge, determining the thickness of the rolled iron plate.

2.The material used for obtaining the knuckle with a good coefficient of wear

In the knuckles of our system, who is a rotating sliding surface is represented by the outer surface of a spider which is fixed on the conic shaft.

This knuckle is made of a steel alloy which is non-magnetic, wear-resistant, with a low carbon content.

The stratum of anti-friction for the knuckle it is a material who it is was obtained by centrifugal casting, using three combinations of the constituents Sn, Sb, Cu (of which it is made) and then the material samples were tested for wear for three weeks.

The three types of alloys used were:

Table 1

N°	**Sn%**	**Sb%**	**Cu%**	**The quantity lost in the wear test at the end of the trial period**
1	65÷67	16÷20	15÷17	30%-35%
2	78÷80	7÷8	14-12	18%-20%
3*	85÷88	6÷7	8÷9	11%-12%

The test-pieces of all the three alloys were cast and then tested to find out the wear resistance, while exposed to shock and humid atmosphere containing abrasive particles.

The best results were obtained for the third group of test-pieces : after weighing, a loss of 11-12% of the original weight was registered after a three week trial period.

A contrastive representation of the microstructure of the material in the first and third group of test-pieces is given in fig 2.

Fig.2

3.Conclusions

In the superficial layer from the interior of the knuckle the wear and the fatigue stresses determine damaging in functionary.

The presence in superficial layers of different nature intruders and their concentration in certain dislocation density absence or microcracks than the rest of material surface.

The slide strips produced by the deformation of areas in wear or fatigue processes are also characterised by great dislocation .

These phenomenon are conditioning the energy levels of surfaces and respectively their strength.

The researches showed that the material containing 85-88% Sn, 6-7% Sb, and 8-9% Cu had the best results for the wear, tests in an abrasive atmosphere.

This material was recommended for the knuckle on the basis of the results of the test. By using of this material is improving with 30% the using characteristic of this knuckle an a less friction coefficient inside them :

A sum of .8500$ knuckle/jack was saved by using this material to make the spider/jacks in our country instead of importing the unit.

The knowledge of the maximal values of the pressure can help at the dimensioning of the all actionnary system looking at the resistance of hydraulic shock.

The application of operationally calculus is used research the waving phenomena into the hydraulic installation.

The differentially equation with partial derivations, integrated like wave equation by help of "φ" function (direct wave) and "ψ" function (reflected wave) for different phases of actionnary mechanism.

References

[1].Pitigoi B. *Fenomene tranzitorii in actionarea mecanismelor din metalurgie* –Revista met. 36/1994
[2].Mateescu C. – *Actionari metalurgice* EDP.Buc. 1992
[3].Oprescu, Grosu – *Utilaje metalurgice* EDP.Buc. 1994
[4].Oprescu I. – *Utilajul şi proiectarea sectoarelor metalurgice,* E.D.P.,Bucureşti,1988
[5].Werner W.- *Siguranţa în funcţionare şi întreţinere nr.17,* Neue Hutte,1992
[6].Lindley R., Higggins P.E.-*Maintenance Engineering* Hill Book,Company,N.Y.1997
[7].Cheng P.-*Control of Maintenance Cost Industrial,* Ed.Modern Surrey, U.K.,1998
[8].Miyoshi H. Tsubuku, T, *Instantaneous deformation of subsurface layer in rolling contact,* In proceedings of the Japan International Tribology Conference, Nagoya, 1990.

ESTABLISHING OF ROLLING - FRICTION COEFFICIENT, FOR HERTZIAN CONTACTS BETWEEN STEEL BALLS AND DIFFERENT KINDS OF THERMOCHEMICAL TREATED STEEL SURFACES

Daniel MUNTEANU

Transilvania University of Brasov
muntean.d@unitbv.ro

ABSTRACT

It is known that for the ball displacement guide paths, the necessary start-moving force of the mobile half-couple is higher than the displacement-motion keeps force.Within the frame of this work, it has been designed and manufactured special pairs of rolling-motion couples, made from 5115AISI case-hardening steel and 4140 AISI heat treatable steel. After that, some of them (in the first blend) were carburized (at 925^{o}C) and others carbonitrided (at 890^{o}C) in gaseous conditions. The rolling - friction tests supposed different arrangements of the half-couples and balls. In order to establish the rolling - friction coefficients for all the thermochemical treated surfaces, a typical method such as the inclined plane slope, was used. Taking into account each kind of superficial treatment category, generally, it has been observed smaller values of equivalent friction coefficient for the carburized surfaces in comparison with the carbonitrided ones. For low - temperature superficial treatments category, a little bit smaller values of equivalent friction coefficient for the nitocarburized surfaces in comparison with the nitrided ones were obtained. The non-treated surfaces have been characterized, in all the cases, by minimum friction coefficient values in comparison with the treated ones. In comparison, the results clearly show a difference between the equivalent friction coefficient values registered for carburized/carbonitrided and nitrided/nitrocarburized surfaces. Thus, in the first case, these values were smaller than in the second case.

KEYWORDS: Steel, Carburizing, Nitriding, Rolling-friction coefficient

1. Introduction

There are several practical applications, including bearings and gears, in which rolling or rolling-sliding punctiform or line contacts are developed. In mechanics, this kind of contacts belongs to the hertzian contacts category. Even for constant loads, the rolling motion produces a variable superficial state of efforts characterized by normal and tangential - shear stresses under impact. The intricacy of researching this kind of contacts is further increased by the presence of lubricant [1]. Thus, for the study it must be considered several factors such as: the load, the speed, the rolling - sliding ratio (if the sliding exists), the lubricant presence and quality, the surface topography, etc.

Owing to the high temperature of carburizing, which could lead to the grain's increasing and deformations appearance, in certain cases the carburizing process has been replaced with

Generally, contact micro surfaces and higher pressures in the contact zones characterize the hertzian rolling contact cases. Therefore, surface deformations must be considered. The appearance and evolution of surface fatigue phenomena have been theoretically explained in literature using the *space stress state condition* and the models of Hertz and Boussinesq [1,2,3].

In this kind of contacts, wear process of hardened steel surfaces usually occurs in a mild way, in comparison with the unhardened surfaces. For instance, in the case of ball - bearings manufacturing, generally are used two steel categories: hypereutectoid steels with chromium and low carbon alloyed steels for carburizing and carbonitriding. Many practical cases, especially for impact stress conditions, showed better mechanical behaviour for bearings manufactured from carburized steels.

nitrocarburizing. Thus, the process temperature became lower.

The steels for bearing manufacturing, especially in the rolling contact surfaces, have to be able to support the strong alternating stresses, which are caused by the compressive forces between balls (rolls) and rolling guide paths.

The hertzian contacts are characterized by the appearance of a typical "material wave" on the rolling guide path, in front of the rolling body (ball or roll) [1, 2, 3, 4]. Depending of the rolling - surface qualities and rolling body dimensions too, this wave could be more or less important in size. Its appearance has an important role in rolling motion because it leads to a rolling - friction moment developing. This moment is in opposite with the rolling motion and plays an important role, not only for the motion but also for the start - moving.

The paper tries to establish an equivalent friction coefficient value for different types of hertzian contacts (ball on carburized, carbonitrided, nitrided and nitrocarburized plane steel surface) for rolling start - moving conditions.

2. Theoretical and experimental background

The rolling - friction process is characterized through a typical friction torque which gives a specific rolling - friction moment M_{rf}. Figure 1 presents a schematic arrangement of a ball rolling motion on a plane surface.

Very often, the practical physical explanations of the rolling - friction process takes into account the plastic deformations appearance in the contact zone [1]. If we consider a rolling contact in which the ball is harder than the rolling plane surface, on the contact zone will appear an indentation cup.

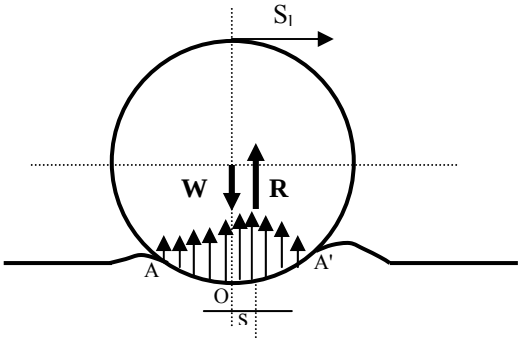

Fig. 1 *Schematic arrangement of a hertzian punctual contact, in plane coordinates; W – ball weight, R – result of typical force-reaction distribution on the contact zone AA', s – the moment arm, S_l – the ball linear speed.*

This phenomenon leads to a specific material accumulation, not only in front of the contact (where is more important) but also behind the contact (figure 1).

Thus, the reaction force R on the AOA' section is given by infinity of elementary forces. The general force - moment of these elementary forces in relate of the theoretical contact point O is the rolling friction moment M_{rf}. These elementary reaction forces are not symmetrically distributed. Thus, in front of the contact, where more material is concentrated, the reaction forces are stronger. Owing to this reason, the elementary reaction forces result, R, give the moment M_{rf}, which is in opposite with the rolling sense of the ball [1,4]. The practical researches showed that for equilibrium state, the value of this moment must be lower than a certain maximum value, as follows:

$$M_{rf} \leq s \cdot R \qquad (1)$$

In relation (1), s represents the rolling - fri coefficient. In comparison with the sliding friction coefficient μ which is dimensionless, the rolling - friction coefficient s has a little dimension, very difficult to measure. It represents the maximum displacement distance of the normal reaction R support relatively to the theoretic contact point O (fig. 1).

For static equilibrium conditions, when the rolling body (ball or role) is not moving and the rolling plane surface is in a perfect horizontal position, the accumulation of material is symmetrically distributed in front and behind the ball. However, for very little inclinations of the plane support, at rolling initiation, because rolling - friction coefficient s is difficult for measure, the friction phenomenon can be evaluated considering *the equivalent (conventional) sliding - friction coefficient μ_0 at start* [5].

Thus, it is known that for the ball displacement guide paths, the necessary start-moving force of the mobile half-couple is bigger than the force, which keeps the displacement-motion. The start-moving force is equal to the normal load $W = R$ multiplied by the equivalent friction coefficient μ_0.

Thus, in order to establish the static friction coefficients for all the samples, a typical method such as the inclined plane slope was used. This system [5] may estimate the friction coefficient value, based on some typical linear size measurements. Thus, correlation between the friction angle α and the

$$tg\alpha = \mu \qquad (2)$$

friction coefficient μ is:

At the same time, a plane inclines the friction couple that is in a rest state, with variable angles, until the sliding phenomenon appears in the couple. The angular value $\alpha_{limit} = \alpha_0$ where the sliding

appears, is in direct correlation with the static sliding - friction coefficient μ_0 at start according with:

$$\mu_0 = tg\alpha_0 \quad (3)$$

3. Experimental arrangements

In order to estimate the equivalent friction coefficient, it has been designed and manufactured special pairs of rolling-motion couples, from E 410 Bohler, Austrian designation, (≈ 5115AISI) case-hardening steel with the following chemical composition: 0.17%C, 0.30%Si, 1.20%Mn, 0.90%Cr and V 320 Bohler, Austrian designation, (≈ 4140AISI) heat-treatable steel with the following chemical composition: 0.41%C, 0.30%Si, 0.70%Mn, 1.10%Cr, 0.20%Mo.

Each half-couple has a parallelepiped form, with 141x100x15 mm. Some of these half-couples have plane (flat) friction surfaces and others have by threes identically longitudinal V-guide paths on the rolling - friction surface.

The relative motion between the half-couples has been achieved with three identically balls, and the point contacts in three different contact zones. The rolling - friction tests supposed different arrangements of the half-couples and balls. Through different changes of the half-couple (plate), each lower plate will become consecutively fixed plate and each upper plate will become mobile plate. Thus, the role of the lower plate and upper plate is replaceable. The upper plate is moving in relate of the lower one by means of bearing balls with different sizes. At each test, all the balls, which form the couple, have to be the same sizes. The minimum number of balls is three, of which two on the edge paths and one on the center path.

It has been used different sizes of identically balls, with 8, 10, 12, 15.9, 18, 19.8, 22, 25 and 26 mm in diameter, made from high speed steel (AISI M2) hardened and three times tempered, characterized by 64 HRC and R_a = 0,06 μm. Each rolling-friction couple was fixed, in a perfect horizontal position of start, on the plateau of a special tribosystem.

In order to establish the rolling - friction coefficients for all the thermochemical treated surfaces, a typical method such as the inclined plane slope, was used. Help of a variable-dropping plane inclines the rolling couple (which is in a horizontally-rest state) the rolling phenomenon appearances in the couple. The angular value $\alpha_{limit} = \alpha_0$ where the rolling appears, is in direct correlation with the equivalent sliding - friction coefficient μ_0 at start.

After that, the samples manufactured from E 410 steel were carburized (at 920°C) and others were carbonitrided (at 860°C) in gaseous conditions, using an endothermic atmosphere completed by 8% CH_4 for carburizing and an endothermic atmosphere completed by 8% CH_4 and 5% NH_3 for carbonitriding. In both cases, the carbon potential in the furnace chamber was kept at 0,9% and the maintaining period at the treatment temperature 7 hours. After the thermochemical treatments, the samples were first case hardened (from 830°C) using oil like quenching agent, and second low tempered (at 180°C).

At the same time, the samples manufactured from V 320 steel were hardened (from 840°C) using oil like quenching agent, and high tempered (at 585°C). After that, the samples were polished and it has been a roughness of Ra = 0.1μm.

Some of samples were gas - nitrided (at 520°C, for 15 hours in $NH_3 + N_2$ atmosphere with ammonia dissociation grade α = 25%) and others were gas - nitrocarburized (at 560°C, for 7 hours in endothermic gas + NH_3 atmosphere).

The hardness values were estimated using a special device Akashi MVK 4-E type, with 0,05 daN load. The roughness values of the surfaces were also established, based on profilometer method, using a Tallysurf 4 (Taylor-Hobson) type profilometer.

4. Experimental results and discussion

Table 1 presents the average experimental values from roughness and Vickers hardness for all the samples manufactured from E 410 case-hardening steel, after removing of extreme values for each kind of measurement.

Table 1.*Roughness and Hardness values of sample surfaces (E 410 case-hardening steel).*

Sample surfaces	Roughness values R_a [μm]	Hardness $HV_{0.050}$
Untreated	0.43	238
Carburized	0.32	816
Carbonitrided	0.36	832

The same characteristics are shown in table 2 for the samples manufactured from V 320 heat-treatable steel.

Table 2. *Roughness and Hardness values of sample surfaces (V 320 heat-treatable steel).*

Sample surfaces	Roughness values R_a[μm]	Hardness $HV_{0.050}$
Just hardened and tempered (+ polished)	0.11	238
Nitrided	0.48	756
Nitrocarburized	0.38	788

The rolling-friction coefficients established by the inclined plane slope method are shown in Table 3.

Table 3. *Average values of rolling - friction coefficient μ_0 for different kind of couples (A, B, C, D, E, F) and for different ball measurements.*

Balls diameter [mm]	**Average values of rolling - friction coefficient μ**					
	A	B	C	D	E	F
8	0.0021	0.0024	0.0021	0.0024	0.0023	0.0026
10	0.0019	0.0022	0.0020	0.0024	0.0022	0.0023
12	0.0020	0.0022	0.0021	0.0022	0.0022	0.0023
15.9	0.0020	0.0023	0.0023	0.0024	0.0023	0.0025
18	0.0022	0.0023	0.0022	0.0023	0.0024	0.0025
19.8	0.0019	0.0021	0.0022	0.0023	0.0023	0.0024
22	0.0016	0.0017	0.0017	0.0022	0.0019	0.0022
25	0.0014	0.0016	0.0015	0.0018	0.0017	0.0020
26	0.0013	0.0014	0.0014	0.0016	0.0014	0.0017

where A, B, C, D, E, F, G were the following couples:

A: Carburized half-couple with longitudinal V-guide paths on the rolling - friction surface (fixed) – Balls – Plane untreated half-couple;
B: Plane carburized half-couple (fixed) – Balls – Plane untreated half-couple;
C: Carbonitrided half-couple with longitudinal V-guide paths on the rolling (fixed) - friction surface – Balls – Plane untreated half-couple;
D: Plane carbonitrided half-couple (fixed) – Balls – Plane untreated half-couple;
E: Untreated half-couple with longitudinal V-guide paths on the rolling - friction surface (fixed) – Balls – Plane untreated half-couple;
F: Plane untreated half-couple (fixed) – Balls – Plane untreated half-couple.

For the nitrided and nitrocarburized samples, the rolling-friction coefficients established by the inclined plane slope method are shown in Table 4, where A', B', C', D', E', F', G' were the following couples:
A': Nitrided half-couple with longitudinal V-guide paths on the rolling - friction surface (fixed) – Balls – Plane untreated half-couple;
B': Plane nitrided half-couple (fixed) – Balls – Plane untreated half-couple;
C': Nitrocarburized half-couple with longitudinal V-guide paths on the rolling (fixed) - friction surface – Balls – Plane untreated half-couple;
D': Plane nitrocarburized half-couple (fixed) – Balls – Plane untreated half-couple;
E': Untreated half-couple with longitudinal V-guide paths on the rolling - friction surface (fixed) – Balls – Plane untreated half-couple;
F': Plane untreated half-couple (fixed) – Balls – Plane untreated half-couple.

Figures 4, 5 and 6 present, for carburized, carbonitrided and thermo-chemically untreated samples, the dependencies between rolling – friction coefficient and couples characterized through different ball sizes (three identical balls). The graphic dependencies denote, for all cases, that increasing the ball diameters in rolling – friction couples leads to a slightly decreasing of the friction coefficient values. Nevertheless, all friction tests revealed the same behaviour for a little tendency of increasing friction coefficient in the middle of ball sizes interval (e.g. 15,9 – 18 mm in diameter). This phenomenon is very difficult to explain but it is possible a little deviation from balls spherical shape in this interval.

For all three graphic represented cases, smaller friction coefficient values were observed for couples which in a half-couple is represented by V-guide paths on the rolling (fixed) - friction surface. This is very important if we are thinking that in these cases, the contact is produced in three points for each ball, two on the V-guide paths and one on the other plane half-couple. Anyway, this aspect could be appear due to the smaller width of the rolling paths in comparison with whole plane surfaces. Thus, the effect of front resistant wave could be reduced because it is developed only on the limited width.

Figures 7, 8 and 9 present, the same dependencies for nitrided, nitrocarburized and thermo-chemically untreated samples.

The graphic dependencies of these kinds of surfaces, denote that increasing the ball diameters in rolling – friction couples leads to a slightly decreasing of the friction coefficient values. Like for the first groups of samples (carburized and carbonitrided), it has been registered a little increasing friction coefficient in the middle of ball sizes interval (e.g. 15,9 – 18 mm in diameter).

In comparison, for nitrided and nitrocarburized surfaces, slightly lower values for friction coefficient were registered in the couple plane – balls – plane types. These results could conclude the importance of the guide paths during the rolling motion. The establishing of rolling-friction coefficient μ_0, lead to the conclusion that the lowest coefficient values generally characterize the carburized surfaces and the highest the untreated surfaces.

Table 4. *Average values of rolling - friction coefficient μ_0 for different kind of couples (A', B', C', D', E', F') and for different ball measurements.*

Balls diameter [mm]	Average values of rolling - friction coefficient μ					
	A'	B'	C'	D'	E'	F'
8	*0.0033*	0.0032	*0.0034*	0.0026	*0.0024*	0.0023
10	*0.0034*	0.0033	*0.0033*	0.0027	*0.0022*	0.0019
12	*0.0032*	0.0030	*0.0033*	0.0028	*0.0021*	0.0018
15.9	*0.0035*	0.0035	*0.0034*	0.0032	*0.0023*	0.0022
18	*0.0034*	0.0033	*0.0033*	0.0030	*0.0025*	0.0023
19.8	*0.0034*	0.0032	*0.0030*	0.0027	*0.0021*	0.0020
22	*0.0033*	0.0031	*0.0022*	0.0018	*0.0018*	0.0016
25	*0.0030*	0.0023	*0.0023*	0.0015	*0.0017*	0.0013
26	*0.0031*	0.0022	*0.0021*	0.0016	*0.0013*	0.0012

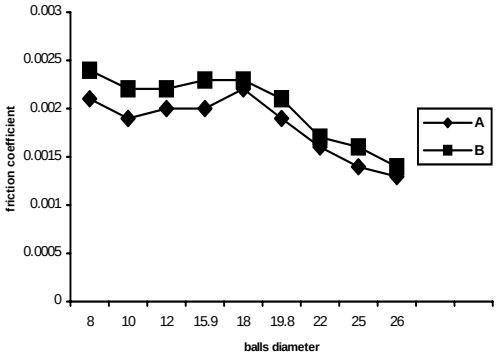

Fig. 4: *The rolling-friction coefficient μ_0 (average values) for different ball sizes. A: Carburized half-couple with longitudinal V-guide paths on the rolling - friction surface (fixed) – Balls – Plane untreated half-couple; B: Plane carburized half-couple (fixed) – Balls – Plane untreated half-couple;*

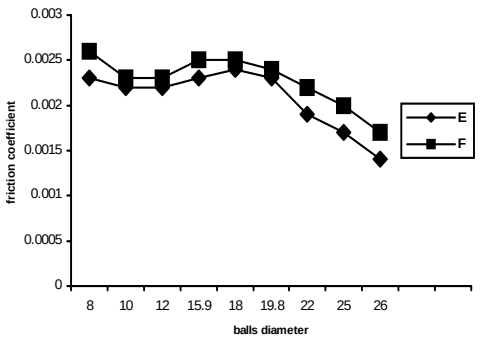

Fig. 6: *The rolling-friction coefficient μ_0 (average values) for different ball sizes. E: Untreated half-couple with longitudinal V-guide paths on the rolling - friction surface (fixed) – Balls – Plane untreated half-couple; F: Plane untreated half-couple (fixed) – Balls – Plane untreated half-couple.*

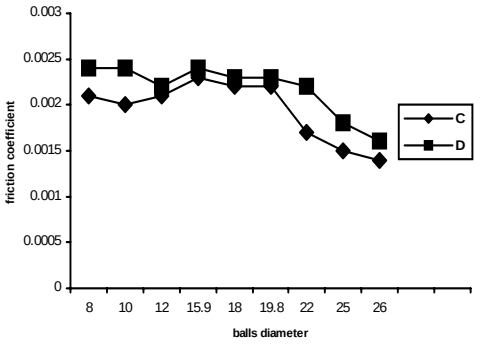

Fig. 5: *The rolling-friction coefficient μ_0 (average values) for different ball sizes. C: Carbonitrided half-couple with longitudinal V-guide paths on the rolling (fixed) - friction surface – Balls – Plane untreated half-couple; D: Plane carbonitrided half-couple (fixed) – Balls – Plane untreated half-couple;*

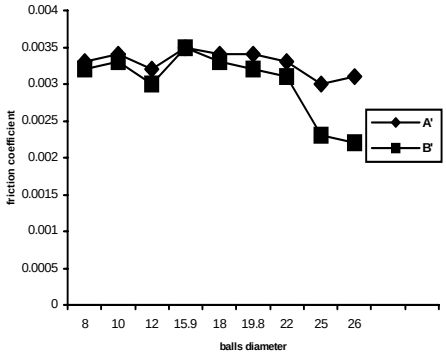

Fig. 7: *The rolling-friction coefficient μ_0 (average values) for different ball sizes. A': Nitrided half-couple with longitudinal V-guide paths on the rolling - friction surface (fixed) – Balls – Plane untreated half-couple; B': Plane nitrided half-couple (fixed) – Balls – Plane untreated half-couple;*

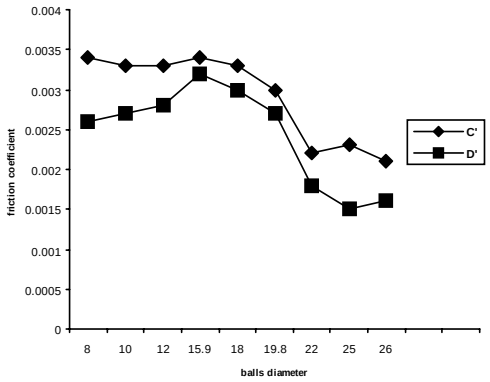

Fig. 8: *The rolling-friction coefficient μ_0 (average values) for different ball sizes. C': Nitocarburized half-couple with longitudinal V-guide paths on the rolling (fixed) - friction surface – Balls – Plane untreated half-couple; D': Plane nitrocarburized half-couple (fixed) – Balls – Plane untreated half-couple;*

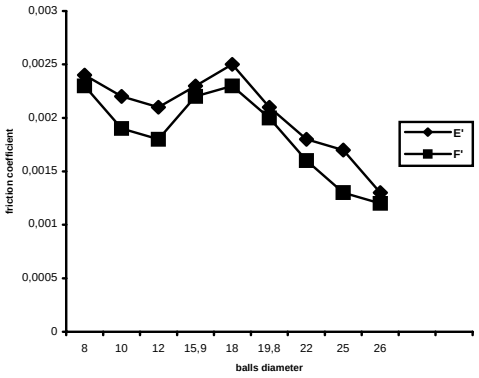

Fig. 9: *The rolling-friction coefficient μ_0 (average values) for different ball sizes. E': Untreated half-couple with longitudinal V-guide paths on the rolling - friction surface (fixed) – Balls – Plane untreated half-couple; F': Plane untreated half-couple (fixed) – Balls – Plane untreated half-couple.*

Referring to this, and according with roughness and hardness measurements from Table 3, it is very difficult to have a clear conclusion about the main influence on rolling-friction coefficient. Anyway, both surfaces (carburized and carbonitrided) are able to decrease the friction coefficient, maybe a little more the carburized ones, but the registered differences could appear owing the roughness differences (smaller in the case of carburized surfaces).

At the same time, both surface treatments achieved on the samples contribute to the superficial hardness enhancement and to the minimizing hertzian deformations on the rolling paths. For this reason, if we consider the surface deformations on the treated rolling paths almost the same, with increasing of ball diameters and weight too, the contact pressures become higher. These increased pressures are able to flattening the roughness and to start the balls earlier. At the same time, with increasing the surface hardness, the "material micro-wave" from the contact zone on the rolling path (in front of it, in the moving sense) becomes smaller and this aspect leads to an earlier ball start moment.

Regarding the rolling-friction coefficient μ_0 of nitrided and nitrocarburized samples, we can observe also almost the same values for all the cases. However, in this case, the high experiments precision revealed that the lowest coefficient values generally characterize the untreated surfaces and the highest the nitrided ones. (see Table 4). Anyway, both surfaces (nitrided and nitrocarburized) are able to increase the friction coefficient, maybe a little more the nitrided ones, but the registered differences could appear also owing to the roughness and hardness differences (smaller in the case of non-treated surfaces).

In comparison, the results clearly show a difference between the equivalent friction coefficient values registered for carburized/carbonitrided and nitrided/nitrocarburized surfaces. Thus, in the first case, these values were smaller than in the second case; this conclude that, besides roughness value, the compund zone developed on the top of nitrided/nitrocarburized surfaces increasing the rolling - friction coefficient. At the same time, the increased values of rolling-friction coefficient in these last cases (nitrided and nitrocarburized paths) could also appear owing to the little bit smaller values of hardness in comparison with carburized and carbonitrided ones.

5. Conclusions

Generally, it has been observed smaller values of equivalent rolling-friction coefficient for the carburized and carbonitrided samples in comparison with the nitrided and nitrocarburized ones..

Using longitudinal V-guide paths on the rolling - friction surfaces, for carburized and carbonitrided rolling surfaces, it could be reached friction conditions better then on the plane rolling – friction surfaces. In these cases, the untreated surfaces were characterized by friction coefficients higher than the treated ones.

In comparison, for nitrided and nitrocarburized rolling surfaces, using longitudinal V-guide paths on the rolling - friction surfaces it could be reached friction conditions lower then on the plane rolling – friction surfaces. Generally, for these cases, it hasve been observed the smallest values of equivalent friction coefficient for the non-treated

surfaces in comparison with the nitrided and nitrocarburized ones.

The minimum rolling-friction coefficient (at start) values were registered, in all the cases, when the contacts have been achieved with balls of maximum diameter (26 mm).

Regarding surfaces topography, carburizing seems to develop smaller roughness values. In fact, we could say that starting from the same untreated substrate roughness (R_a = 0.538 μm) both surface treatments lead to decreasing the final roughness. Anyway, the roughness decreasing after carburizing is a little higher than after carbonitriding, nitrocarburizing and nitriding. This could be contribute to a little decreasing of the friction coefficient and, if the final polishing is not taking into account (like in this work), this aspect is very important for some practical applications that imply hertzian contact.

The results clearly show a difference between the equivalent rolling-friction coefficient values registered for carburized/carbonitrided and nitrided/nitrocarburized surfaces. Thus, in the first case, these values were smaller than in the second case; this conclude that, besides roughness value, the compund zone developed on the top of nitrided/nitrocarburized surfaces increasing the rolling - friction coefficient.

With increasing the surface hardness, the "material micro-wave" from the contact zone on the rolling path (in front of it, in the moving sense) becomes smaller and this aspect leads to an earlier ball start moment and also to the decreasing of rolling-friction coefficient.

References

[1]. N. Popinceanu, M. Gafitanu, *The Basic Problems of the Rolling Contact*, Technical Publishing House, Bucharest, 1985.
[2]. D. Pavelescu, *Tribotechnics,* Technical Publishing House, Bucharest, 1983.
[3]. D. Pavelescu, A. Tudor, *Tribology,* Pedagogical and Didactical Publishing House, Bucharest, 1980.
[4]. D. Munteanu, A. Munteanu, in *Journal of the Mechanical Behaviour of Materials*, 8 (4), 331 (1997).
[5]. S. Bobancu, R. Cozma, V. Cioc, *Tribology and Inventics, Practical Applications,* "Transilvania" University of Brasov Publishing House, 2000.

BEHAVIOR OF Rp3-HIGH SPEED STEEL ON SHORT TIME NITRIDING IN FLUIDIZED BED

ADOLF BÂCLEA[1], NELU CAZACU[2], SORIN DOBROVICI[2], ELENA DRUGESCU[2], OCTAVIAN POTECAŞU[2]

[1] S.C.Cosena S.R.L Constanța,
[2]"Dunarea de Jos"University of Galati,
Nelu.Cazacu@ugal.ro

ABSTRACT

For steel nitriding, treatment time is a important factor. Gas and plasma nitriding are usual method to increase surface properties by nitriding. A close retort is used. Total time for treatment are higher because are necessary transition time for heating and cooling. Fluidized bed offer a short time for heating and cooling because furnace having an open retort. Work paper is based by nitriding experiments by experimental fluidized bed furnace. A gas mixture of ammonia and nitrogen was used. For samples were used HHS (Rp3) . Results were investigated micrographic, surface hardness test (HV5) and micro hardness (HV0,05)..

KEYWORDS: Nitriding, fluidized bed, HSS, Rp3, short cycle

1.Introduction

High speed steel (HSS) having a good properties for cutting tools (resistance, hardness, wear resistance, thermal stability) and these properties is determined by chemical compositions (high quantity of alloying elements) and specific heat treatments. A carbon presence in chemical compositions of steel is necessary to a high quantity of complex metallic carbides dispersed in metallic matrix. For these properties HSS are actually used for many other applications: tools for die press forging, extrusion tools and hydraulic parts. For all tools is important hardness over surfaces and surface porosity to maintaining wear agent for a long time that increasing using time of tool. Some thermochemical treatments are used for increased hardness and surface profile control (nitrocarburizing, nitriding). The paper is based by nitriding in fluidized bed experiments. Some goals are following by thermochemical treatments:

higher values of superficial hardness
stability at high working temperature
corrosion resistance
decreasing values for friction coefficient
increasing durability.

Nitriding treatments of HSS is based by subcritical values of treatment temperature that conduced to low values of inside transformation in material. The treatments is localised at surfaces and a new hard complex with fine distribution is possible to appear before nitrogen diffused in material and alloying elements. Using a fluidized bed technology a short time for nitriding treatment is obtaining and a supplementary hardness appear because secondary brittle by Fe_4N fine dispersed in metallic grain is avoided.

2.Experiments

1. Base of experiments are intense chemical activity of fluidized bed made by granular solid (0,10…0,16mm, burned clay) and mixed gas from ammonia (33%) and nitrogen, 0. Working with open chamber make a reduced total nitriding time because samples is take off after nitriding time (1h, 2h and 3h) and was cooling in air. That procedure has a normal benefits by reducing total time of treatments and by eliminate a Fe_4N precipitates that decreasing hardness, 0. Nitriding in fluidized bed experiments were made on laboratory conditions and nitriding furnace is showing in

2. Fig. 1. For experiments was used samples from Rp3 steel (

Tab. 1). For all experiments a constant debit for mixed gases was used.

Tab. 1. *Chemical composition for Rp3 (HSS - T1-AISI, STAS 7382/90).*

C	Mn	Si	Cr	W	Mo	V	Co
0,7…0,8	max.0,45	0,30…0,40	3,62…4,40	17,5…19,5	max.0,60	1,0…1,4	-

Fig. 1. *Fluidized bed laboratory installation.*

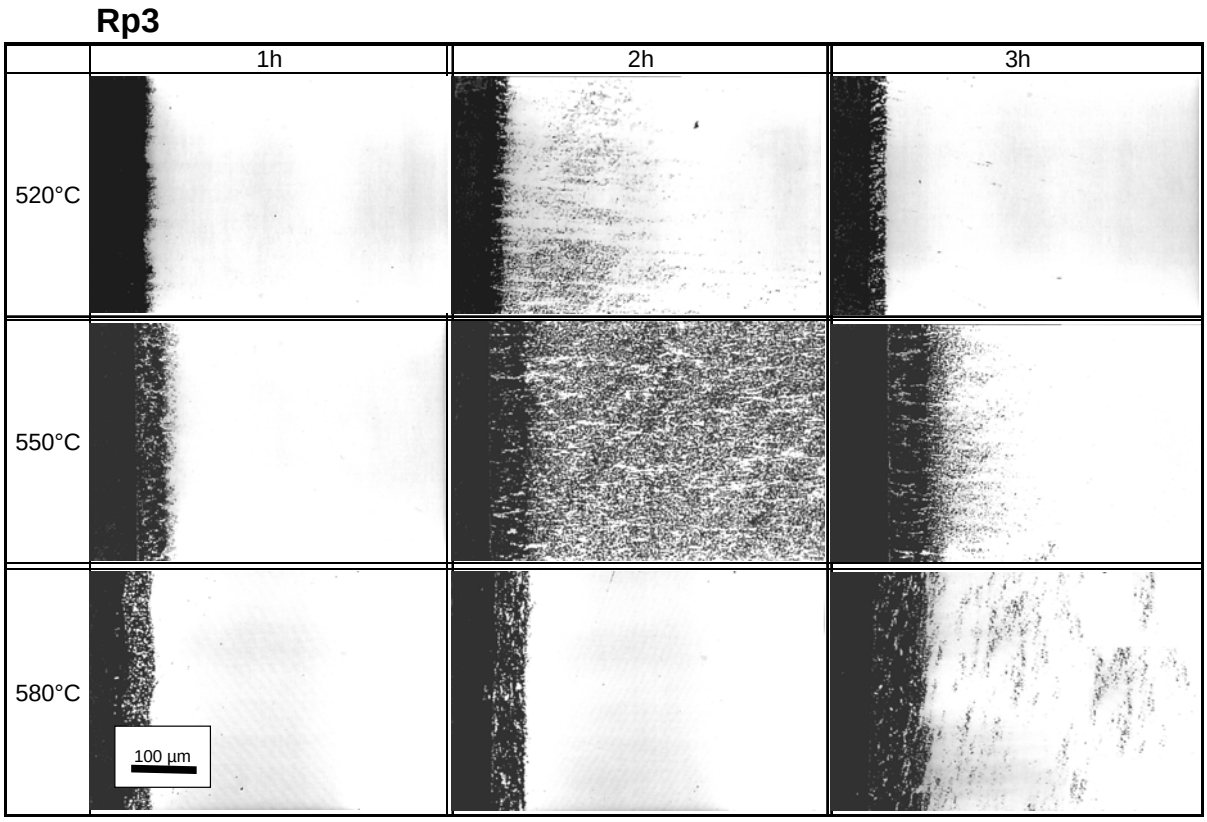

Fig. 2. *Micrographs for Rp3 steel samples after fluidized bed nitriding.*

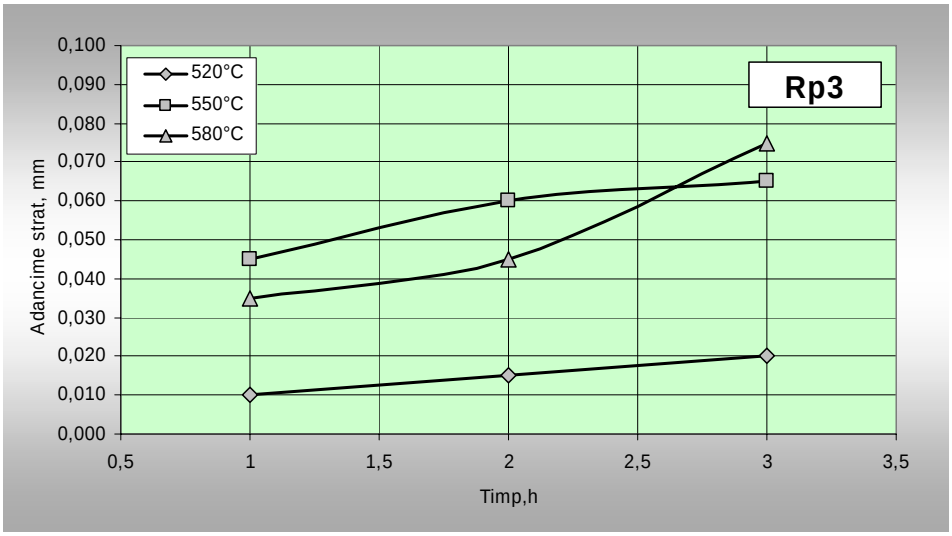

Fig. 3. *Nitriding layer depth variations with nitriding time and nitriding temperature.*

4.Results and discussion

For Rp3 steel samples micrographic analysis is showing in Fig. **2**. For etching was used *royal water*. Micrographs showing a nitriding layers for all regimes, that are depending with nitriding time and nitriding temperature. Depth layer measurements on micrographs is showing in

Fig. **3**. Hardness measured on the nitriding surface is the most important properties after nitriding treatments.

3. The hardness after nitriding in fluidized bed is showing in Fig. 4 (measured by Vickers TPP-2, CIS, with load 5kgf). Hardness increasing with high values for nitriding temperature 550° C and 580°C, and for short time nitriding time (maximum 3h). Chemical and thermal activity of fluidized bed media are important for reducing time of treatments. After treatment the samples (parts or tools) was immediately take of that conduced to maintaining a hardness at high values, eliminated a secondary embrittlement of nitriding layer by Fe_4N (γ') acicular separation. Microhardness (Fig. 5, Fig. 6 and Fig. 7) was measured by nitriding section (metallographic samples) PMT-3 (CIS) microhardness tester with 50g load (0,050kgf). A cross section profile of hardness was determined using microhardness and this profile is in concordance with superficial hardness and micrographs.

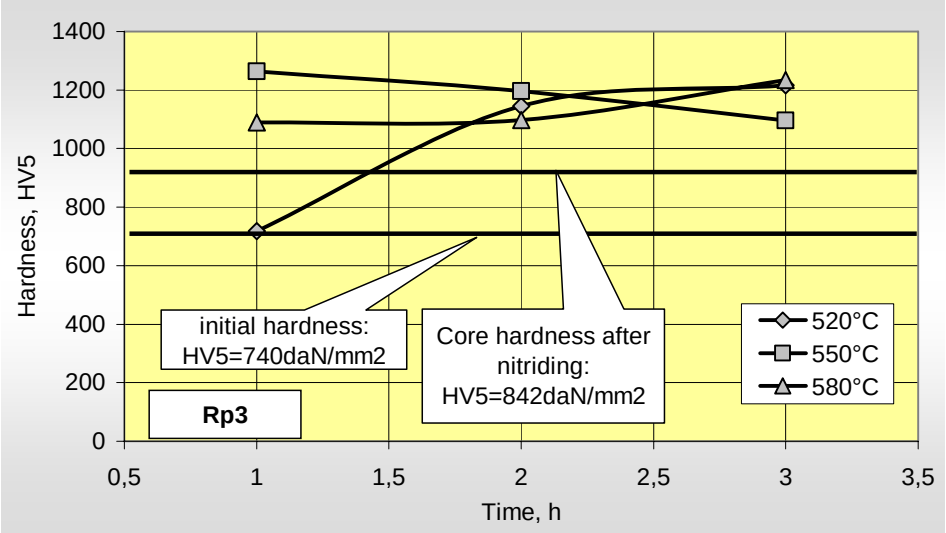

Fig. 4. *Hardness HV_5 after fluidized bed nitriding in function of nitriding temperature and nitriding time.*

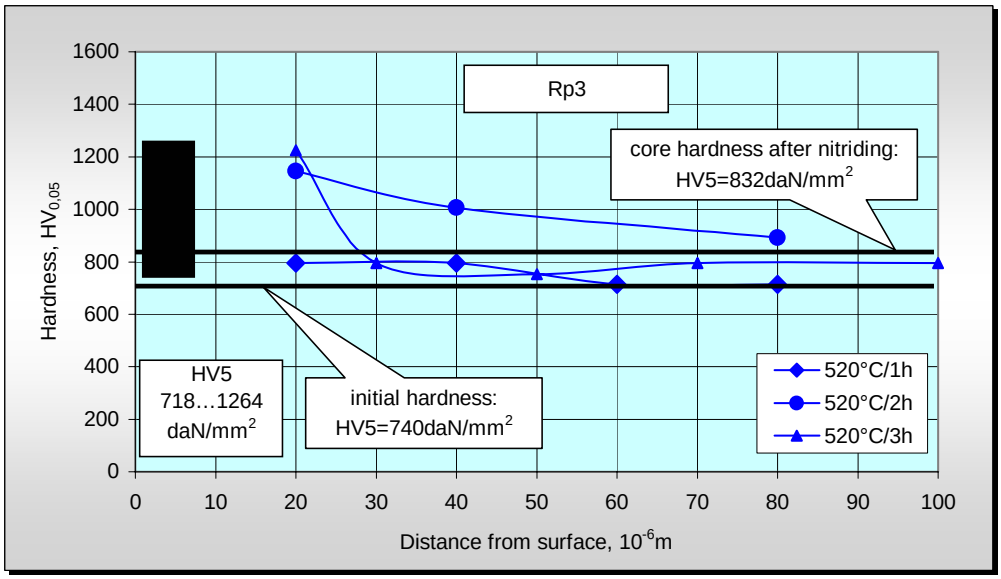

Fig. 5. *Micro hardness for Rp3 samples after fluidized bed nitriding at 520°C.*

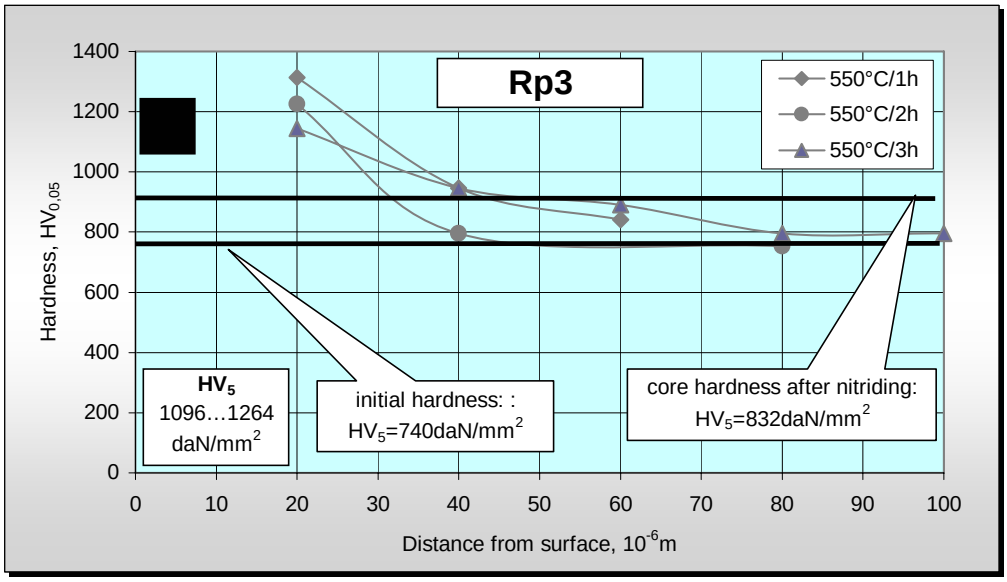

Fig. 6. *Micro hardness for Rp3 samples after fluidized bed nitriding at 550°C.*

Microhardness was measured by nitriding section (metallographic samples) PMT-3 (CIS) microhardness tester with 50g load (0,050kgf). A cross section profile of hardness was determined using microhardness and this profile is in concordance with superficial hardness and micrographs.

5.Conclusions

The Rp3 steel (HSS) having high quantity of alloying elements in chemical compositions. A very hardness metallic carbides dispersed in base matrix material. By nitriding a supplementary quantity of hard an thermal stable nitrures were dispersed by nitrogen diffused from nitriding media and by alloying elements from steel. A supplementary hardness increasing is associated by a superficial porosity increasing, and all conduced to a good behaviour of tools in cutting process. After nitriding in fluidized bed superficial hardness increasing with 250…400daN/mm^2.

The most higher value of hardness, 1234daN/mm^2 is obtaining at 580°C nitriding temperature and 3h for nitriding time. Microhardness ($HV_{0,05}$- 50 grams load) measured by metallographic sections showing a decreasing profile for hardness in sections. A secondary increasing of hardness is present in core of samples. Micrographs showing a structure with only a diffusion layer. An oxide layer is present on the surface of samples. Is appears because the samples is take out in air from fluidized bed at nitriding temperature and oxidation is present.

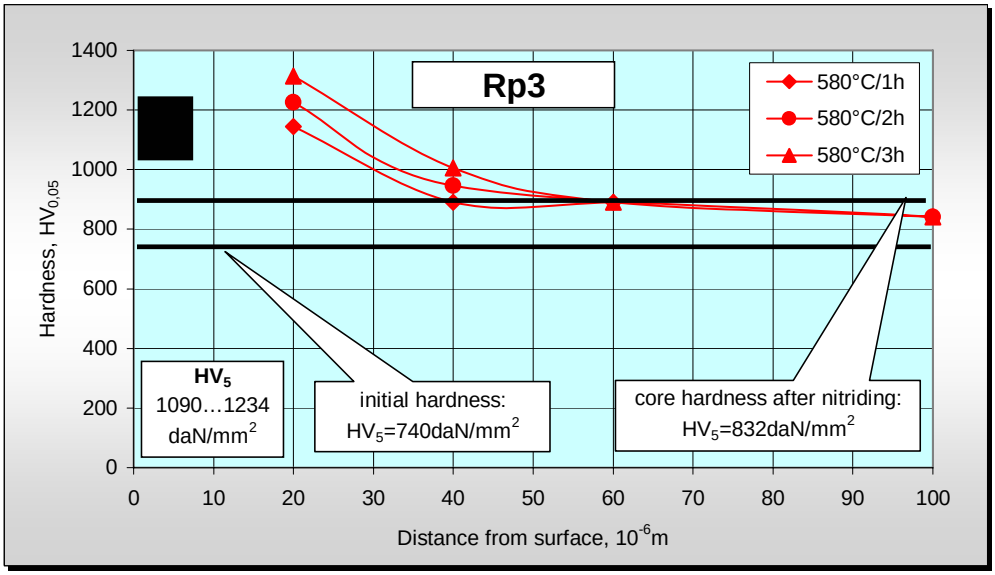

Fig. 7. *Micro hardness for Rp3 samples after fluidized bed nitriding at 580°C.*

The depth layer measured metallographic is depending by time and temperature. In fluidized bed conditions the total time of treatments is decreasing.
The furnace is at working temperature and is simple to introducing another parts to nitriding. The total efficiency of installations increasing when compare with ion nitriding and gas nitriding where heating and cooling represents higher values of time in correlation with effective nitriding time.

Fluidized bed nitriding is a favourable applications of internal and external fluidizations properties. High values of thermal conductivity an acceptable values of mass diffusivity are internal properties that determine high values for mass and thermal global coefficient of transfer. The nitriding surface having an apart gray nuance of colour because a thin ferrous oxide layer is present after nitriding when samples is cooling in air at atmosphere temperature.

Applications of fluidized nitriding thermochemical treatments for Rp3 steel is recommended to be at third tempering regimes for material.

References

[1]. Bâclea,A., *Some aspects concerning fluidized bed nitriding*, Proceeding of the MOC'40 Seminar, Odessa, 26-27 April 2001, pg.145;
[2]. Kunii,D., Levenspiel,O, *Fluidization engineering,* John Wiley & Sons, Inc., New York, 1969;
[3]. Bâclea.A., Drugescu.E., Cazacu.N., Dobrovici.S., *Some aspects concerning the nitriding steels in fluidized bed,* International Conference On Advances in Material and Processing Technologies, AMPT01, Leganes, Madrid, Spania, 18-21 Septembrie, 2001, Proceedings of The International Conference on Advanced Processing Technologies AMPT'01, vol. I, pag.131.
[4]. Ivanuş Gh, Todea I., Pop Al, Nicola S, Damian Gh, I*ngineria fluidizării,* Editura Tehnică, Bucureşti, 1996;
[5]. Drugescu E, Udvuleanu A, *Metalurgie fizică şi tratamente termice*, Lucrări de laborator, Universitatea din Galaţi, 1981;
[6]. Drugescu E, Udvuleanu A, Dobrovici S, *Tratamente termice. Lucrări de laborato*r, Universitatea din Galaţi, 1985;
[7]. Carţiş,I .Gh.,Tratamente termice. Tehnologie şi utilaje, Editura Facla, Timişoara,1982
[8]. Florian, E., Dulamiţă,T., *Tratamente termice şi termochimice*, Editura Didactică şi Pedagogică, Bucureşti,1982
[9]. Murry Guy, *Une nouvelle norme europeenne "Acier pour nitruration"*, Traitement Thermique, nr.339, mai 2002, pag.30
[10]. Dulamiţă. T., *Producerea si utilizarea atmosferelor controlate pentru tratamente termice*, Editura Tehnica, Bucureşti 1976;
Revista Tratamente termice şi ingineria suprafeţelor (ATTIS), Vol II, nr.1/2002, pag 39…40
[11]. Vermeşan,G., *Tratamente termice. Indrumător,* pag.167÷180, Editura Dacia Cluj Napoca, 1987.

THE VALUE OF THE STRUCUTRAL REMANENCE AND THERMIC TENSIONS IN THE FORGED PIECES

Aurel CIUREA, Marian BORDEI

"Dunarea de Jos" University of Galati
e-mail: ciurea.aurel@ugal.ro

ABSTRACT

The plastic deformation, the heating and the cooling of the pieces submitted to plastic deformations acumulate remanent tensions inside the pieces.

Knowing the environmental where they are produced and avoiding its superposition in an important problem for a specialist who aims to get through the forging process some pieces dimentionally corresponding and without defects. This works will analyse the value of the structural remanent and thermal tensions in the case of some forged pieces.

KEYWORDS: forged pieces, tensions, cracks

1. Introduction

At the end of the deformation process of the forged pieces, remanent tensions remain, tensions which type and size can be determined especially by suplimentary tensions which operated on the metal at the moment of the end of the deformation. Also, during the cooling process, in the forged piece structural transformations can be produced accompanied by the corresponding tensions. Finally, during the cooling process in the press thermal tensions appear too. Thus, the final stage of the forged press tension is determined by the sum of the above mentioned tensions. Each of the mentioned tensions or their algebraic sum may achieve the resistance tensile strength of the metal and provoke its distruction:

$$\sigma_i > \sigma_r \qquad (1)$$

$$\sum_{i=1}^{n} \sigma_i > \sigma_r \qquad (2)$$

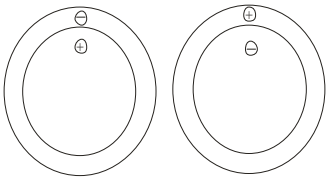

Fig. 1. *The possible diagrams of the tension state of the round forged piece after the ending of the forging process (the remanent tensions of the forging process).*

At the end of the deformation process in the forged pieces, the tension state can correspond to one of the following diagram of figure 1.

These tensions are provoked by the remanent deformation tensions.

The destruction of the metal starts inside the forged piece (in their breaks) or un their surface (superficial cracks).

At the forged pieces, from steels that do not have phase transformation, superficial cracks are possible which may become gradually deeper inside their body. At the pieces forged in a round shape these cracks orientate radially. The characteristics difference consists in the fact that yhey are visible during the cooling process of the forged piece up to 500^0C and are hardly to discover sfter its complete cooling. The cooling cracks after the quenching process start from the surface of the forged piece. They appear under the action of the structural tensions, the most frequently after the complete cooling of the piece.

We will analyse further on the variation of the tension state diagram during the cooling process of a cylindrical forged piece from the moment of the end of the forging process (T_f = 900-1000^0C) till the environmental temperature(T_0 = 20^0C), for both types of tensions described in figure 1, applicate for steels of three types:

a. without phase transformation
b. perlitic transformation
c. martensitic transformation.

The variation of the tension state diagram of a cilyndrical forged piece, having phase transformation is swown in figure 2.

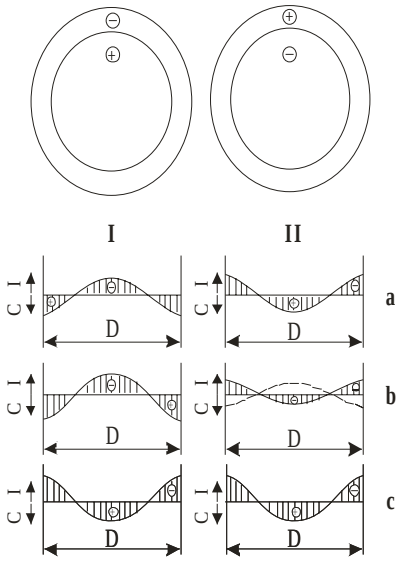

Fig.2. *The variation of the tension state of a cylindrical forged piece made of steel without phase transformations during the cooling process after the forging process with different remanenet tensions of deformation.*

a. the deformation remanenent tensions before cooling;

b. the diagram tensions before of the cooling piece surface up to 200-500^{0}C

c. the diagram of the tensions after complete cooling up to 20^{0}C.

In figure 2 one can notice the variation of the tension state during the cooling process of the forged piece, with remanent tensions of forging, of compression at the external side and elongation in the axial area.

From figure 2 in this case it results that maximum tensions of elongation, superficial can be obtained in case I b, and maximum axial elongations in I c and II c bodies.

In the last case all the other conditions remain equal, the extent of internal elongation tensions gets the maximum value. It results that the formation the interior cracks of cooling in the forged pieces of steel without phase transformations is possible in I c and II c bodies only after complete cooling.

The formation of the superficial cracks is the most probable only in case I b. in the II b case, at a sufficiently intensive cooling of the forged piece, the formation of the elongation superficial tensionsis possible (the dots line figure 2, II,b).

However under identical cooling conditions the value of these elongation tension is always smaller than in case I b.

The variation of the sign and tenisions value during the cooling process from 1000^{0}C to 20^{0}C of two forged pieces regarding the variants I and II from above, can be noticed in figure 3.

On the left side there are the remanent tensions of forging existent inside the piece before the beginning of the cooling process and on the right the final tensions obtained after the complete cooling process.

In conclusion, at both variants, after the complete cooling process, in the internal area of the forged piece, remanent thermal volumetric of elongation tensions are maintained, tensions that usually lead to the formation of internal cracks.

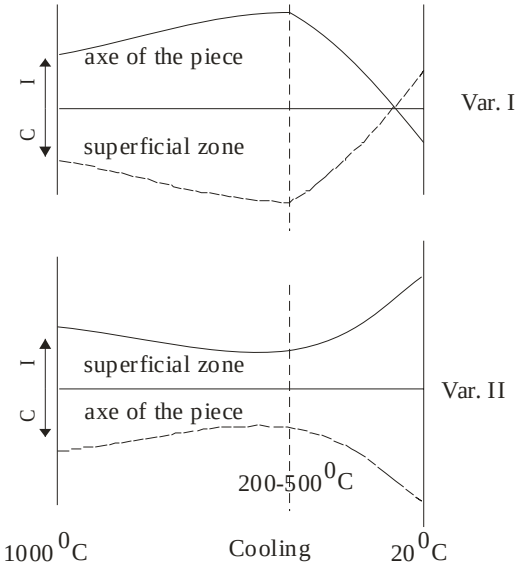

Fig.3. *The curves of the variation of the tension sign in different areas of the forged pieces analysed in figure 2, during the cooling process up to the room temperature.*

At the next heating process for a reheat treating in the axial area of this forged piece, radial internal suplementary tensions of elongation appear, tensions that are added to those thermal of cooling, with the same sign, which operates in the same area. That is why, the formation of the internal crack in the forged piece with volumetric internal remanent elongation is more probable during the heating than the cooling processes.

During the heating of these forged pieces, suplementary measures must be taken to aim at making the difference between the internal and pheripherical temperatures the smallest possible.

During the cooling and heating process in the forged pieces of steel without phase transformations, thermal tensions are appear to which the remanent tensions of forging with a sign or other are added.

The value of these tensions depends on:

a. the maximum difference between the axial area temperature and the superficial one of the forged piece during cooling and heating;

b. the coefficient of linear expansion of the metal.

The biggest the difference of temperatures and the coefficient of linear expansion of the metal which appear. Besides this fact, a significant importance for the possibility of formation of the intenal or external cracks has the reserve of the plasticity of the metal. The smallest the plasticity is, the smallest value of the tensions where cracks may appear is.

During the forged piece made of a steel with phase transformations, besides the thermal tensions, structural tensions appear, because the structural constituents of the steel: austenite, perlite and martensite have an unequal specific volume.

During the transformation of the austenite in martensite, the value of the local volumetric variations is incomparably bigger than the perlitic transformation. The value of the forged pieces tensions which bears a martensite transformation gets values. They often surpass the tensile strength of the hardened steel and produce the destruction of the forged piece.

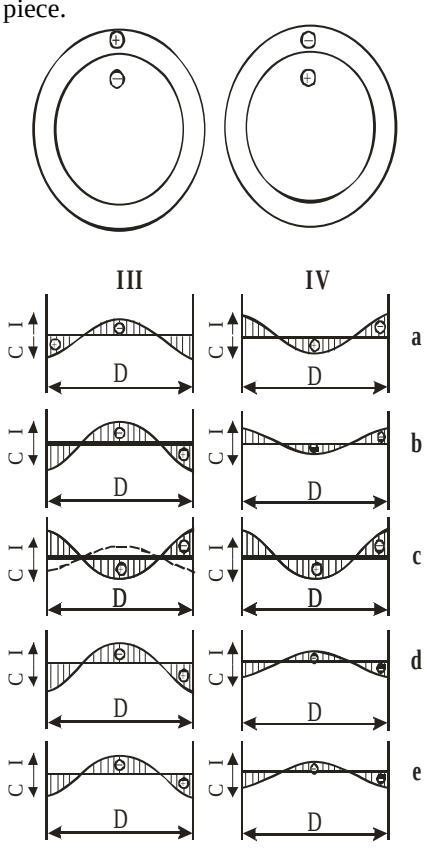

Fig. 4. *The variation of the strengthening state of the round forged piece of steel where a perlite transformation takes place.*

In figure 4 one may see that the round forged pieces made of perlite steel, variation while their cooling process from the forging temperature till that of the ambient temperature at different diagrams of the streighning state before cooling:

a. remanent tensions of deformation before starting the cooling;

b. diagram of the tensions before starting the perlite transformation in the superficial area;

c. diagram of the tensions after the perlite transformation in the superficial area;

d. diagram of the tensions after the perlite transformation in the centre.

e. diagram of the tensions after the complete cooling of the forged piece.

I-elongation; C-compression; S-diameter.

In the same case IV c, the highest internal tensions may be obtained, but into practice, they do not produce the formation of internal cracks. The maximum value of the strengthening superficial tensions may be noticed in cases III b, d,e. however the external cracks can be formed only in case III e.

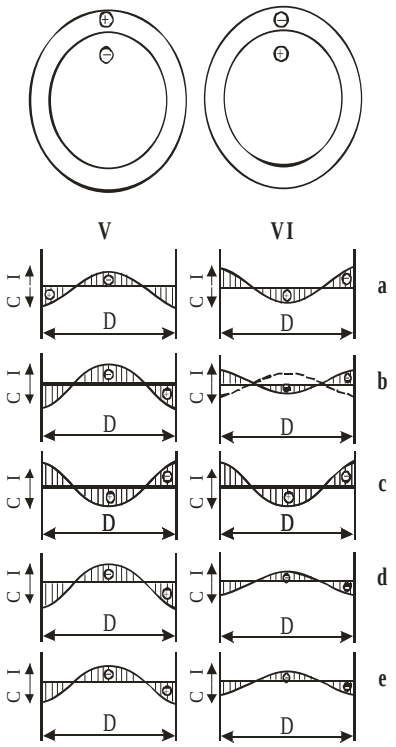

Fig. 5. *The variation of the tension state of the round forged piece made of steel where the martensite transformation takes place.*

In figure 5 the same thing is shown as in figure 4, but for forged pieces, where during the cooling process the austenite transformation in martensite is produced.

a. the remanent tensions of deformation before the begining of the cooling process;

b. diagram of the tensions before starting the martensite transformation in the superficial area;

c. diagram of the tensions after the martensite transformation in the superficial area;

d. diagram of the tensions after the perlite transformation in the centre.

e. diagram of the tensions after the complete cooling of the forged piece.

I-elongation; C-compression; S-diameter.

The principle on the whole developing period of the process of cooling, the tension state of the forged piece do not differ from the state of tension from the previous pieces.

Howver the tension state is here more evident. After the martensite transformationis higher and the hardness and the brittleness of the metal with martensite structure.

These circumstances condition a higher probability of the cracks. Usually, the elongation internal tension which appear in the forged piece at the cooling process after the variants V and VI do not produce internal cracks and inside the cooled forged piece, these tensions are absent practically.

During the cooling process, the elongatin tensions may reach high values in the superficial area of the forged piece, but practically they do not surpass the following limit of the metal because of the remanent formation.

The same tensions in the forged piece which was cooled (andd which has already a martensite structure) reach values that surpass the tensile strength of the metal and produce its breaking.

This type of cracks are usually called hardening cracks. The appearanceof these cracks starts from the surface of the forged piece and is the most probable in "V" and "U" bodies.

Conclusions

The formation of the hardening cracks may be eliminated by avoiding the possibility of developing the martensite transformation, creating conditions for obtaining the perlite transformation of the austenite, if the perlite transformation cannot be obtained, then by creating the martensite transformations conditions simultaneously an the whole section forged piece.

The tension state of the forged piece or the cooled semi-finished product has also a great importance during their following treating process.

At the heating process of the big forged pieces be established taking into account the cooling remanent tensions, in order to avoid the sum of tensions with the some sign.

At the cutting process of the forged piece or of the semi-finished product with circular saw or side milling cutters a gradual tightening of the disk or the side milling cutter takes place. This hapens under the action of the compression remanent tensions from the peripheric area of the forged piece. The more evident the tension state of the forged piece is, the stronger the disk may get stuck, and the cutting of the piece becomes more difficult. At the cutting process with the same saw or side milling cutter of the forged piece which has a diagram of the tension state in accordance with figure 1 b, the width of the cut grows gradually and the possibility that the disk get stuck is excluded.

The practical experiments show that at equal cooling conditions, in the forged pieces made of steel, the martensite of the remanent forging tensions with a sign or another, can accelerate or show down the formation of herdening cracks inside them. An important role regarding the kind and value of the remanent tensions at the forged pieces has the shape of the tools with which the plastic deformation is produced.

References

[1]. I. Dragan, I. Ilca, S., E. Cazimirovici – *Tehnologia deformarilor plastice*, Ed. Didactica si Pedagogica, Bucuresti, 1979
[2]. Dieter Jr. – *Metalurgie mecanica*, Ed. Tehnica, Bucuresti, 1970
[3]. Bakofan A. W. – *Superplasticity. Ductility*, New York, ASM, 1968
[4]. Gubkin, SL., *Metalurghizdat*, Moskova,1960.

THE COMPUTATION OF THE CALENDER ROLLS DEFLECTION USING THE STONE-GAEVSKI FORMULAE

Daniela FLORESCU, Iulian FLORESCU

University of Bacău

ABSTRACT

This paper presents new models for the change of the internal configuration of the paper calender rolls with extension to those for plastics and rubber, and the deflection calculation procedure using Stone-Gaevski formulae.

KEYWORDS: rolls deflection, stress, Stone-Gaevski formulae

1.New models suggested for the rolls deflection computation

1.1. Hypotheses used in the drawing up of the models

There have been conceived two computation models in which there are used plane elements for the stresses transmission, obtained by sectioning the rolls with longitudinal planes. There have been considered the following hypotheses:

- the load is constant, uniformly distributed along the calender rolls surface's for paper pressing (p_2 = 62 N/mm)
- the model undergoes a plane strain, due to the fact that the shearing strain of the plane element is actually impeded because of the rolls portions which have been removed and which have high stiffness
- the roll is supported at its ends; the length of the bearings and the bending moments due to the reactions with respect to the planes of the rolls ends are negligible
- the friction forces are negligible taking into account both their reduced values ant their influence on the other parameters. This hypothesis is confirmed by the experimental results
- the rolls dimensions are:
- external cylindrical surface ∅ = 100 × 500 (mm × mm)
    - internal cylindrical surface ∅ = 40 × 50 (mm × mm)

1.2. The determination of the shape and dimensions of the computation models

The hypotheses used in conceiving new computation models of a calender roll elements stress lead to structures whose plane dimensions depend on the rolls geometry and on the paper tape width.

The roll under consideration has the following dimensions:

- external diameter D_2 = 100 mm
- minimum internal diameter D_1 = 50 mm
- total length L = 1 100 mm

For the following models we consider the possibility to obtain opposite rolls deflections by introducing a non aggressive work medium, under pressure, within the rolls

Further on we have in view to determine the deflections which appear in the calender rolls, when a uniformly distributed load, occurring during the rolling of the paper tape, acts upon them. In this respect, different internal shapes of the calender roll are considered.

Model I

We consider a calender roll whose internal surface has a cylindrical section along its entire length, (fig. 1).

The dimensions of model I are:

- external diameter D_2 = 100 mm;
- minimum internal diameter D_1 = 50 mm;
- total length L = 1000 mm;
- active length l = 500 mm.

Model II

A calender roll with an ellipsoidal internal section is considered. Fig. 2 shows the work diagram in the case.

The equation of the ellipsoid is:

$$\frac{x^2}{a^2}+\frac{y^2}{b^2}+\frac{z^2}{c^2}=1 \qquad (1.1)$$

where a = b = R_1 stand for the ellipsoid small semi-diameters.

Because the calender rolls are thought to be thick-walled cylindrical bodies, they are characterized by the between the external and internal radius

$$\beta=\frac{R_2}{R_1}\geq 1{,}2 \Rightarrow R_1 \leq \frac{R_2}{\beta} \quad (1.2)$$

in which R_2 = 50 mm;

R_0 = radius necessary for the roll to operate, R_0 = 20 mm

c_1 = basic size, mm

$$c_1=\frac{L}{2}-h=\frac{1000}{2}-30=470\,\text{mm}.$$

$$R_1=\frac{R_2}{\beta}=\frac{50}{1{,}22}=41\,\text{mm}.$$

The ellipsoid equation in the roll longitudinal plane is:

$$\frac{y^2}{b^2}+\frac{z^2}{c^2}=1 \Rightarrow y=\pm a\cdot\sqrt{1-\frac{z^2}{c^2}} \quad (1.3)$$

Limiting conditions:

$y = R_0 \Rightarrow z = c_1$ (1.4)

Replacing we obtain:

$$c=\pm\frac{R_1 c_1}{\sqrt{R_1^2-R_0^2}}$$

c = 538 mm (1.5)

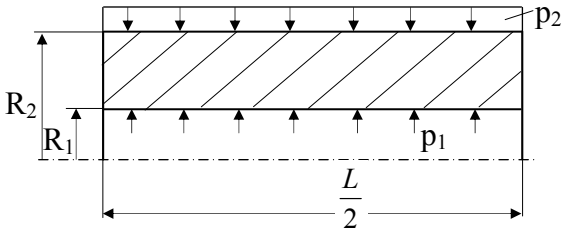

Fig. 1. *Diagram of the constant internal section model shape roll*

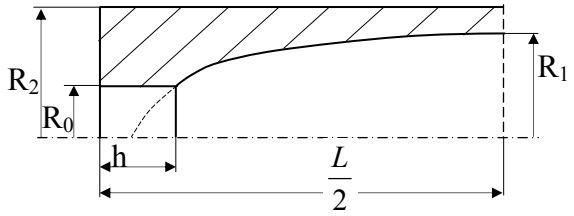

Fig. 2. *Diagram of the ellipsoidal internal*

Model III

We consider the internal section in the shape of truncated cone, from the radius r, with current radius, to zero, on the length L.

Fig. 3. shows the diagram for the case under consideration.

The characteristic constructive dimensions are: =l = 500 mm;

$$\frac{r_i}{x}=\frac{r}{l}\Rightarrow r_i=\frac{r}{l}x$$

r = R = 20 mm, the external radius

R_2 = 50 mm.

Model IV

A calender roll with double truncated cone internal surface is considered. Fig. 4. shows the diagram for the roll under consideration.

The constructive dimensions of the model IV are:

- total length L= 1000 mm;
- computation length l = 500 mm.

distance from the center bearing median line to the paper tape margin, h = 30 mm

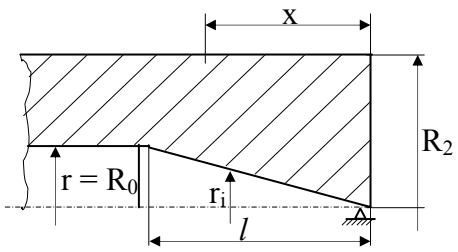

Fig. 3. *The diagram of a calender roll with double cylindrical-truncated cone internal section*

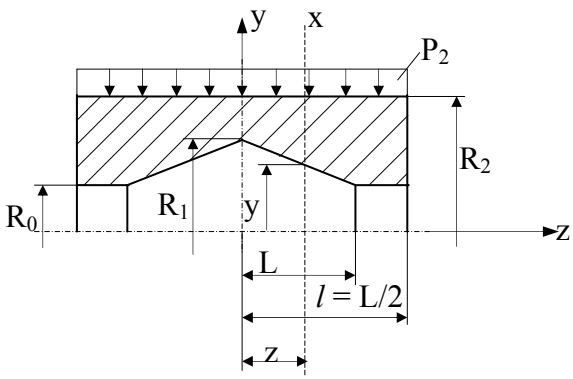

Fig. 4. *The diagram of a calender roll with double truncated cone internal section*

2. Deflections computation

Stone's formula for calculating the maximum deflection of a roll is:

$$f_{\max} = \frac{5p_2L^4}{384EI_z}\cdot\left[1+\frac{24}{5}\cdot\frac{h}{L}+2\cdot\left(\frac{D_2}{L}\right)^2\right] \tag{2.1}$$

where:

p_2 – the external rolling pressure, N/mm
E – Young's modulus of the roll material
I_z – moment of inertia of the cylinder casing
D_2 – external diameter of the cylinder casing, mm
h – distance from the center bearing median line to the paper tape margin, mm

The first term in the square brackets introduces the bending produced by the uniformly distributed load, the second is due to the center bearing deflection, and the third stands for the curvature produced by the shearing forces. The magnitude of this last term is generally 5 %, but it can increase to 10 %.

Gaevski's formula for calculating the rolls total deflection is:

$$f_{\max} = \frac{5p_2L^4}{384EI_z}\cdot\left\{\left[1+\frac{24}{5}\cdot\frac{h}{L}+2\cdot\left(\frac{D_2}{L}\right)^2\right]\right\}-\left\{8\cdot\left[\frac{3}{5}+\frac{12}{5}\frac{h}{L}+\left(\frac{2R_2}{L}\right)^2\right]\right\} \tag{2.2}$$

After doing the substations in the formulae (2.1) and (2.2) table 1 is drawn up for each case, and the deflections variation for the rolls under consideration is shown in Fig 5.

Table 1

Lenght L,mm	0	10	50	100	150	200	250	300	350	370	390	400	430	450	500
Model	1	2	3	4	5	6	7	8	9	10	11	12	13	14	15
I.a - Series I	1,278	1,275	1,264	1,219	1,145	1,044	0,918	0,768	0,597	0,52	0,448	0,41	0,291	0,118	0,01
I.b - Series 2	2,19	2,189	2,165	2,088	1,962	1,789	1,572	1,315	1,023	0,9	0,768	0,702	0,498	0,315	0,112
II - Series 3	1,44	1,439	1,423	1,373	1,29	1,176	1,034	0,865	0,673	0,59	0,505	0,461	0,327	0,215	0,111
III - Series 4	1,398	1,398	1,382	1,333	1,253	1,142	1,004	0,84	0,653	0,57	0,49	0,448	0,318	0,252	0,05
IV - Series 5	1,3	1,299	1,284	1,239	1,164	1,062	0,933	0,78	0,607	0,53	0,456	0,416	0,295	0,11	0,001

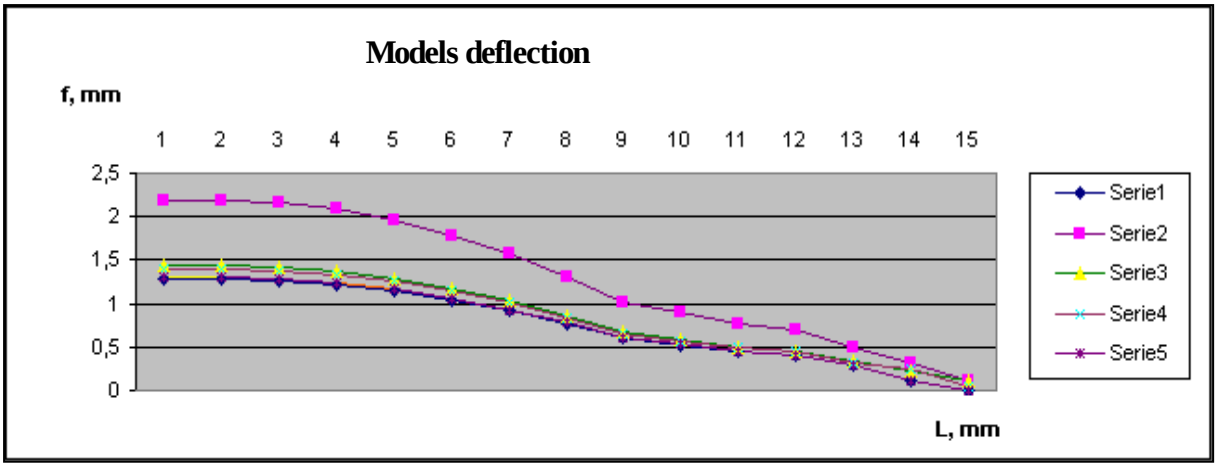

Fig. 5. *The variation chart of the calculating models*

References

[1]. Florescu, D. *Theoretical and Experimental Research Concerning the Realization of a Uniformly Distributed Load Along the Generatrix of the Paper*, Ph.D. Thesis, University of Bucharest, 2001.

[2]. Florescu, D., Iatan, R. *Theoretical Study Concerning the Determination of the Calender Rolls Deflection, Mechanical Engineering*, Bucharest, 2002, (54), no. 1-2.

[3]. Gaevschi, B.A. *Maşina i aparata bumajnoi promaslenosti*, Editura Maşghiz, Moscow, 1955, p. 239 – 240.

ASPECTS REGARDING THE WIDIA PLATES BEHAVIOUR COVERED WITH TiN DURING THE CUTTING PROCESS

Mihai GAITA, Marian BORDEI

"Dunarea de Jos" University of Galati
e-mail: gaita.mihai@yahoo.com

ABSTRACT

The microscopic property that depends on the interfacial structure and on the tension to which the interface is submitted is called adherence. The strong connection in the interfacial area, low tension gradients, the absence of cracks and of degradation in the course of time are properties that define a good adherence at the layer-underlayer interface. The good adherence of the thin layer to the underwear implies the non- deterioration in normal conditions or while tensions application of the interfacial area. In order to establish the degree of adherence of the tin titanium – nitride layers deposed on the widia plates, there were researches made about the behaviour of the covered plates during the cutting process. In this way the dependence between the durability (T) of the widia plates and the cutting speed (v) was determined as a result of experiments.

KEYWORDS: widia plates, thin layer, cutting

1. Introduction

The durability of the widia plates is measured in minutes, is noted "T" and depends on the following factors:

- the tool material
- the quality of the worked material
- the cooling and the greased liquids
- the tool geometry
- the cutting depth "t"
- the tool advance in the material

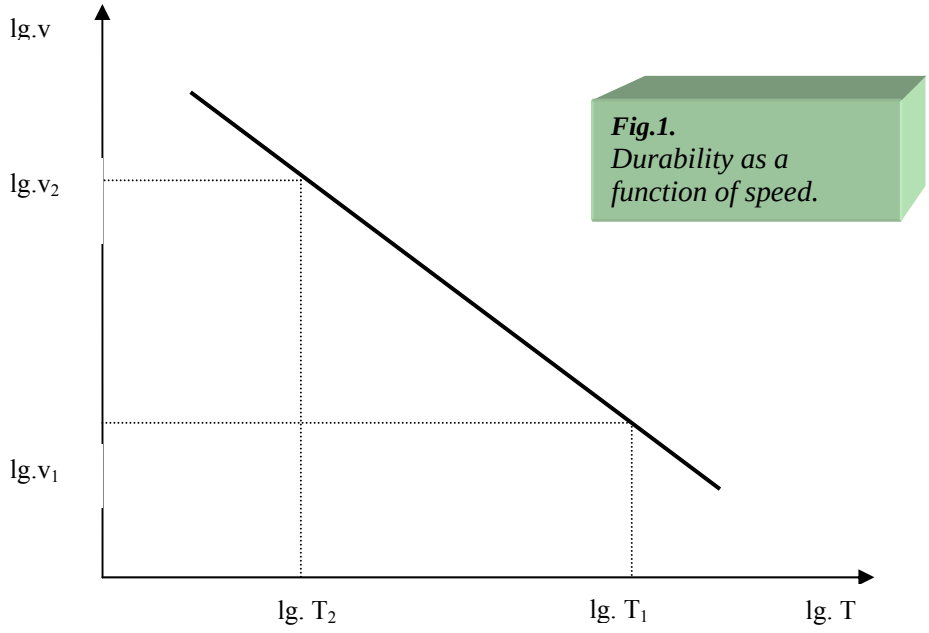

Fig.1. *Durability as a function of speed.*

The greatest influence on the durability comes from the cutting speed which is mathematically defined by Taylor relation:

$$v = \frac{C}{T^m} \quad [m/min]$$

where "m" is the durability index and "C" is a constant that depends on the worked material properties, on the cutting depth "t" and the advance "s".

For a limited area of speed variation, the"m" index can be considered a constant value although this is not a constant size but dependent on factors that influence the cutting wear.

When m=constant, in double logarithimic co-ordinates, the equation (1) represents a straight line under the following form:

$$\log v = -m \log T + \log C \qquad [1]$$

where: $m = tg\ \alpha$

The smaller the "m", is the nearer to the horizontal line the straight line is and to a small variation of the cutting speed "v" corresponds a big variation of the durability.

The dependence of the durability as a function of the speed T=F (v) is shown in fig.1.

From relation 1 we get $T_1^m \cdot v_1 = T_2^m \cdot v_2$ and the gradient "m" in double logarithms coordinates can be determined by the following relation:

$$m = tg\ \alpha = \frac{\lg v_2 - \lg v_1}{\lg T_1 - \lg T_2};$$

2. Experimental conditions

For the experiments plates from P30, CNMG 12-04-08-PN group were used, covered and uncovered with TiN.

The table 1 shows the cover process manner and both the constructive and active geometry of the plates used.

Table 1. *The constructive and active geometry of the plates*

Plate type	The worked material	The plate geometry [º]							
		Constructive				Active			
		α	γ	χ	λ	α	γ	χ	λ
CNMG 12-04-08-PN	Oțel OLC45	0	12	40	0	8	-6	45	0

2.1. Worked materials

At the CROMSTEEL INDUSTRIES firm Târgoviște, the CNMG 12-04-08-PN plates type are used for working the steels.

The chemical composition of OLC45 steel used for test was shown in table 2 and the mechanical properties in table 3..

The samples used for the tests were OLC45 bar shape, 40 mm diameter and 200 mm length for CNMG 12-04-08-PN plates (microstructure is presented in figure 2).

Table 2. *Chemical composition*

C	S	Mn	Si	P
[%]				
0.46	0.014	0.65	0.27	0.016

Table 3. *Mechanical properties*

Flowing limit	Tensile resistant	Elongation	Resilience	Hardness (in normalized state)
$R_{p0,2}$ [N/mm²]	R_m [N/mm²]	A_5 [%]	KCU [J/cm²]	[HB]
480	690-840	14	60	235

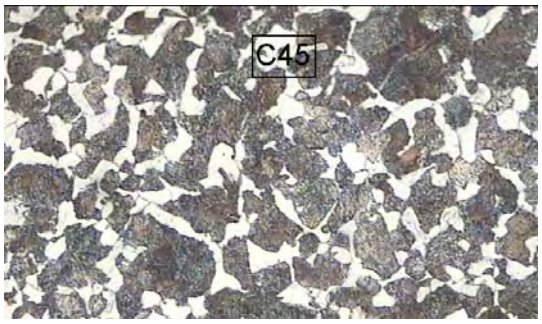

Fig.2. *Microstructure of the OLC 45 samples (x50) .*

2.3. Experiments

There were made experiments on a lathe with numerical control MAZAK.

The working operations consisted in longitudinal turning under the conditions of the cutting process (t, s, v_1). Keeping unchanged the working conditions for all the tests it is determined the wear dependence as function of the tool working time.

The tool wear measurement is made at equal intervals (at every passing). The experiment is repeated for a new value of the cutting speed v_2, maintaining the other parameters constant.

In order to eliminate the faults due to the thermal deformation of the tool, this one is cooled at the medium surrounding temperature before making the measurement. The measurement of the tool wear is made with the measurement accuracy of 1 micrometer on the microscope from the Technic alQuality Control laboratory.

In order to establish the characteristic points the dependence curve depending on time is marked out. (fig. 3, 4, 5 and 6).

The standard representation of the wear dependence depending on time is shown in figure 3 and points out three characteristic areas: OA - the initial wear; AB - the proportional wear; BC - the catastrophic wear.

The cutting conditions parameters are chosen in the domain of the values used on the working machines from CROMSTEEL Targoviste. In the table 4 there are some examples of using the CNMG 120408 PN plates.

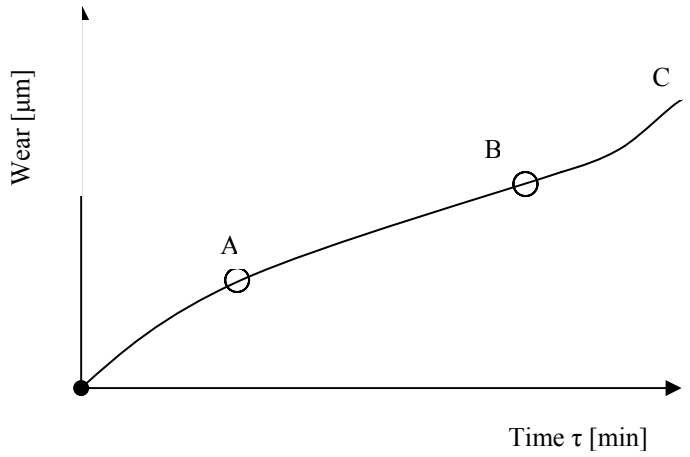

Fig. 3. *Wear depending on time.*

Table 4. *Cutting conditions*

Plate type	Processing type	Processed material	Cutting conditions		
			V_{max} [m/min]	s [mm/rot]	t [mm]
CNMG 12-04-08-PN	Turning	OLC45 Steel	200	0,060	1,0
			314	0,060	1,0
			314	0,048	0,8

The cutting speeds were calculated by means of the following relation:

$$V = \frac{\pi \cdot D \cdot n}{1000} \text{ [m/min]},$$

where: D – bar diameter [mm]
n – rotation speed [rot/min]

For the OLC45 steel bars:

$$V_1 = \frac{\pi \cdot 40 \cdot 2228}{1000} = 280 \, m/\min;$$

$$V_2 = \frac{\pi \cdot 40 \cdot 2500}{1000} = 314 \, m/\min.$$

In the table 5 the domains of the parameters values of the cutting conditions are shown.

Table 5. *Domains of the parameters values of the cutting conditions*

Plate type	Processed material	Conditions	n [rot/min]	v [m/min]	s [mm/rot]	t [mm]
CNMG 12-04-08-PN	OLC45	1	1592	200	0,060	1,0
		2	1751	220	0,060	1,0
		3	1910	240	0,060	1,0
		4	2069	260	0,060	1,0
		5	2228	280	0,060	1,0
		6	2500	314	0,060	1,0

4.The experimental results

After making the experiments, the wear values (VB) of the CNMG 12-04-08-PN plates were established. These values resulted from some periods of time, corresponding to one, two, respectively to three turning passings of the sample.

The calculus of the passing period is made by means of the relation:

$$\tau = \frac{L}{n \cdot s} \cdot i \text{ [min]};$$

where: L-the length of the bar
n-the rotation speed
…….s-forward flow
…….i-number of successive passings
For the OLC45 bars:

$$\tau_1 = \frac{200}{2228 \cdot 0{,}06} \cdot 3 = 4{,}50 \text{ min}$$

$$\tau_2 = \frac{200}{2500 \cdot 0{,}06} \cdot 3 = 3{,}00 \text{ min}$$

The experimental data were centralized in table table 6:

Table 6. *The experimental data.*

Plate type	Processed material	Cutting speed [m/min]	Passing number	Wear VB [µm]		Time [min]
				Plate covered with TiN of 8µm PN/CG4015	Plate uncovered PN/GC4035	
CNMG 12-04-08-PN	OLC45	280	1	1,73	4,30	4,50
			2	2,32	5,60	9,00
			3	2,88	12,93	13,50
			4	4,84	-	18,00
		314	1	1,92	5,99	3,00
			2	2,61	7,84	6,00
			3	3,46	14,48	9,00
			4	5,62	-	12,00

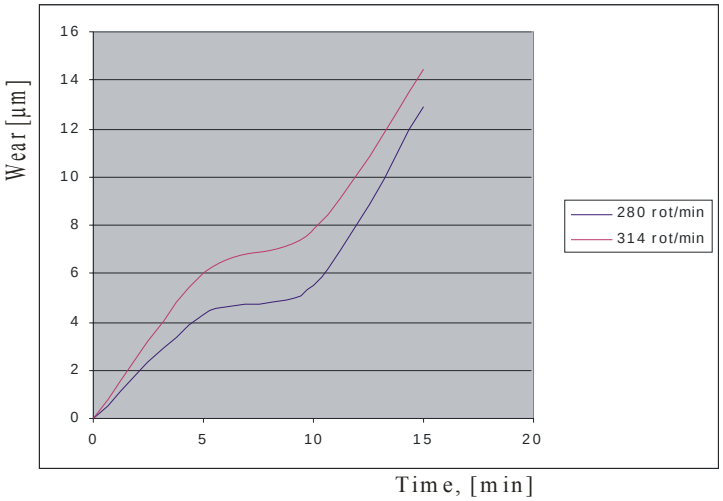

Fig.4. *The wear of the uncovered plates, during the turning of the OLC45 steel.*

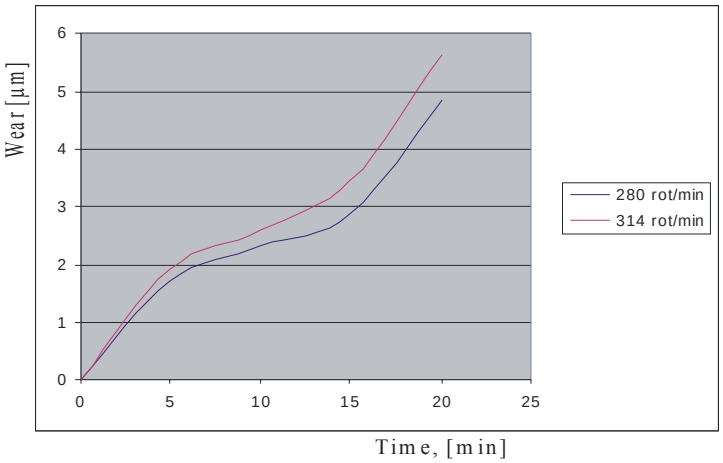

Fig.5. *The wear of the plates covered with TiN, during the turning of the OLC45 steel.*

5.Conclusion

Examining the shape of the durability curves depending on the cutting speed T = f(v) (figure 6) one can notice the fact that at the same time with the cutting speed growing the same durability of the layers during the working period deceases. This aspect is valuable both in the case of the covered plates and in that of the uncovered plates.

One can notice from the covered plates. The plates covered with titanium nitride behave better during the steel processing with a low content of carbon.

The durability of the covered plate is 2.3 bigger at low speeds and 3.1 times bigger at high speeds, compared with the uncovered plates, fact that indicates that the covered plates are more resistant to higher cutting speeds. When the covered plate wear with TiN gets the shape corresponding to the catastrofic wear, a sudden rise of this one takes place during a very short cutting period.

One can notice that when the wear of the TiN covered plate gets the shape corresponding to the catastrophic wear, a sudden rise of this one takes place in a very short cutting time.

This behaviour can be explained by the fact that in the limits of the rational wear. The hand layer resulted from coating surphasses and gets to the base material that does not resist any more to the high cutting speeds with which it had been worked.

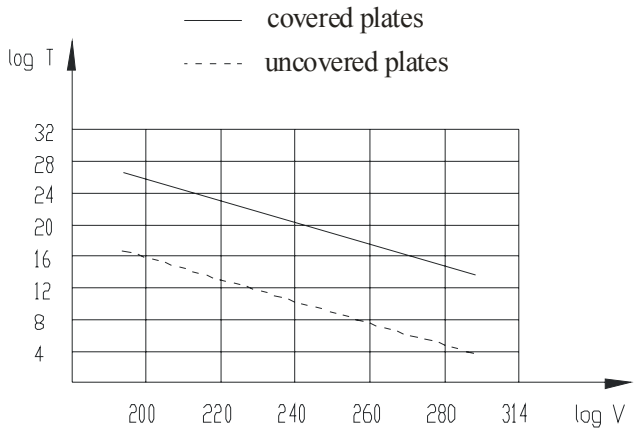

Fig. 6. *The durability T=f(V) for the TiN covered and uncovered plates during the turning of the OLC45 steel; s= 0,060 mm/rot; t=1,0 mm.*

References

[1]. R.V. Berry – *Thin Film Technology*, Van Nostran & Company, Princeton, New Jersey, Toronto London, 1970.
[2]. E. Moll and E. Bergman – *Hard Coatings by Plasma Assisted PVD Technologies*, Industrial Practice, Surface and Coating Technology, 37, 1989
[3]. J.L. Vossen – *Thin Film Processes*, Academic Press Inc., London, 1977
[4]. K. Ughiyama – *Performance of Cuttin Tool Treated by Physical Deposition Process*, Nachi Engineering Review, vol 35, 1979
[5]. STAS 5744-89 – *Protectia suprafetelor metalice prin acoperiri metalice si prin formarea de compusi chimici metalici*
[6]. Abruna H.D. -*In 'Electrochemical Iinterfaces. Modern Techiques for In-Situ Interface Characterization*' Ed.H.D. Abruna, Ithaca, New-York, VCH Publishers,
[7]. Bernard J.-*Adsorption on metal surface*, Elsemer, 1993.
[8]. Briggs D., Peach M.P. – Practical Surface analysis, 1994.
[9]. Ciocirdia C., s.a.-*Aliaje dure sinterizate den carburi metalice*, Ed. Tehnica, Bucuresti, 1984
[10]. Cahu R. W.-*Processing of Metals and Alloys*- vol. 15, New- York 1991
[11]. Wiley J., Sans N. Y.-*Practical Surface analysis,* 1993
[12]. Winand R.-*Application of Polarization Measurements in the Control of Metal Deposition* –Ed. I.H. Warren,Elsevier.

CORROSION RESISTANCE OF THE COMPOSITION MATERIALS SYSTEM (Cu–Al)–Mo, OBTAINED BY THE EB-PVD METHOD

V.GRECHANYUK, Y.ARTYUH

Kiev National University of Building and Architectures
Kiev, Ukraine

ABSTRACT

For development of new composition materials for the electric contacts, which would differ by high electric conductivity, mechanical properties, corrosive and erosion resistance in conditions of high temperature's influence, it is necessary to decide the task of choice optimum of composition of matrix alloy and dispersion inclusions of hardening phases.

KEYWORDS: corrosive and erosion resistance, EB-PVD method

1. Introducing

One of the most widespread methods of material's hardening is introduction of particles of the second phase to the metallic matrix. As is generally known from literature's data, traditional low-alloyed alloys on the copper basis, bronzes, containing a chrome, aluminum or tin, insignificantly reduce electric- and thermal conductivity of copper matrix and substantially multiply its mechanical properties [1].

2. Results of researches

In this papers the researches of composition materials on the basis of low-alloyed copper matrix and hardening phase of molybdenum were conducted, which obtained by simultaneous evaporation from independent crucibles, with subsequent condensation of vapor stream on substrate, heated to the temperature 700±20 °C are submitted[2].

As alloying addition to the copper matrix the aluminum additions of which were brought into copper matrix within the limits of formation of hard solution in accordance with the state diagram for given components was used, that is the hard-solution's hardening of copper matrix was used.

At alloying of copper matrix by an aluminum it's maintenance did not exceed 6 %. Such composition was chosen on a next considering, from one side, taking into account insignificant reduction of conductivity of the system Cu- 6% Al and with, other, – at maintenance of aluminum more than 6 % in vacuum condensates the new phase appears with the parameter of lattice a = 0.87952 nm, accorded for the composition of Cu_9Al_4 phase. The presence of the second phase multiplies heterogeneity of the system and is instrumental in the decline of its corrosive resistance.

At maintenance in a copper matrix a 6 % Al middle width of grain diminishes from 35 mcm in condensates of pure copper to 15 mcm in condensates Cu– 6 % Al, being hard solution of aluminum in the copper. This electric resistance is $7.6 \cdot 10^{-8}$ Ohm·m on comparison with the copper $1.69 \cdot 10^{-8}$ Ohm·m, micro-hardness of condensates multiplied and during concentration of aluminum to 6 % exceeds more than micro-hardness of pure copper in 3 times. It enables to assume that composition materials on the basis of the matrix alloy Cu– 6 %Al with enough high electric conductivity and mechanical property it is possible to use for producing of electric contacts.

The choice of molybdenum for dispersion hardening phase is conditioned to those, that it suits, produced to the dispersion phase in a matrix on the basis of copper. From literature's data, solubility of molybdenum in a copper in equal terms is practically was absence till 1300 K [3]. In addition, a molybdenum differs by the high temperature of melting, and low diffusive mobility in a copper matrix. It well moistens by copper, the corner of molybdenum moistening by pure copper is equal 0° [4], that indicates on high compatibility of dispersion inclusions of molybdenum with copper. The specific of important advantage of molybdenum's using is its low value electric resistance ($5.7 \cdot 10^{-8}$ Ohm·m), which approximately in 3 times is more than for copper, therefore it follows to expect that introduction of molybdenum to the copper matrix will not strongly conductivity's reduce of the system.

As solubility of molybdenum in a copper is insignificant, that introduction to condensate of the system Cu- 6 % Al additions of molybdenum results in formation of heterogeneous structure. According

to the results of X-ray analysis, formation in condensates α- hard solution on the basis of copper and molybdenum was found out.

The values of periods of lattices of hard solution on the basis of copper, definite by a X-ray analyze, are showed in the table 1. Hard solution of matrix of copper-aluminum alloy have face-centered cubic lattice (fcc), similar to the pure copper the parameters of which are multiplied with the rise of maintenance of aluminum, that as atomic radius of aluminum on 10 % is more than atom's radius of copper.

Table 1

Composition of samples, mass.%			**Parameter of lattice *a*, nm**	
Cu	**Al**	**Mo**	**initial sample**	**after annealing, at 750°C, during 1 hour**
100	-	-	0.36189±0.00009	0.36182±0.00011
base	6	-	0.36592±0.00011	0.36589±0.00014
base	6	2	0.36574± 0.00009	0.36611±0.00026
base	6	4	0.36586±0.00022	0.36581±0.00024
base	6	6	0.36563±0.00014	0.36569±0.00015
base	6	10	0.36550±0.00015	0.36542±0.00032
base	6	12	0.36527±0.00013	0.36503±0.00025

Reduction of value of period of lattice for the system (Cu- 6% Al)- Mo with the increase of maintenance of molybdenum can be accounted for by formation of hard solution of aluminum in a molybdenum.

X-ray analyze are confirmed by electronic-microscopic researches (fig. 1). Researches of structure showed that size of grains of hard solution (Cu- 6% Al) in the system (Cu- 6%Al)- 2% Mo does not exceed 1.3 mcm.

In grains the dispersion particles of molybdenum, which size does not exceed 20-300 nm. Increase of molybdenum maintenance in the system (Cu- 6% Al)- Mo till 10 % results in the substantial growing of grains from 0.1 to 0.3 mcm, are evenly distributed, here the size of dispersion inclusions of molybdenum is multiplied to 50-2000 nm.

Corrosion resistance of the system (Cu- 6% Al) -Mo was studied by the gravimetric method in the distilled and plumbing water of middle inflexibility ($7 \cdot 10^{-6}$ mol-eqv./l) by standard method [5]. Time of test was 100 hours, measuring made each10 hours.

The gravimetric researches of corrosive resistance of composite (Cu- 6% Al) -Mo showed that insignificant maintenance of molybdenum (till 1 %) corrosive resistance same by level of the system Cu- 6% Al. With the increase of maintenance of molybdenum in the system (Cu- 6% Al)-Mo loss of mass diminish both in plumbing, and in the distilled water. This phenomenon is conditioned by reduction of dissolution of aluminum in connection with the presence of other metal with negative potential which competition and also participates in formation of galvanic couple with a copper. In behalf on such presentation the increase of concentration of molybdenum testifies in a corrosive environment (to water) after 100 hours of tests (table 2).

Table 2

Mode:	**Composition of environment, mg/l**			**ρ, Ohm·m**	**pH**
	Cu	**Al**	**Mo**		
initial plumbing water	1.94	0.05	3.5	$3.8 \cdot 10^{-6}$	7.43
plumbing water after 100 hours of test	1.71	0.034	9.74	$3.92 \cdot 10^{-6}$	7.77
initial distilled water	2.71	0.25	0.60	$9.27 \cdot 10^{-8}$	6.55
distilled water after 100 hours of test	2.33	0.27	3.05	$3.6 \cdot 10^{-7}$	7

Electrical conductivity of environment appropriately increases with the increase in solution of ions of molybdenum, pH increase because of that salts appearing at cooperation with carbon acid give the alkaline reaction. It should be noted that in the distilled water there is greater reduction of mass of standards, on comparison with plumbing water, in however the character of change of motion of curves

depending on concentration of molybdenum remains identical for two environments.

Except for marked factors to reducing of losses of mass in the system (Cu- 6% Al)- Mo with the increase of maintenance of molybdenum has influence appearing on the surface of insoluble salts, which arise up because of cooperation of more electronegative aluminum with carbon acid appearing in investigation of dissolution of carbon dioxide from an atmosphere in water.

Conclusions

Introduction of molybdenum to the alloy (Cu-6%AI) is instrumental in the increase of mechanical properties and results in growing of structure's dispersion.

Corrosion resistance of the system (Cu- 6% Al)- Mo relies on maintenance of the entered components.

References

[1]. Arzamasov B., *Construction materials: reference book by red*. – M: 1990. - 687 p.

[2]. Movchan B., Malashenko I. *Heat-resisting coating, deposited in vacuum*. K: 1983. – 230 p.

[3]. Eroshenko I., Zaharov A., Olenicheva V. *Diagrams of the state of metallic system*. M: 1983. - 531 p.

Naydich Y. Contac's phenomena in metallic fusions. K: 1972.– 196 p.

[4]. *Compatible method of laboratory tests of efficiency of inhibitors of corrosion in the water system*s. – Riga: 1980. – 29 p.

EXPERIMENTAL RESEARCH OF SINTERED POROUS MATERIALS OF BRONZE POWDERS

I.VIDA-SIMITI, N. JUMATE, T. BOLOG, G. BATIN

Technical University of Cluj-Napoca,
e-mail: ivida@personal.ro

ABSTRACT

Porous sample were fabricated by sintering of bronze (Cu Sn10) with different particle size range. The paper investigates the influence of the particle size distribution, temperature and sintering time on the structural characteristics (porosity, pore size, dimensional changes) of the porous parts studied. A porous structure with small-sized pores and a uniform distribution of the pore sizes is obtained in conditions of a narrow range of particle size distribution, small size of the powder particles and optimal sintering parameters.

KEYWORDS: porous materials, sintering materials, bronze powders.

1.Introduction

Porous elements obtained by Powder Metallurgy methods are used with excellent results as filters, flame arresters, noise suppressors, distributors of gases in fluids, electrochemical catalyzers etc.

A uniform porous structure with small sized pores ensures the main conditions required for these applications.

Structural parameters (porosity and size of pores) are influenced by the following technological processing parameters: the powder size range, compacting pressure, sintering temperature, sintering time [1,2,3,5,6,7]. A previous paper [8] studied the influence of the compacting pressure on the porous structure parameters of permeable sintered materials from 316 L stainless steel powder.

This study provides new comparative results regarding the influence of powder size ranges of free bronze sintered powder on the permeable porous structure in conditions of changing the sintering time .

2.Experimental method

Porous samples in the shape of disc tablets, 25 mm diameter and approximately 2 mm thickness, were made by sintering from free bronze powder poured into a matrix. The powder size ranges and thesintering time were the technological parameters that were changed in order to study their influence on the main structural characteristics.

Sintering was performed in a vacuum oven ($5*10^{-5}$ torr) at a relatively low temperature of 750^0C in order to ensure the intercommunicating characteristic of the pores and to avoid their closure in case of intensive sintering conditions.

The powder size ranges obtained by sifting and selected for the samples were: -40 μm; (+40 - 63) μm; (+63 - 80) μm; (+80 - 100) μm; (+100 - 125) μm; (+125 -160) μm.

During sintering the samples were maintained for 30, 45 and 60 minutes.

The porous structure was examined by a scanning electron microscpe (JEOL 5600 LV) and microphotos were obtained. The porosity of the samples with regular geometric shape was determined by calculation, based on their weight and calculated volume.

3.Results and discussion

Experimental sintering tests were performed at 850^0C, according to prescriptions found in literature [6]. It was found that the powder samples of high powder size ranges were melted and underwent marked contractions (fig.1).

Using the temperature of 750^0C, sintering was performed for 30, 45 and 60 minutes. It was found that at sintering time s of more than 45 min. the powder size ranges (100 - 125 μm; 125 -160 μm) were highly contracted (fig.2).

This may be explained by the fact that with vacuum sintering the heat transfer is mainly by thermic radiation. Due to the high porosity of the free powder having a powder size between 100 - 125 μm and 125 -160 μm, the "absorbant black body" phenomenon occurs.

A certain part of the thermic radiation is absorbed by the sample material, a part is reflected by the sample surface and another part penetrates into the pore cavity where heat accumulates, leading to the

local temperature increase. The diffusion process at the level of the sintered bridges is enhanced. The increase of the temperature by 20^0C practically doubles the diffusion coefficient and triggers the transfer of material around the bridges between particles. Consequently, the effect of local temperature increase following the heat transmission by radiation leads to intensified sintering, reduction of porosity and increase of contractions.

Fig. 1. *Bronze powder samples sintered at 850^0C*

Fig. 2. *Bronze powder samples sintered at 750^0C*

This accounts for the high contraction in the powder samples with powder size s between 100 – 160 µm.

Figure 3 graphically presents the influence of the sintering time on the total contraction of samples for all the powder size rangees studied at a constant sintering temperature (750^0C). High contractions may be noted with powder size rangees (+100 - 125) µm; (+125 -160) µm.

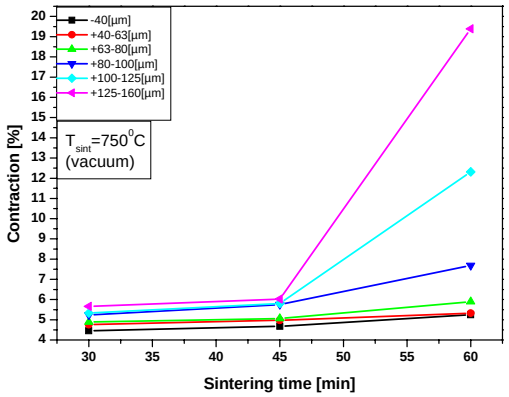

Fig. 3. *The influence of sintering time and powder size on the contraction*

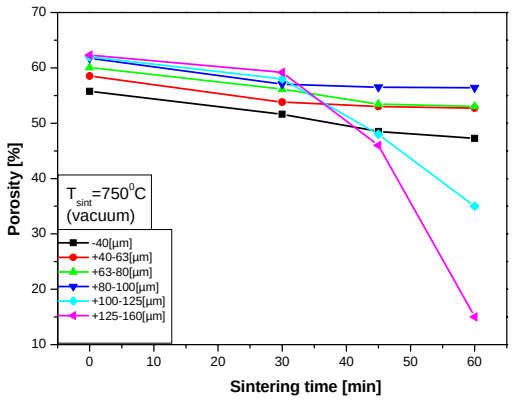

Fig. 4. *The influence of sintering time and powder size on the porosity*

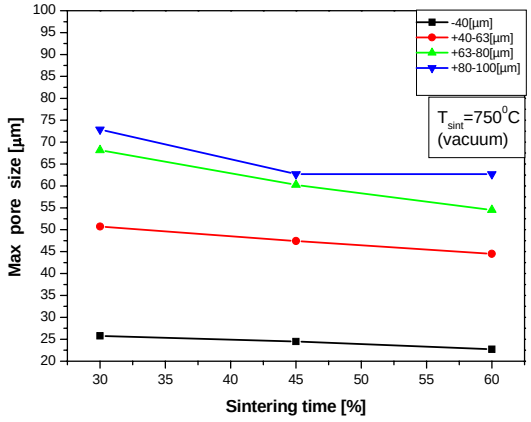

Fig. 5. *The influence of sintering time and powder size on the maximal pore size*

A more marked reduction of the porosity in the -40 μm powder size range (fig. 4) may be accounted for by the initially higher degree of packing of the small particles. The same findings are expressed by figs. 5 and 6, which show the variation of the size of the largest pore and the average pore size respectively in relation to the sintering time . The pore size undergoes small, even insignificant changes when sintering time increases. The mechanism of material transfer around the inter-particle bridges during sintering is not very intense. Consequently the pore size does not decrease too much with sintering time.

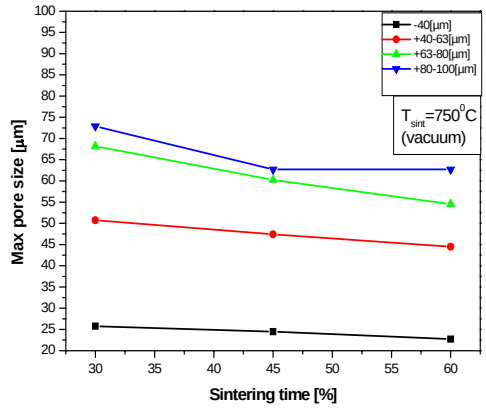

Fig. 6. *The influence of the sintering times and powder powder size on the average pore size*

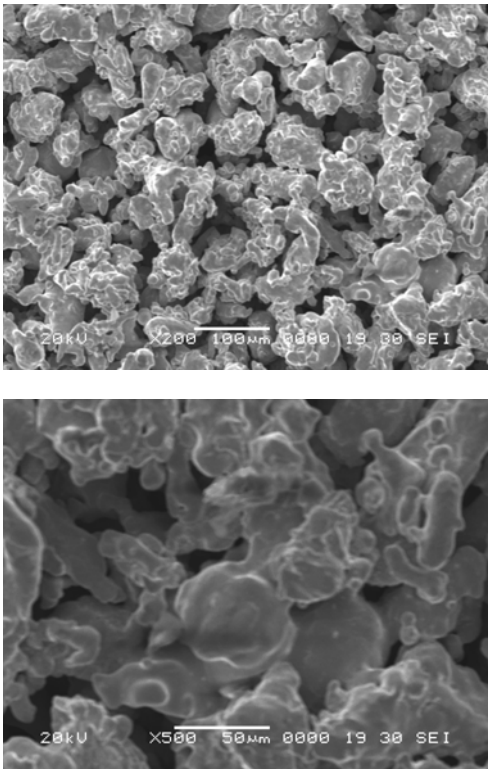

Fig. 7. *SEM image (x 500) of the bronze porous structure (45 mon.)*

The SEM images (fig.7) of the porous structures evidence the fact that the pore size and the inter-particle bridges reduction are not significantly changed. However, it may be noticed that the particle surface is smooth, following the material transport into the superficial layer by sintering. The surface defects and the roughness disappear following the sintering mechanisms.

Fig. 7 shows the image of the porous structure of the sample made of +63 – 80 μm granulometric powder sintered for 45 minutes.

The images evidence the inter-particle bridges formed after sintering only in the small areas of initial contacts between the free powder particles.

The narrow powder size ranges, formation by free spreading into the mold as well as the relatively low sintering temperature (750^0C) ensures a uniform porous structure with intercommunicating pores, favourable to fluid flow and filtration.

Conclusions

The sintering time has a marked influence on the porous structure parameters (porosity, pore size) in the case of the samples sintered from free bronze powder with (-100 – +160) μm.powder size .

Thesintering time does not influence the porous structure parameters (porosity, pore size) significantly in the samples obtained from free powder with (-40 – 100) μm powder size .

By sintering the powder particle surface becomes smooth, due to the transport of substance into the superficial layer of the material.

References

[1]. Albano-Müller, *Filter Elements of Highly Porous Sintered Metals*, Powder Metallurgy International, 1982, 14, **2**, 73-79.
[2]. M. Bram, H. P. Buchkremer, D. Stöker, *Development of Porous Composites Membranes for Microfiltration Devices*, Conference Proceedings, Euro P M 2004, 183-188.
[3]. I. N. Podrezov, *Structural Engineering of High-Porous PM Materials, Conference Proceedings*, EuroPM 2004, 125 – 130.
[4]. P. Neuman, *Porous Metal Structures Made by Sintering Processes and Applications*, Mat. Wiss. u. Werkstofftechn, 2000 (**31**), 422.
[5]. O. I. Getman, L. I. Chernysher, *The Porous Structure of a Permeable Nickel Material with a Bimodal Pore – Size Distribution*, Powder Metallurgy and Metal Ceramics, 2003, (42),11-12, 630-637.
[6]. I. Vida-Simiti, *Sintered Permeable Materials* (in roumanian), Ed. Casa Cărții de Știință, Cluj-Napoca, 1998.
[7]. A. Palfalvi, I. Vida-Simiti, I. Chicinaş, *Influence of Porosity on the Mechanical Characteristics of Sintered Porous Stainless Sheets*, Powder Metallurgy International, 1998, **4**, 16-19.
[8]. I. Vida-Simiti, *Researches on Some Characteristics of The Permeable Porous Structures from Sintered Powders* (in roumanian), Construcția de Mașini, București, 1997, 11, 1-4.

RESEARCHES REGARDING IMPROVEMENT OF THE FATIGUE LIMIT BY HEAT TREATMENTS OF THE AL-ALLOYS FOR AERONAUTICS INDUSTRY

Ana DONIGA, Elisabeta VASILESCU, Miltiade ISTRATE, Ioan VASILESCU, Silviu MACUTA

"Dunarea de Jos" University of Galati
e-mail: doniga.ana@ugal.ro

ABSTRACT

The laboratory experiments were made on the two aluminium alloyed qualities used for aeronautical industry. The structure and mechanical characteristics were analyzed and the gotten results were compared using those two types of the thermal treatments. Also, the conventional thermal treatment was used, consisting of the solution quenching and artificial heat ageing, mode in more working condition. A significantly improvement of the mechanical characteristics was ascertained to the thermical treated test-specimen.

KEYWORDS: thermomechanical treatment, aluminium alloy.

Introduction

The special aluminium alloys are complex systems where the alloying elements: Mg, Si, Cu, Mn, Zn set up solid solution with aluminium, thus improving, the plasticity characteristics.

When the content of the alloying elements is low, the gotten solid solution is stable at any temperature, and the growth of the mechanical characteristics is moderated one.

At higher percentage of the alloying elements, the gotten solid solutions are metastable at the environmental temperature and, consequently, the alloys might be structural hardened by some components precipitation from the solid solution, that determinate an important increase of the alloy strength but with some decrease of the plasticity.[1]

This structural hardening could be achieved by some thermal treatment, applied only to certain alloys which are grouped in aluminium alloys *hardened by thermal treatment*, known as duralumin; The alloying elements are forming the resoluble compounds at heating, for example: $CuAl_2$, Al_2CuMg, Mg_2Si as well as non-soluble compounds Fe, and Mn as: $(Mn,Fe)Al_6$, Al_7Cu_2Fe.

In annealing condition the duralumin consists of the solid solution and secondary precipitated compounds. Heated at about 500^0C, $CuAl_2$ and Mg_2Si are dissolved in Al while Mn and Fe compounds are not.

By quenching, from this temperature, the alloy will consist of suprasaturated solid solution and Fe and Mn compounds. As result, the thermal treatment, typical to Al complex alloy are the hardening (quenching) in solution and the heat (artificial) ageing.

By heat ageing, the compound precipitation of the solid solution is achieved, determining an hardening of the alloy, a growth of the strength characteristics, respectively, with a slight plasticity dropping. The temperature range, both, for quenching and heat ageing, is large enough, in accordomewith the alloy type (alloys elements) and the characteristics that should be gotten. Thus, for aluminium alloys processed by plastic deformation, the temperature range for solution quenching is 450 – 540^0C and for heat ageing is between 90 – 160^0C. [2]

2.Materials and working conditions

The experiments have been made on Al-Zn-Mg-Cu aluminium alloys, for aeronautics having chemical composition shown in table 1.

Table 1. *Chemical composition of Al-Zn-Mg-Cu alloys (%)*

Cu	Zn	Pb	Fe	Mn	Si	Mg
1.219	2.470	0.0025	0.290	0.470	0.310	2.06

During the laboratory experiments more thermal treatments ranges have been used as quenching in solution and heat ageing with different parameters (temperature and holding time) in accordance with table 2 and figure 1.

Table 2. *Experimental conditions of the thermal treatments*

No.	Heating temperature (^{0}C)	Time (hours)	Cooling	Artificial ageing temperature (^{0}C)	Time (hours)	Hardness HB
1	500	0,5	water	120	12	81
2	500	1	water	120	12	85
3	500	2	water	120	12	102
4	500	4	water	120	12	112
5	500	2	water	160	12	98
6	500	2	water	200	12	80
7	500	2	water	120	6	81
8	500	2	water	120	8	89

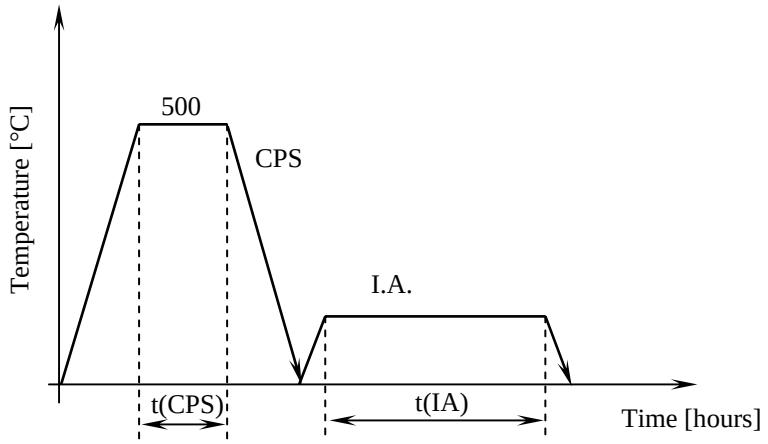

Fig.1 *Variant thermal treatments applied on alloys Al-Mg-Zn-Cu*

3.Experimental results

In the paper framework three variant ways of the thermal treatment have been studied:

a) The influence of the holding time, for quenching in solution, on the hardness.

The following operation have been made:

- heating for 500^{0}C quenching in solution;
- various time of holding (t = 0,5; 1; 2; 4 hours);
- 80^{0}C cooling in water;
- heat (artificial) ageing 12 hours at 120^{0}C.

The gotten results are shown in figure 2.

A light growth of the hardness results to holding time.

b) The influence of the heat (artificial) ageing holding time on the hardness. The following condition had been carried out:

- quenching in solution (500^{0}C, 2 hours holding, cooling in water);
- 120^{0}c heat (artificial ageing; holding time: 6; 8; 12 hours).

The hardness have been measured (fig 3).

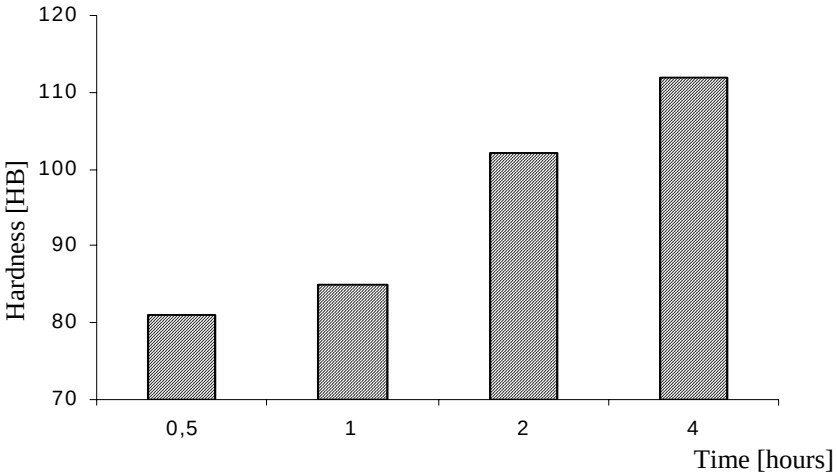

Fig.2 *Hardness variation to the heating time for quenching in solution.*

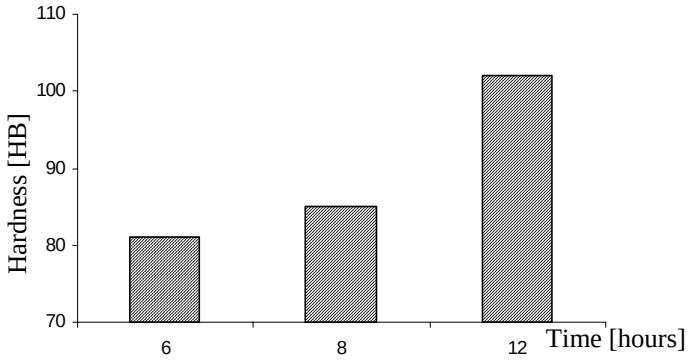

Fig.3 *Hardness variation to the artificial ageing holding time*

A light growth of the hardness with holding time is established (hardness values are very near ones).

c) The influence of the ageing temperature on the hardness, in the following conditions:
   - quenching in solution (500^0C, 2 hours, cooling in water);
   - artificial ageing, 12 hours, at various temperature: 120^0c; 160^0C; 200^0C.

The gotten hardness have been recorded in figure 4.

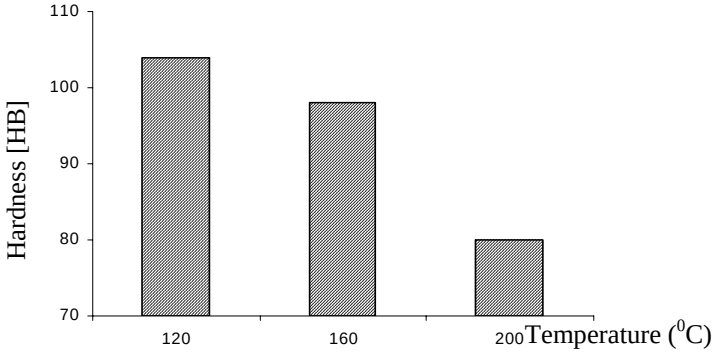

Fig.4 *Hardness variation to ageing temperature.*

A light lowering of the hardness to the growth of the ageing temperature was resulted.

The hardness increase during such treatments a) and b) variant ways is determined by the partly dissolution of the secondary phase precipitates into solid solution, during quenching into solution and, later-on, by the reprecipitation during artificial ageing. By these condition, the getting of certain grain-size and their uniform distribution is watched. The precipitates carrying-out is determining a material hardening.[3]

An increase of the holding temperature could determinate a hardness lowering due to the begining of the coalescence proces of the precipitates (fig.4). These phenomena are, evidently, due to microstructure aspects too, as could be seen in figure 5.

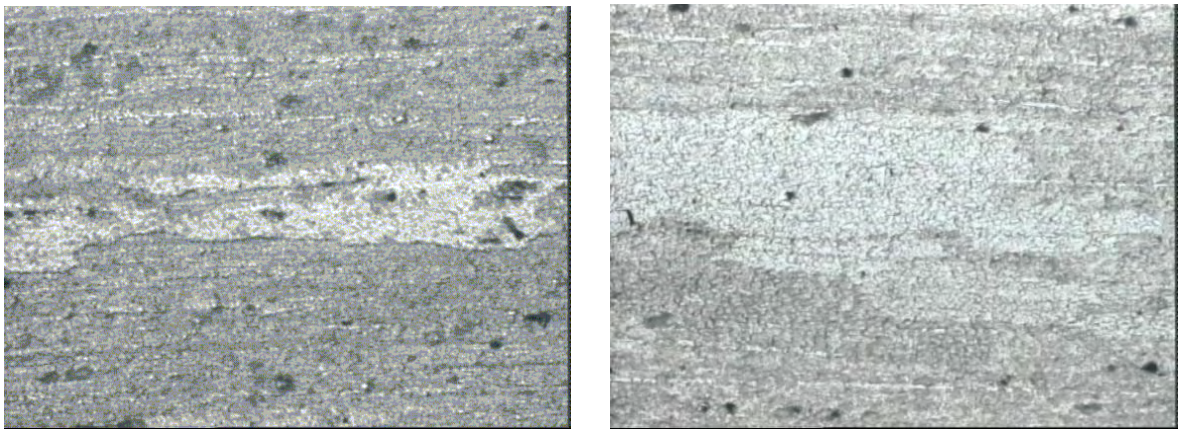

a b

Fig.5 *The microstructure aspect after thermal treatment (magnification x500)*
a) 120^0C ageing temperature; b) 200^0C.

Conclusions

The following conclusions have been resulted from the experiments:
holding time of the quenching in the solution is determining a light growth of the hardness;
heat (artificial) ageing influences the hardness by the heating temperature and holding time;
- for Al-Mg-Zn-Cu type alloys, the treatments of the quenching in solution and artificial ageing are characteristics ones leading to the strength growth, on the one hand, and to the good corrosion and fatigue resistence of the material, on the other hand.

References

[1] Popescu N., - *Tratamente termice neconventionale* ET – Bucuresti 1990
[2] Dulamita T., Florian E, - *Tratamente termice si termochimice* EDP – Bucuresti 1982
[3] Cazimirovici E.,-*Laminarea aliajelor speciale* Ed. BREN 1998.

PHYSICO-MECHANICAL CHARACTERISTICS OF HARD ALLOYS MADE OUT OF MANY CARBIDES

Stela CONSTANTINESCU

"Dunarea de Jos"University of Galati,
e-mail: Stela.Constantinescu@email.ro

ABSTRACT

The Hard alloys of type WC-TiC-Co can be used to process materials with long chips, such as steels [1].

Titanium carbide or TiC-WC solid solutions, added as alloying constituents in the compositions of WC-Co pseudo-alloys increases their corrosion resistance, hardness and refractoriness.

Moreover, the thermal conductibility of WC-TiC-Co alloys and their tendency to weld the chips is an indisputable quality in favor of the cutting process of steels and other metallic materials with long chips. The physico-mechanical characteristics of WC-TiC-Co alloys vary with the increase of titanium carbide amount.

In the factory programme of prestigious manufactures of hard alloys, made out of sintered metallic carbides, the alloys of type WC-Ti-Co have been replaced by the alloys type WC-TiC-TaC(NbC)-Co, intended to cutting process of steels. Of course, this is due to better endurance and cutting process performance. Alloys of type WC-TiC-TaC-Co offer better mechanical strength and also better craking strength values. These alloys are used both in cutting long and short chip materials, due to their characteristics and forming the so called universal alloys.

KEYWORDS: density, hardness, bending fracture strength, thermal conductibility, coefficient of thermal expansion, magnetization up to saturation.

1. Introduction

Hard alloys made out of metallic carbides manufactured to an industrial scale for cutting processing can be divided in two categories, according to their use. The second category of industrial products comprises the alloys out of many carbides used in cutting process of materials with long and continuous chips (all sorts of steel).

According to chemical composition, there are the following types of alloys: WC-TiC-Co; WC-TaC(NbC)-Co and WC-TiC-TaC(NbC)-Co.

Alloys based on many carbides with small or medium amount of TiC or TaC(NbC) can also be used for cutting materials with short chips and this way the so called "universal alloys" have emerged. These alloys can be used to cut any material, under certain cutting conditions. Almost all the sintered hard alloys made out of metallic carbides comprises a high amount of ternary or quaternary carbide type WC-TiC-TaC(NbC)-Co instead of secondary WC-TiC-Co or WC-TaC-Co. The specialised literature shows that the composition that offers the optimum tenacity values is: 50-70%WC, 3-10%TiC, 10-35%TaC and 5-15%Co.

This composition offers a better cracking strength than the alloys type WC-TiC-Co and a generally better endurance of the tool than WC-TaC-Co.

Hard alloys made out of carbides type WC-TiC-TaC-Co have been sucessfully inserted in the factory programmes of prestigious manufacturers worldwide in order replace the alloys based on only two carbides. It has to be emphasized that, due to higher costs of tantalum carbide and tantalum itself, the alloys containing quaternary complex carbides type WC-TiC-TaC(NbC)-Co are more expensive than the alloys containing only binary carbides type WC-TiC-Co.

2.Researching and experimental results

The density of pure titanium carbide TiC (4.90g/cm^3), considerably lower than the density of tungsten carbide (15.7g/cm^3) influences the density of the alloys type WC-TiC-Co, decreasing with the increase of TiC amount (fig.1).

Due to possible content of undesirable elements of TiO or TiN to be found in the titanium carbide or in the TiC-WC solid solutions, micropores can emerge and density measurement has to be done not only for sintering degree purposes, but also for the purity of the WC-TiC-Co alloys.

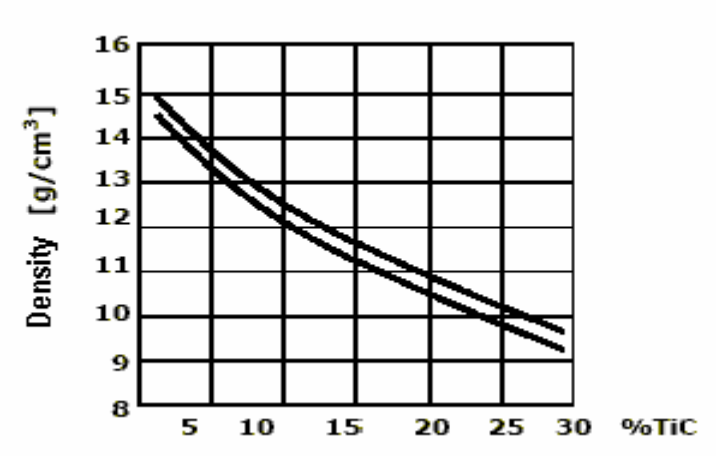

Fig.1 . *The dependence of WC-TiC-Co alloy density with the amount of titanium carbide (TiC%)*

Table 1 . *Compositions and characteristics of WC-TiC-Co alloys*

Composition %			Density [g/cm³]	Hardness HRA	Hardness Vickers [daN/mm²]	Banding cracking strenght [daN/mm²]	Compression stregth [daN/mm²]	Thermal conductibilit [cal/cms°C]	Coeff. of thermal expans. [10⁻⁶/°C]
WC	TiC	Co							
94	1	5	14,5-14,7	90-91	1500-1600	140-160	557	0,19	5
87,5	2,5	10	14,0-14,2	89-90	1400-1500	160-178	458	0,16	-
84,5	2,5	13	13,7-13,8	87-89	1300-1400	178-200	447	0,15	5,5
86	5	9	13,2-13,4	89-91	1450-1550	150-160	458	0,15	5,5
82	5	13	12,8-13,0	88-90	1350-1450	160-178	-	-	-
82	10	8	11,8-12,0	90-91	1500-1600	150-170	-	0,079	-
78	14	8	11,1-11,3	90-91	1550-1650	130-140	417	0,08	6,2
78	16	6	11,0-11,2	90-91,5	1600-1700	110-124	427	0,09	6
76	16	8	10,9-11,1	90-91	1550-1650	120-130	-	0,069	6
69	25	6	9,6-9,8	91-92	1650-1750	90-110	-	0,05	7
61	32	7	8,7-9,0	92-93	1650-1750	79-100	408	0,04	-
34	60	6	6,5-6,8	92-93	1750-1850	70-79	388	0,03	7,5

The dependence of physico-mechanical characteristics of WC-TiC-Co alloys with the increase of TiC amount is given in the table nr.1 [2]-[3].

Hardness of WC-TiC-Co alloys is affected by a large number of elements connected to the raw material, purity and component dispersion in the pseudo-alloy and the solid solution quality and grain size of components.

In the factory process, these elements are playing an ultimate role in effective hardness measurement of the material with a given chemical composition (fig.2).

Generally speaking, the hardness of WC-TiC-Co alloys increases with the TiC amount and decreases with cobalt amount increasement (fig.3).

The bending cracking strength values of WC-TiC-Co alloys decreases with the TiC amount increasement , this decreasement can only partially be counter-balanced by cobalt amount increasement.

The compression strength oh WC-TiC-Co alloys decreases with the TiC amount increasement.

Fig.2. *Metallographic appearance of pseudo-alloy with 80%WC, 12%TiC, 8%Co, x1500*

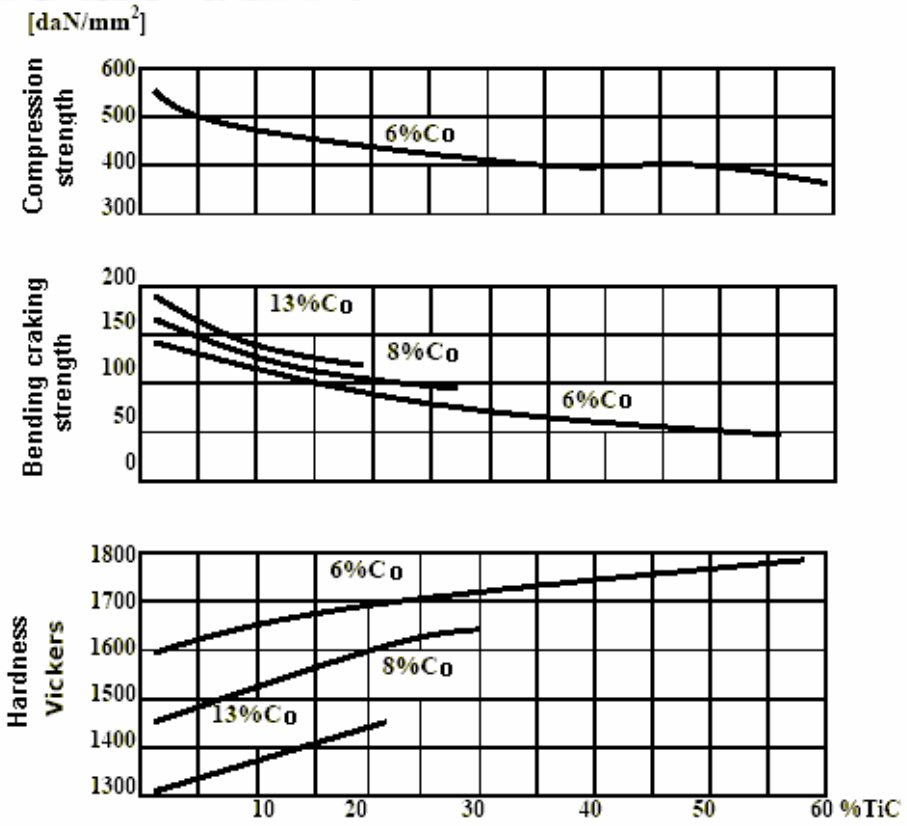

Fig.3. *The dependence of hardness, bending cracking strength and compression strength with the amount of titanium carbide (TiC%)*

The titanium carbide is a weak thermal conductor – the thermal conductibility of WC-TiC-Co alloys is lower than of WC-Co avearange alloys and keeps decreasing with TiC amount increasement. Tabel nr.1 shows the values of thermal conductibility of certain WC-TiC-Co compositions. For purposes of comparison, it is specified that the thermal conductibility value of rapid steels is 0.6[cal/cm s ^{o}C].

The coefficient of thermal expansion increases with titanium carbide amount increasement, but is smaller than that of rapid steels in all the WC-TiC-Co alloys.

The magnetic characteristics of WC-TiC-Co alloys are given in the tabel nr.2. Since the titanium carbide is not ferromagnetic, the magnetization up to saturation decreases with TiC amount increasement in the alloy. Thus, the values of the magnetization up to saturation, together with those of coercive force can describe the TiC amount of alloy.

.

Table 2. *The magnetic characteristics of WC-TiC-Co alloy*

Composition, %			Magnetization to saturation $4\pi\sigma$	Coercitive force HC
Wc	TiC	Co		
88	3	9	160-165	185
88	5	7	107-112	120-130
78	14	8	140-145	100-110
78	16	6	97-100	100-110
69	25	6	89-92	80-90
34	60	6	89-95	70-80

Consequently to those showed above, as well as due to a better corrosion resistance values of WC-TiC-Co alloys compared to average alloys [4], [5], there results in a better cutting processing behaviour of the first mentioned.

In the factory programme of prestigious manufactures of hard alloy, made out of sintered metallic carbides, the alloys of type WC-TiC-Co have been replaced by the alloys type WC-TiC-TaC(NbC)-Co, intended to cutting process of steels (fig. 4).

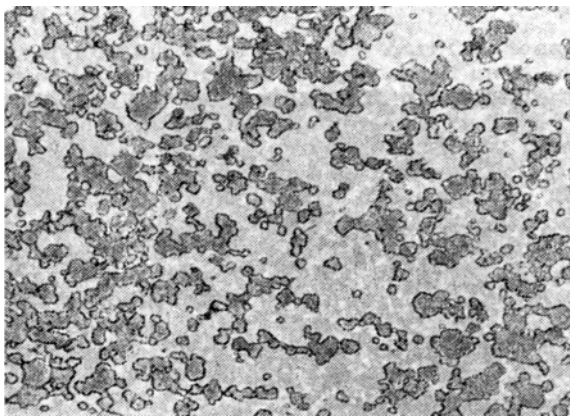

Fig 4. *The metalographic aspect of the pseudo alloy*
11% TiC, 14% TaC(NbC), 8% Co si 67% WC, x1500

Of course, this is due to better endurance and cutting process performance. Alloys of type WC-TiC-TaC-Co offer better mechanical strength and also better craking strength values. These alloys are used both in cutting long and short chip materials, due to their characteristics and forming the so called universal alloys.

3.Conclusions

The density of WC-TiC-Co alloys decreases with TiC amount increasement.

The hardness of WC-TiC-Co alloys increases with TiC amount increasement and decreases with cobalt amount increasement.

The bending cracking strength of WC-TiC-Co alloys decreases with TiC amount increasement. The compression strength of WC-TiC-Co alloys decreases with TiC amount increasement. The thermal conductibility WC-TiC-Co alloys keeps decreasing with TiC amount increasement. The coefficient of thermal expansion increases with titanium carbide amount increasement. The magnetization up to saturation decreases with TiC amount increasement in the alloy. Hard alloys made out of carbides type WC-TiC-TaC-Co offer better cracking strength than the alloys type WC-TiC-Co and a generally better endurance of the tool than WC-TaC-Co.

References

[1]. Mitoşeriu O., Constantinescu S., ş.a., *Advanced methods of investigation the properties of metallic materials*, Universitatea „ Dunărea de Jos „ Galaţi 1998 .

[2].Constantinescu S.,Radu T., *Advanced methods of obtaining thin coats,* Ed.Ştiinţifică F.M.R.Bucureşti, 2003

[3]. Constantinescu S., *Metals properties and physical control methods* ,Didact. and Pedag. Publishing House , Bucharest , Romania , 2004

[4].Chiriac A.,Tadu T.,Constantinescu S., *Nonferrous alloys: structure and properties ,* Ed.Ştiinţifică F.M.R.Bucureşti, 2004.

[5]. Ciocârdia C., Drăgulănescu E.,şi I., *Hard sintered alloys made from metallic carbons* ,Ed. Tehnică , Bucureşti, 1985 .

[6]. Moroşanu C., *Chemical deposition of thin coats by vaporizing* ,Ed. Tehnică , Bucureşti, 1981 .

THE ANNALS OF "DUNAREA DE JOS" UNIVERSITY OF GALATI
FASCICLE IX METALLURGY AND MATERIALS SCIENCE, ISSN 1453 – 083X. NR 2 – 2005

LASER CLADDING OF HIGH-SPEED STEEL ON A STEEL SUPPORT

Dan Teodor LEVCOVICI[1], Radu BOICIUC[1], Sanda Maria LEVCOVICI[2], Constantin GHEORGHIEŞ[2]

[1]S.C. Uzinsider Engineering S.A. Galați,
[2]University "Dunarea de Jos" of Galați,
e-mail: dan.levcovici@uzineng.ro,

ABSTRACT

Multilayer cladding by injection of high-speed steel powder with 0.82%C, 4.7%Mo, 6.4%W, 4.1%Cr, 2.02%V, 0.3%Mn, as chemical composition, in melted bath by CO_2 continuous wave laser connected to x-y-z coordinate table was tested in order to increase the wear resistance and heat proving of tool active surfaces made of 0.45%C steel. Layers made by different laser running were characterized by macro and microstructure analysis, as well as phase quality analysis by X ray diffractometry, microhardening analysis and hardness finding on coated layer surface in order to establish the optimal cladding run. Lathe tools made by this procedure showed a good behavior when steel shaping.

KEYWORDS: laser, cladding, high-speed steel, tool, powder, injection.

1. Introduction

In case of making the lathe tool of high-speed steel, an important part of tool body is not used during the facing process but only for setting it into the tool machine. A solution that removes this disadvantage is represented by cladding [1, 2, 3, 6, 7, 8] the high-speed steel in the active area of lathe tool made by carbon steel.

Therefore, the multilayer cladding was made by high-speed steel powder injection in melt bath by CO_2 continuous wave laser connected to x-y-z coordinate table.

High-speed steel powder as addition material mainly with 0.82%C, 4.7%Mo, 6.4%W, 4.1%Cr, 2.02%V, 0.3%Mn was used as prior researches emphasized a higher capacity of this material to be quenched since liquid phase, like specific case in laser cladding. [4].

Carbon steel was used like base material. Optimal running found by laboratory testes were used in order to make several lather tools by laser cladding. These lathe tools presented a good behavior when steel facing.

2. Experimental conditions

„M2 Coldstream B-7800, Sweden" powder with 0.82%C, 4.7%Mo, 6.4%W, 0.3%Mn, 4.1%Cr, 0.32%Si, 2.02%V, Fe balance, as chemical composition for cladding was used. By sieving the granulometric fractions, inside the 80÷90 μm range, were separated in order to be used as addition material. Powder had spherical shape, therefore, it provided a fluid floating of addition material through the injection system. Powder dried at 110°C for 15 minutes before addition material feeding inside the injection system tank. Coatings were performed on 25 x 25 x 15 mm^3 samples made of 0.45% C carbon steel in improved condition.

Laboratory trials were performed in a CO_2 continuous wave laser installation as GT type of 1400 W (made in Romania), with coordinate working table and running computer program, provided by dust injection system onto laser melted surface. For laboratory tests an 1100 W power laser beam with 1.8 mm in diameter on machined surface was used, by which parallel strips partly superimposed cladded. Final cladding layer thickness resulted by

superimposing of 5 layers. In order to establish the optimal laser deposit running the addition material flow and the sweeping speed of charging surface as well as transverse motion pass varied. In table 1 layers running conditions and thickness for several experimental running are given.

Table 1: *Experimental conditions and layers thickness.*

Code	AM flow [mg/s]	v [mm/s]	p [mm]	h [mm]
1	251	7	1.5	3.82
2	251	9	1.5	2.29
3	134	5	2	1.50
4	251	5	1.5	3.59
5	119	5	1.5	2.09
6	119	5	1	1.49
7	134	7	2	1.74

Note: AM - added material flow, v - sweeping speed, p - trransverse motion pass, h - layer thickness.

Cladded layers were tested by: macroscopic analysis on deposited layer surface as well as in cross section to laser processing direction after its metallographic preparation, chemical analysis by spectral methods, microstructure analysis and $HV_{0.98}$ (0.98N load) microhardness profile drafting in cross section of laser strips, phase quality analysis by X ray diffractometry to cladded layer surface using copper anticathode, single diffracted chroming beam, U=34kV, I=30mA, F_1=2mm, F_2=0.5mm, ω=1°/min, v_{strip}=720mm/h, at diffraction angle variation between 2θ = 20°....75° limits.

3. Results and Discussion

Macroscopic analysis pointed out the cladded surface quality, tightness, cladded layer thickness and its adherence onto support. Figures 1 and 2 show code 1, 2 and 3 code sample macrostructure having 3.82 mm, 2.29 mm and 1.50 mm in thickness, respectively. Thick layers with good adherence on support may be observed.

Fig. 1. *Samples cladded by thick layers of high-speed steel.*

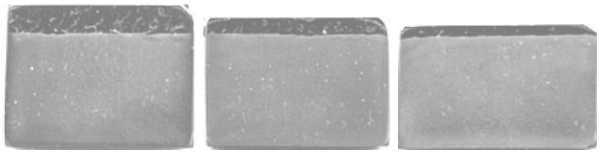

Sample 1 Sample 2 Sample 3

Fig. 2. *Macrostructures in cross section. Nital attack 2%.*

Chemical composition of laser claded layers surface is given in table 2 together with support composition (BM) and powder used as addition material (AM).

Table 2: *Chemical composition.*

Sample code	Chemical composition (%)				
	C	W	Mo	V	Cr
1	0.77	6.41	4.60	2.09	3.95
2	0.78	6.34	4.62	2.19	4.07
3	0.77	6.30	4.71	1.84	3.75
4	0.76	6.50	4.72	2.07	3.97
5	0.76	6.31	4.63	1.99	4.02
6	0.77	6.32	4.65	1.97	4.03
7	0.78	6.48	4.75	2.16	4.02
BM	0.49	-	-	-	0.19
AM	0.82	6.40	4.70	2.20	4.10

It was found the lack of any support influence upon chemical composition through cladded layer surface after five charging passes.

Dilution level resulted by support melting in order to achieve the support layer adherence may be found as a result of metallographic analysis by high multiplying, in orthogonal plan onto direction of strips generated by laser beam. Figure 3 shows, for sample 3, the cladded layer surface microstructure (CL), and figure 4 gives the cladded layer adherence area microstructure, of high-speed steel, on carbon steel support (BM). Throughout laser cladded cross section there is a dendrite structure with many carbides of wolfram, molybdenum, chrome and vanadium disposed between dendrites and at border of solid solution grains.

Good cladded layer adherence to support may be observed.

Tightness defects or non – metallic inclusions do not exist on diffusion border.

Dilution area (DA), resulted as a superficial support melting, which conducts to intermediary composition getting between cladded layer and support, is decreased. Measurements made by optical microscope empathized a dilution layer thickness of

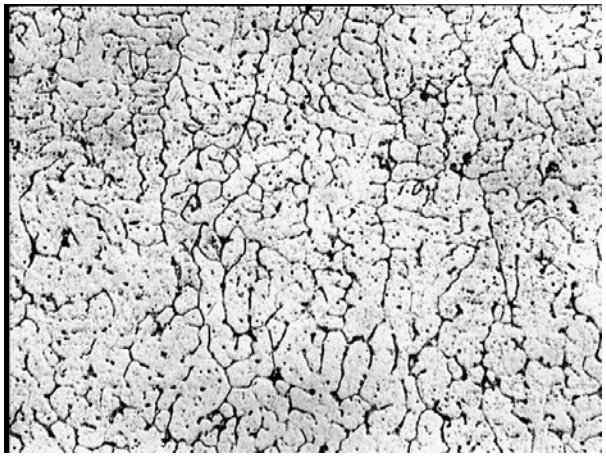

Fig. 3. *(x300) Sample 3. Laser cladded layer surface area microstructure. Nital attack 2%.*

40 μm about. As layer was made by several passes, it was found a large granulation decreasing since fusion border toward surface, as a result of successive recrystallisation determined by repeated heating.

According to the quantity analysis (figure 5), cladding microstructure includes martensite, residual austenite and carbide eutectic colonies, main hardening base being the Cr_7C_3. In layer bottom may be seen a narrow dilution area that makes transition to the support material.

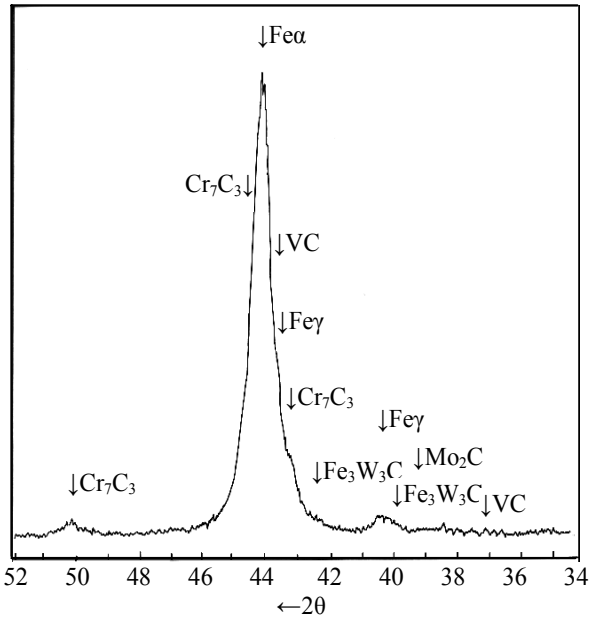

Fig. 5. *Fragment from diffractograme of high-speed*

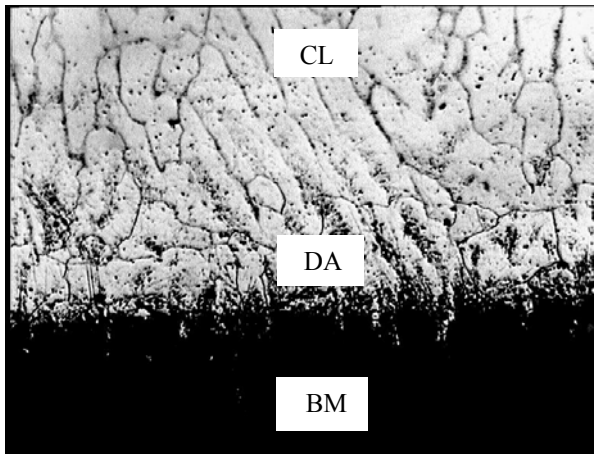

Fig. 4. *(x300) Sample 3. Adherence area micro-structure of layer cladded to carbon steel support: BM - support; DA - dilution area; CL - cladded layer. Nital attack 2%.*

$HV_{0.98}$ micro-hardness measurements generally confirmed the acknowledgements made on microstructure analysis, related to structural homogeneity of cladded layer and reduced dilution degree determined by the applied running. However, making a comparison between curves of micro-hardness variation on laser cladded layers depths on samples 3 and 6 (figure 6) processed by powder flow of 134 mg/s and 119 mg/s, respectively, in condition of steady keeping the other running parameters, a difference between dilution layer thickness resulted. Because of larger flow used to process sample code 3, the powder jet sucked a large quantity of laser beam energy intended to heat it up to melting. Therefore, a smaller quantity of energy was available to make melted baths that resulted with a smaller depth and found the minimum dilution.

HV_{49} hardness measurements pointed out higher hardness values than those measured on parts from same material, volume treated or superficially treated by laser [9]. Table 4 shows these measurements results.

Table 4. Cladded layer surface hardness.

Samples code	1,4, 5, 6	2, 3, 7
HV_{49} (MPa)	10130	10270

High-speed steel laser cladding on active surface of lathe tool was made by laboratory technology matching to the specific by the tool geometry assessed. A lot made of three identical tools was processed.

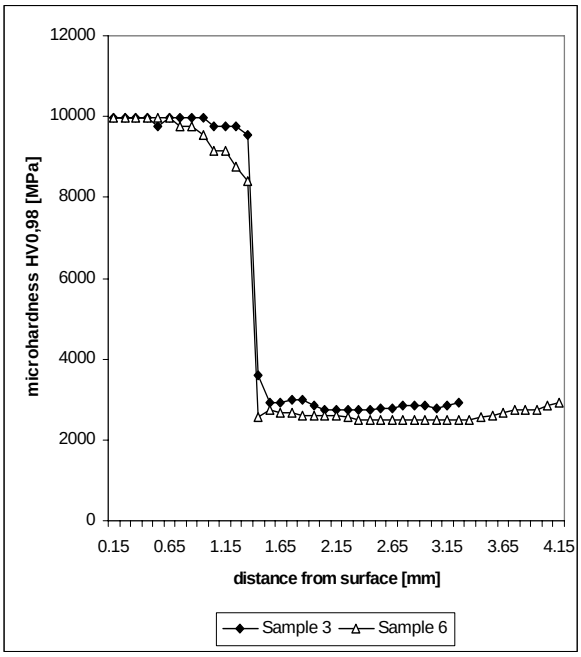

Fig. 6. *$HV_{0.98}$ hardness variation curves in laser cladded layer at samples 3 and 6.*

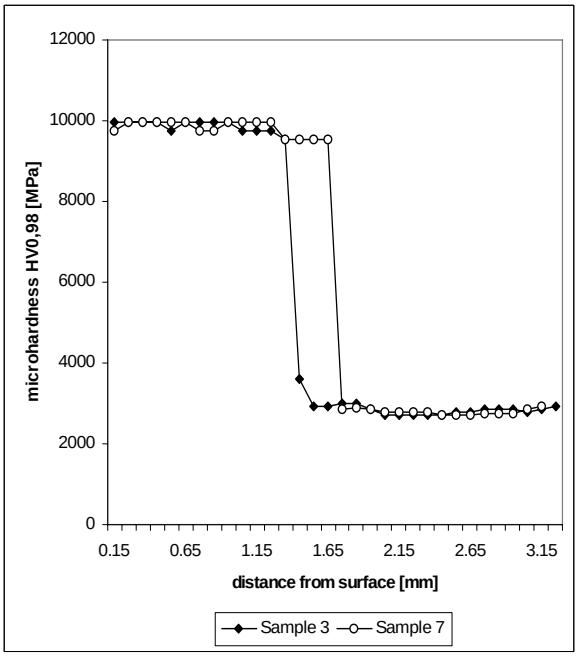

Fig. 7. *$HV_{0.98}$ hardness variation curves in laser cladded layer at samples 3 and 7.*

Fig. 8. *Semi-product after laser cladding.*

Fig. 9. *Lathe tool after sharpening.*

Fig. 10. *Longitudinal turning test.*

After cladding the high-speed steel in 3.5 mm thickness layers (figure 8) of each tool, these were submitted of a under cooling treatment to –60^{o}C, aiming to reduce the residual austenite quantity. 550^{o}C double annealing thermal treatment was eliminated.Comparation of microhardness variation curves got on samples 3 and 7 (figure7) that used the same powder volume but processed by different sample surface sweeping speeds (5mm/s on sample 3 and 7 mm/s on sample 7), confirms the structural homogeneity of laser cladded layers and the low dilution level

Different laser cladded layer thickness in this case is explained by difference between k ($k = P/v \cdot d_s$) power factor values. Thus, sample 3 was processed by k = 122,2 J/s power factor and sample 7 k = 87,3 J/s power factor, respectively. Layers cladded onto the two surfaces were made by five superimposed passes. Power factor difference resulted in different losses by vaporization. It is known that temperature in laser beam is higher then metallic material vaporization temperature. As consequence, each laser beam superimposed pass vaporized a larger material quantity of sample 3 rather than of sample 7, that made the larger layer thickness of sample 7 to be.

Each tool sharpened in order to provide the cutting capacity (figure 9).

Steel processing tests, without cooling liquids use, were accomplished by these tools (figure 10).

Comparatively speaking of a tool entirely made of the same kind of high-speed steel, submitted to specific volume treatment, laser processed tools had a higher behavior, determined by one hand of higher superficial hardness and by the other hand of larger steel carbon body capacity to spread the heat from the active area (steel thermal conductivity decreases in the same time with alloying degree increasing).

4. Conclusions

By laser clading of high-speed steel powder with 0.82%C, 4.7%Mo, 6.4%W, 0.3%Mn, 4.1%Cr, 0.32%Si, 2.02%V, Fe reminded, as chemical composition, high hardness layers with 10130 – 10270 MPa and 1.5 – 4 mm in thickness were achieved, which allow the cutting angles making and taking over of technological wear.

Laser cladding tests by different running, pointed out the fact that powder flow has an decisive influence upon dilution degree. Also, when processing the laser cladding layers by several superimposed passes, it was found that k power factor magnitude determines the losses increasing by vaporization.

Turning test pointed out the fact that laser processed tools had a higher behavior, determined by one hand of higher superficial hardness and by the other hand of larger steel carbon body capacity to spread the heat from the active area.

References

[1] Eboo, M., Lindemanis, A.E., *"Advances In Lasercladding Technology"*, Proc. ICALEO '83, SPIE, vol. 527, (1983), pp. 86-94.
[**2] Grünenwald, B., et a**l., "*Laser Cladding with a Hetero-geneous Powder Mixture of WC/Co and NiCrBSi*", Proc. ECLAT '92, (1992), pp. 411-416.
[3] Lensch, G., Kröhnert, G., Bady, T., "*Hochleistungsoptiken für die Laserbearbeitung von Innenräumen*", Proc. ECLAT '96, (1996), pp. 823-828.
[4] Levcovici, S.M., Levcovici, D.T., *"Surface Hardening of Rp5 Steel by Continuous Wave CO_2 Laser"*. The Annals of University of Galati, fascicle IX, Metallurgy and Materials Science, Year XIV (XIX), (1996), pp.95-100.
[5] Levcovici, D.T., Munteanu, V., Levcovici, S.M., Benea, L., Mitoşeriu, O., Paraschiv, M.M., *"Laser Processing of MMC Layers on a Metal Base*", Materials and Manufacturing Processes (USA), July 1999, vol. 14, no. 4, pp. 475-487.
[6] Monson, P.J.E., Steen, W.M., "*Comparison of Laser Hardfacing with Conventional Processes"*, Surface Engineering, vol. 6, no. 3, (1990), pp. 185-193.
[7] Pelletier, J.M., et al., "*Influence of Processing Conditions on Geometrical Features of Laser Claddings Obtained by Powder Injection*", J. of Materials Science, vol. 28, (1993), pp. 5184-5188.
[8] Schnieder, M.F., *"Laser cladding with powder"*, Ph. D. Thesis University of Twente, Enschede, Haarlem, (1998), pp. 80-84.

RESEARCHES REGARDING THE ROLLING OF THE SINTERIZED METALLIC POWDERS STRIPS

Sorin Miltiade ISTRATE, Ionel PETREA

"Dunarea de Jos" University of Galati
e-mail: **petrea.ionel@ugal.ro**

ABSTRACT

This paper work is distinguishing the size modification of those two material layers gotten by the bimetallic strip rolling, joined by the sintering. The iron powders sediment was achieved on the steel strip backing. After sintering and rolling, the geometrical and technological characteristics were analyzed and correlation between the average rolling pressure, from bimetallic strip and reduction of the powder layer thickness lengthways rolling as wells correlation between hardness of the powder layer and thickness reduction after were studied.

Keywords: the reduction of the powder layer

1. Introduction

The combinate rolling or the multiple layers rolling is a procedure of rolling by which two or more metallic material layers are joined to get a set of particular characteristics:

- high strength as following of the strength increase on the flat – rolled section
- wear strength of the surface;
- chemical corrosion strength
- antifriction characteristics as following of the friction coefficient decrease.

Besides their characteristic, the multiple layers are gotten with lower costs using metallic powders, saving important expensive materials.

At present, ht rolling is the most used method to get the multiple layers processing.

The rolling assures the strength and continuously joining between layers.

H_M, h_M – initial and final thickness of the (powder) soft layer;

H_T, h_T – initial and final thickness of the steel backing.

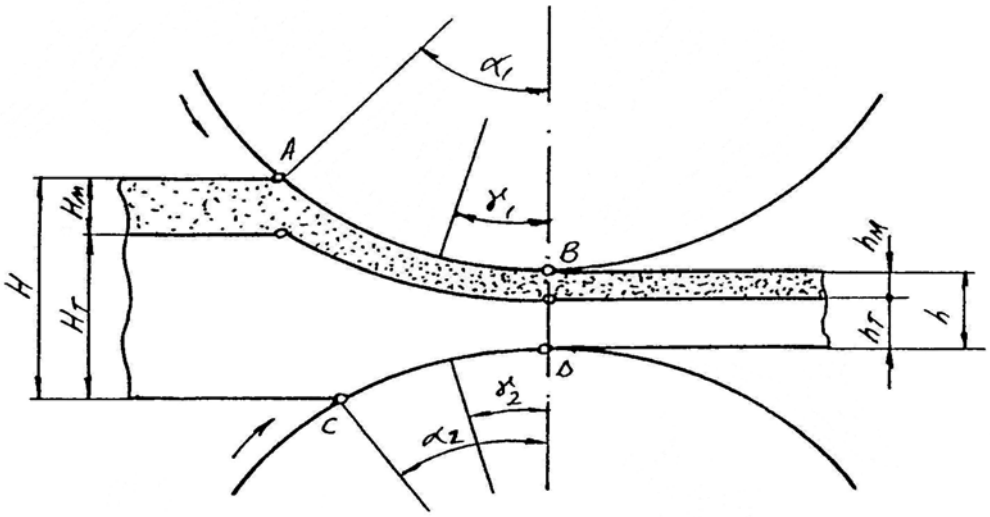

Fig.1. *Deformation zone in case of the multiple layers rolling, joined by sintering.*

2. Materials and working conditions

For experiments the iron powder grain – size of 0,063 … 0,4 mm were used and deposited on the cold rolled and pickled steel strip backing.

After settling, the thicknesses of the powder layers were: 4,31; 2,66; 2,08; 1,87 mm for a steel strip backing thickness of 1.2 mm.

After settling, each set of the test – specimen was sintered at 1200^0C in the hydrogen atmospheric in various sintering lasting – time of: 1 h, 1,5 h, 2h.

The powder settled in the various thickness layers on the steel strip backing, getting, thus, 4(four) sets of test specimens with various ratios between the thickness of the powder layer settled and the thickness of the steel backing.

After sintering, by a test –specimen measuring, a modification of the powder layer thickness – size resulted due to contraction according to fig.2.

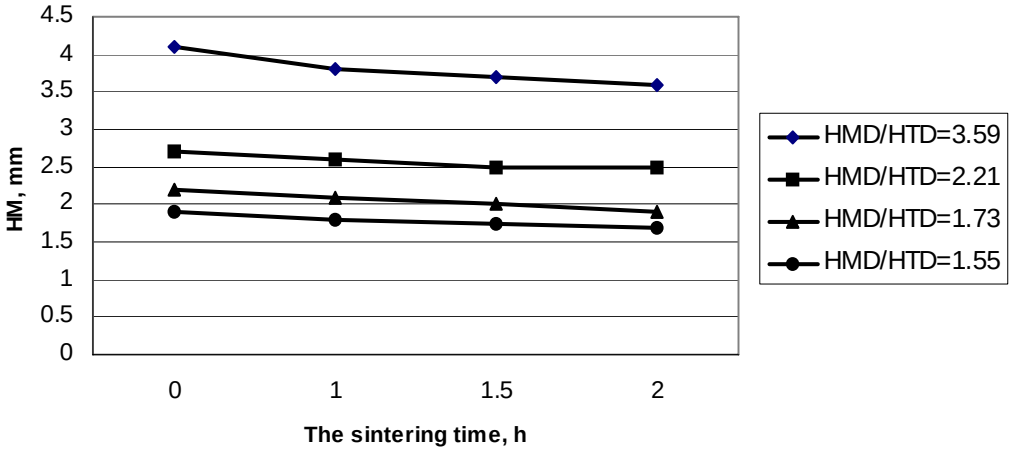

Fig.2. *The settled powder layer thickness change to the sintering time and HMD/HTD ratio*

HMD – the thickness of the powder layer settled before sintering;

HTD – the thickness of the steel backing, before sintering.

After sintering the test – specimen were rolled in three succesive passing, measuring, each time, the rolling pressure, the thickness of those two layers and Brinell Hardness of the powder layers.

3. Results and discussion

These experiments were made to watch the influence of the dimellic test – specimen rolling characteristics on the average rolling pressure and hardness.

The results are shown in fig.3.

Fig.3*. The reduction of the powder layer*

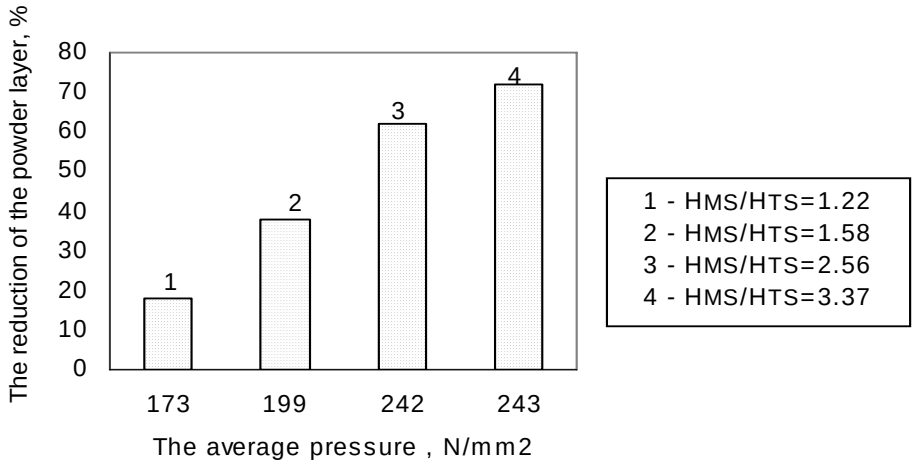

The average pressure change to the reduction of the powder layer and the ratio: HMS/HTS.

HMS – thickness of the settled layer after sintering;

HTS – thickness of the steel backing, after sintering.

An increase of the average pressure to the increase of the all test – specimen reduction is established. The application of the relative reduction on the passing up to 70% was possible on the first passing only for the test – specimen which have HMS/HTS = 3,2. The diminution of this ratio led to the reduction lowering at first passing.

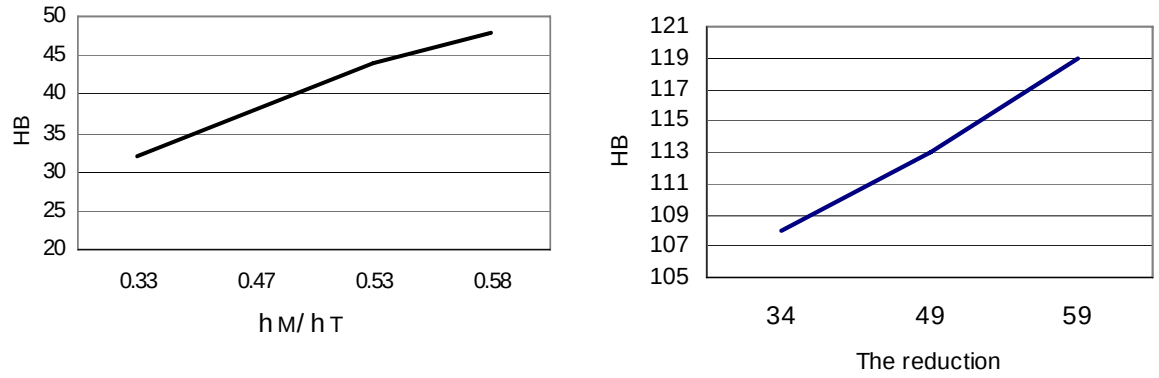

Fig.4. *Hardness change to the reduction and h_M/h_T ratio*

The application of the high reduction on the passings is possible due to powder layers compacting. As following the powder layers may suffer the reduction up to 70% while the steel backing is reduced with 1,7 … 2,6% only.

The increase of the sintering time is determining the powder layer compacting, which leads to the ratio lowering h_M/h_T (thickness ratio of those two layers after rolling).

The average pressure is recording a light diminution while the ratio h_M/h_T lowers and sintering time increases.

Finally, the change of the powder layer hardness was watched on the sintered and rolled test – specimen.

An increase of the powder layer hardness is established while the reduction degree increases.

4.Conclusions

The test – specimen sintering having various ratios of HMD/HTD led to the thickness diminution of the settled layer to the sintering time.

- the average cold rolling pressure of each passing increases to the increase of the total reduction of the powder layer;

- the hardness was measured after each rolling passing.

Generally, are increase could be remarked with the increase of the passing number and therefore an increase of the total reduction per passing as following of the layer compacting and hardening. The hardness increase is removing to the higher reductions and HMS/HTS ratios.

References

[1].Istrate, M., Researches regarding the rolling of bimetal with porous layer, *National Conference of Metallurgy and Materials Science*, 2001, 438-442

THE USE OF SYSTEMS ANALYSIS IN ENVIRONMENTAL ENGINEERING

Spiru PARASCHIV, Lizica Simona PARASCHIV, Ion V. ION

"Dunarea de Jos" University of Galati
e-mail: sparaschiv@ugal.ro

ABSTRACT

The depletion of energy resources has been of primary concern in the `70s and `80s. In recent years, the decline of the environment due primarily to our energy-related activities has become severe and raises serious concern too. For this reason, method to analyze, improve and optimize energy-intensive systems have to deal not only with energy consumption and economics, but also with the pollution and degradation of the environment.

KEYWORDS: energy resources, pollution and degradation of the environment

1. Introduction

Linear programming is about making the most of limited resources. Specially, it deals with maximizing a linear function of variables subject to linear constraints. Applications range from economic planning and environmental management to the diet problem. The aim is to provide a simple introduction to the subject.

2. Linear programming

Linear programming, a specific class of mathematical problems, in which a linear function is maximized (or minimized) subject to given linear constraints. This problem class is broad enough to encompass many interesting and important applications, yet specific enough to be tractable even if the number of variables is large.

The general form of a linear program is

$$\begin{aligned} &\text{Maximize} && c_1x_1 + ... + c_nx_n \\ &\text{Subject to} && a_{11}x_1 + ... + a_{1n}x_n \le b_1, \\ & && ..... \\ & && a_{m1}x_1 + ... + a_{mn}x_n \le b_m, \\ & && x_1 \ge 0, ..., x_n \ge 0 \end{aligned}$$

Here $c_1, \ldots, c_n$, $b_1, \ldots, b_m$ and $a_{11}, \ldots, a_{mn}$ are given numbers, and $x_1, \ldots, x_n$ are variables whose values are to be determined, maximizing the given objective subject to the given constraints. There are *n* variables and *m* constraints, in addition to the nonnegativity restrictions on the variables. The constraints are called linear because they involve only linear functions of the variables. Quadratic terms such as x_1^2 or $x_1 \cdot x_2$ are not permitted. If minimization is desired instead of maximization, this can be accomplished by reversing the signs of $c_1, \ldots, c_n$.

The most remarkable mathematical property of linear programs is the theory of duality.

The *dual* of the linear program given above is

$$\begin{aligned} &\text{Maximize} && b_1y_1 + ... + b_my_m \\ &\text{Subject to} && a_{11}y_1 + ... + a_{m1}y_m \ge c_1, \\ & && ..... \\ & && a_{1n}y_1 + ... + a_{mn}y_m \ge c_n, \\ & && y_1 \ge 0, ..., y_m \ge 0 \end{aligned}$$

This is a linear program in the variables $y_1, \ldots, y_m$. It is not hard to show that if $(x_1, \ldots, x_n)$ is in the feasible region for the first linear program and $(y_1, \ldots, y_m)$ is in the feasible region for the dual linear program, than the first objective function $c_1x_1+\ldots+c_nx_n$ is less than or equal to the dual objective function $b_1y_1+\ldots+b_my_m$. The remarkable fact is that these two objectives are always *equal* for any $(x_1,\ldots,x_n)$ and $(y_1,\ldots y_m)$ which are, respectively, optimal solutions for the two linear programs. This is of great practical importance for both the interpretation of the solutions of linear programs and the methods for calculating their solutions.

3. Debate on the economy aspects of an environmental problem

A production unit in the consumers goods field (aliments) is the unit that produces this kind of goods at the cost of 15 currency units, each product unit being worth/costing 3 such units. Unfortunately, in the production process, a waste-pollutant is

generated: 2 waste units for each product unit. A part of a pollutant is left untreated and gets into an emissary (water course); another part is removed by treatment in a special station, the treatment cost for an unit of product being 1 currency unit. But the unit of polluted water treatment cannot treat more than 10 waste units, with a reduction by 80% of the level of pollutant. The requested tax for each waste unit discharged untreated into the water is 2 currency units and the environmental protection authority limits the waste quantity that can be discharged by the producer to 4 waste units.

The system manager wants to know the optimum level of finite objects production in the above-mentioned conditions.

For the problem equalization, we will use the following notations:

x_1 – the level of finite consumers goods' production;

x_2 – the quantity of pollutant that is left untreated and is discharged in the environment (by a water course);

y – objective function, for which the maximum is searched for;

y function is the difference between the gross benefit and a sum formed by the production costs, waste treatment costs and of the part that is discharged into the affluent.

The pollutant mass $2x_1 - x_2$ passes through the waste water treatment plant.

y function is given by the relation:

$$y = 15x_1 - 3x_1 - 1(2x_1 - x_2) - \\ - 2[x_2 + 0{,}2(2x_1 - x_2)] \quad (1)$$

that means:

$$y(x_1, x_2) = 9{,}2x_1 - 0{,}6x_2 \quad (2)$$

$$2x_1 - x_2 \le 10 \quad (3)$$

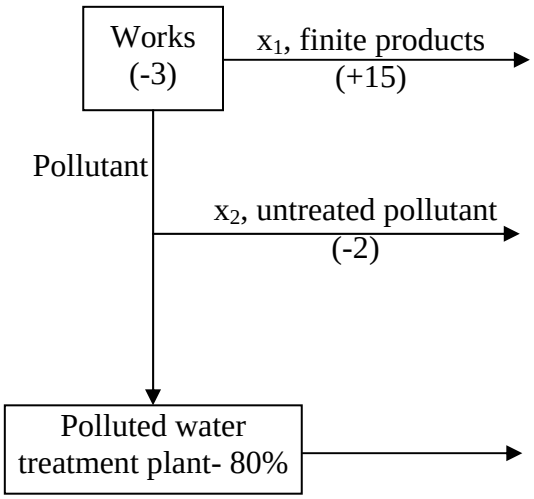

Figure 1. *– The scheme of the production unit*

$$0{,}4x_1 + 0{,}8x_2 \le 4;\ x_1 + 2x_2 \le 10 \quad (4)$$

$$2x_1 - x_2 \ge 0 \quad (5)$$

Condition number (5) is the expression of the fact that in all the cases we have to possess sewerage for polluted water through the waste treatment plant. The scheme for this situation is:

4.The dual problem of linear programming

We will make the following notations:

$$2x_1 - x_2 = a \quad (6)$$

$$x_1 + 2x_2 = b \quad (7)$$

a and b units of measure can vary from a=10 and b=10, as regards their value.

The objective function y is considered in the optimal conditions, that means y_0. The issue that has to be taken into account is how to find the way in which y_0 depends on a and b parameters.

Considering the function $y_0(a,b)$ we can write:

$$dy_0 = \frac{\partial y_0}{\partial a}da + \frac{\partial y_0}{\partial b}db \quad (8)$$

We will make the following notations:

$$(z_1)_0 = \frac{\partial y_0}{\partial a};\quad (z_2)_0 = \frac{\partial y_0}{\partial b}; \quad (9)$$

(8) relation will be noted:

$$dy_o = (z_1)_0 da + (z_2)_0 db \quad (10)$$

(8) relation expresses y_0 variation when a and b vary infinitesimal. From (6) and (7) relations we can easily find, by differentiation, the following relations:

$$da = 2dx_1 - dx_2 \quad (11)$$

$$db = dx_1 + 2dx_2 \quad (12)$$

y_0 value which is, in our case:

$$y_0 = 9{,}2(x_1)_0 - 0{,}6(x_2)_0 \quad (13)$$

where $\{(x_1)_0, (x_2)_0\}$ is the solution of the system 6+7, that means:

$$(x_1)_0 = \frac{2}{5}a + \frac{b}{5} \quad (14)$$

$$(x_2)_0 = -\frac{a}{5} + \frac{2}{5}b \quad (15)$$

As $x_i \geq 0$ (the unnegativity condition) (i=1,2) from (15) the following condition results:

$$-\frac{a}{5} + \frac{2}{5}b \geq 0 \quad (16)$$

or:

$$b \geq \frac{a}{2} \quad (17)$$

Taking into account the relations (14) and (15), the relation (13) becomes:

$$y_0(a,b) = 3{,}8a + 1{,}6b \quad (18)$$

$$dy_0(a,b) = 3{,}8da + 1{,}6db \quad (19)$$

Comparing it to (10) we find:

$$(z_1)_0 = 3{,}8; \quad (z_2)_0 = 1{,}6 \quad (20)$$

In our case:

$$dy\left(x_1, x_2\right) = 9{,}2dx_1 - 0{,}6dx_2 \quad (21)$$

$$dy\left(x_1, x_2\right) = Z_1 da + Z_2 db \quad (22)$$

Using the relations (11) and (12), the relation (22) becomes:

$$dy\left(x_1, x_2\right) = (2z_1 + z_2)dx_1 + (-z_1 + 2z_2)dx_2 \quad (23)$$

Comparing (21) and (23) we can note the following relations:

$$2z_1 + z_2 = 9{,}2 \quad (24)$$

$$-z_1 + 2z_2 = -0{,}6 \quad (25)$$

Solving the above system we find the values of the new variables in the optimal solution point.

$z_1 = 3{,}8; \; z_2 = 1{,}6$

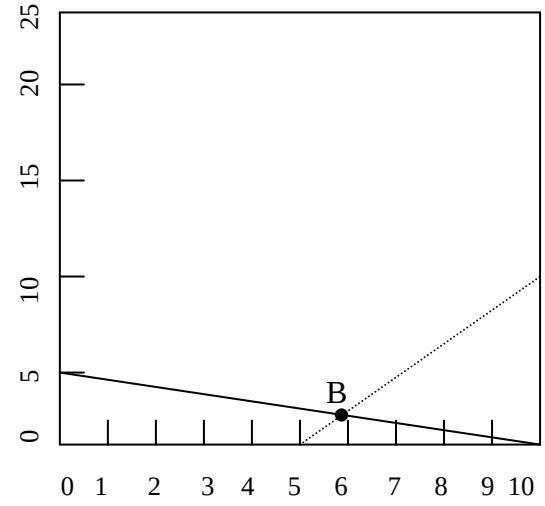

$x_1 + 2x_2 = 10$

$2x_1 - x_2 = 10$

The optimal admissible solution is for point B(6,2) and:

$y_0 = y_{optim}(6,2) = 54$ *currency units*

Conclusion

The main objective in an optimization problem is to find the maximum or minimum of an y objective function. In most of the cases, this function depends on a series of variables x_1, x_2,....x_n, called control variables, whose value we can chose in order to achieve a certain goal.

References

[1]. Nicolae Oprita, Ioan Paunescu, Gigel Paraschiv, *Metode matematice in biotehnica si ingineria mediului*, Matrix Rom Bucuresti , 2002.

[2]. Thomas S. Logsdon – *Basic Programming with Structure and Style*, Boyd &Fraser Publishing Company Boston, 1985

[3]. Neculai Andrei – *Pachete de programe, modele si probleme pentru programarea matematica* , Editura Matrix, 2002.

THE ANNALS OF "DUNAREA DE JOS" UNIVERSITY OF GALATI
FASCICLE IX METALLURGY AND MATERIALS SCIENCE, ISSN 1453 – 083X. NR 2 – 2005

RESEARCHES REGARDING THE THERMOMECHANICAL TREATMENTS INFLUENCE ON THE STRUCTURE AND CHARACTERISTICS OF THE ALUMINIUM ALLOYS FOR AERONAUTICS

Elisabeta VASILESCU, Ana DONIGA

"Dunarea de Jos" University of Galati
e-mail: bica2_2003@yahoo.com

ABSTRACT

The laboratory experiments were made on the two aluminium alloyed qualities used for aeronautical industry. More working conditions of the intermediary (PTMI) and finally (PTMF) thermomechanical treatments were used on the industrial rolled test-specimen. Also, the conventional thermal treatment was used, consisting of the solution quenching and artificial heat ageing, mode in more working condition, test. The structure and mechanical characteristics were analyzed and the gotten results were compared using those two types of the thermal and thermomechanical treatments. A significantly improvement of the mechanical characteristics was ascertained to the thermomechanical treated test-specimen.

KEYWORDS: thermomechanical treatments, aluminium alloys, mechanical characteristic

1. Introduction

Thermomechanical processing (PTM) of the special aluminium alloys is a too litle studied field, eventhough, from the made experiments, it has been established that it resulted some high characteristics, so that they should be more practically used than conventional methods.

The metallurgical technologies used for special aluminium alloys that, watches the grain size finishing and getting of the average or high strength, are two types:

- technological processing that acts on the crystallin grain-size of some aluminium alloys during first stages of the processing at high temperature by the partial elimination of the structural heterogeneity, by the control of the chemical composition of the casting cycles and homogenizing of these alloys. In the sequel the hot plastic deformation is applied (rolling), finally, a recristallized structure is getting, with fine and uniform grain size;

- technological processing applied on the high strength aluminium alloys particularly used for the aeronautics. They consists of more stages of the plastic deformation and thermal tratments, these constituing the thermomechanical processing (PTM) two types of the thermomechanical processings are applied: intermediar (PTMI) and final (PTMF).

The intermediar thermomechanical processing (PTMI) is used in the world to improve the plasticity, toughness and corrosion strength of the special aluminium alloys without mechanical strength reduction comparatively to the conventional processing.

The final thermomechanical processing (PTMF) is applied to get the final strength characteristics combined with a good plasticity, corrosion strength and fatigue strength.

The thermal treatment characteristics of the aluminium alloys, particularly of those Al-Zn-Mg-Cu system, are: solution quenching and heat (artificial) ageing. Combined in a certain succesion to the plastic deformation the important improvment of the strength characteristics could be gotten. Figure 1 shows some exemples of PTMI combined to the conventional thermal treatment or PTMF. [1].

2. Materials and working conditions

The experiments have been made on Al-Zn-Mg-Cu aluminium alloys, for aeronautics having chemical composition shown in table 1.

The laboratory experiments have been made combining thermal treatment specific to such alloys; solution hardening (quenching) and heat (artificial) ageing with deformation degree rolling $\varepsilon = 3…50\%$.

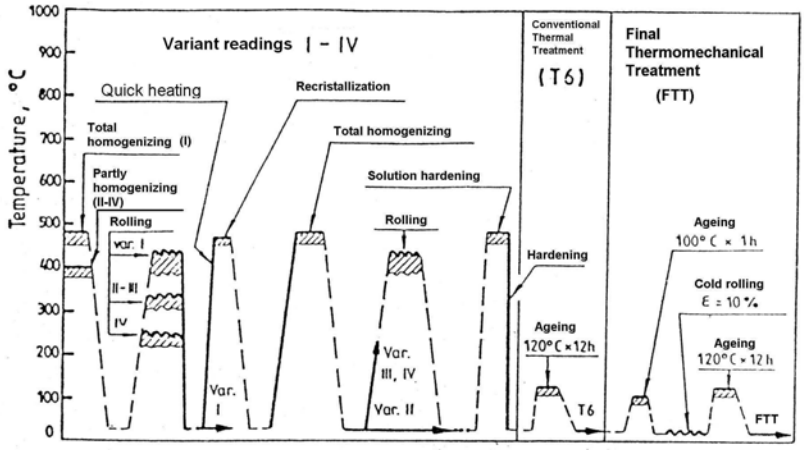

Fig. 1 *Working conditions of PTMI, conventional treatment and PTMF for Al-Zn-Mg-Cu types alloys.*

Table *1Chemical composition of Al-Zn-Mg-Cu alloys (%)*

Cu	Zn	Pb	Fe	Mn	Si	Mg
1,219	2,470	0,0025	0,290	0,470	0,310	2,06

3. Experimental results

In the frame of this paperwork two variant experiments have been studied:

a) The influence of the hot plastic deformation degree on the mechanical characteristics.

In this variant way the working conditions of the thermomechanical treatment is shown in figure 2.

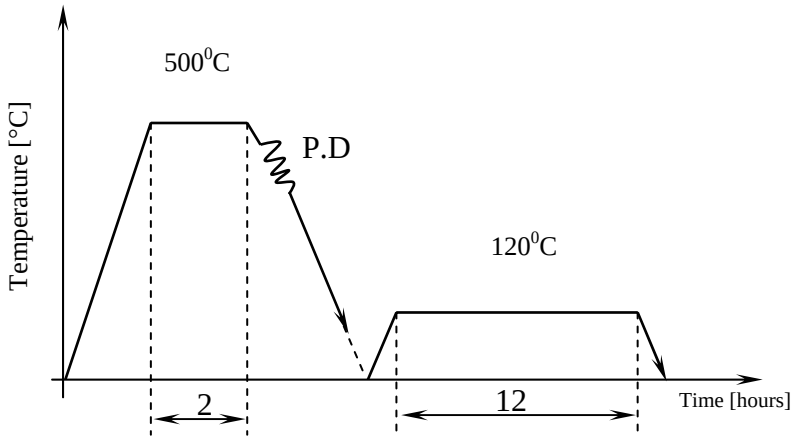

Fig.2 *Experimental conditions of the a) variant thermomechanical treatment*

The operation succesion was the following:

- 2 hours holding at 500^0C heating;
- rolling with ε = 3; 8; 13; 40; 50% deformation degree of the pass;
- water cooling at about 80^0C;
- finally – an heat ageing was carried out at 120^0C for 12 hours.

Therefore, in this case, the quenching in solution was combined with hot plastic deformation into one operation only.

For comparison, a test-specimen was submitted to quenching in solution plus heat ageing, without plastic deformation.

The gotten results are shown in the table 2.

With data of table 2 – the diagrame was drown from figure 3, the variation of the hardness to deformation degree, at rolling.

Table 2. *The experimental working conditions*

No.	Heating temperature (^{0}C)	Time (hours)	Rolling ε (%)	Heat ageing temperature (^{0}C)	Time (hours)	Hardness HB
1	500	2	50	120	12	129
2	500	2	40	120	12	117
3	500	2	13	120	12	114
4	500	2	8	120	12	102
5	500	2	3	120	12	98
6	500	2	0	120	12	85

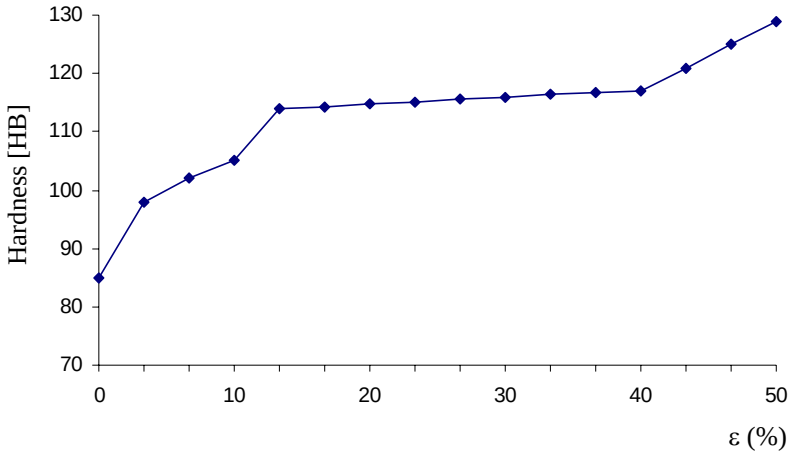

Fig.3 *Hardness variation to hot deformation degree.*

An increase of the hardness to deformation degree is established.

Also, could be remarked that hardness values are higher in case of the carried out plastic deformation against to classic treatment of the quenching in solution, followed by the heat ageing.

b) The influence of the cold deformation and of the heat ageing conditions on the structure and mechanical characteristics.

In this way, a cold plastic deformation have been chosen between two treatments of the heat ageing (fig.4).

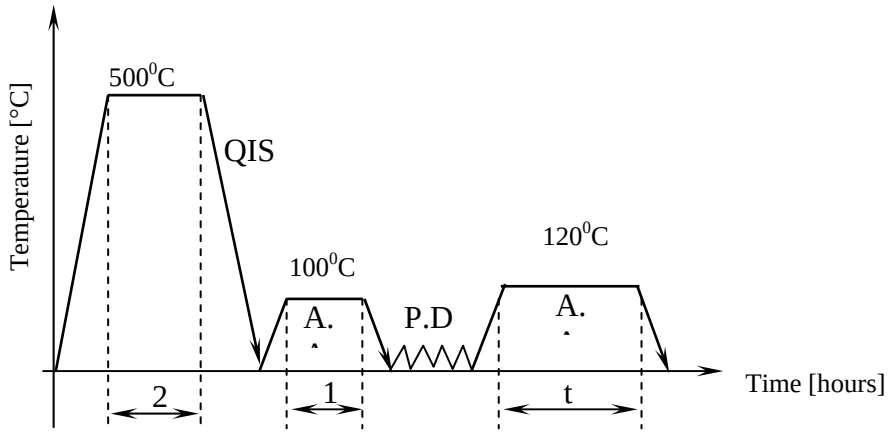

Fig.4 *Conditions of the thermomechanical treatment in b) way*
QIS – quenching in solution ; PD – plastic deformation; AA – artificial ageing;

For comparison, a test-specimen (pieces) was submited to natural ageing (2 days holding at usual temperature).
The gotten results are shown in figure 5.

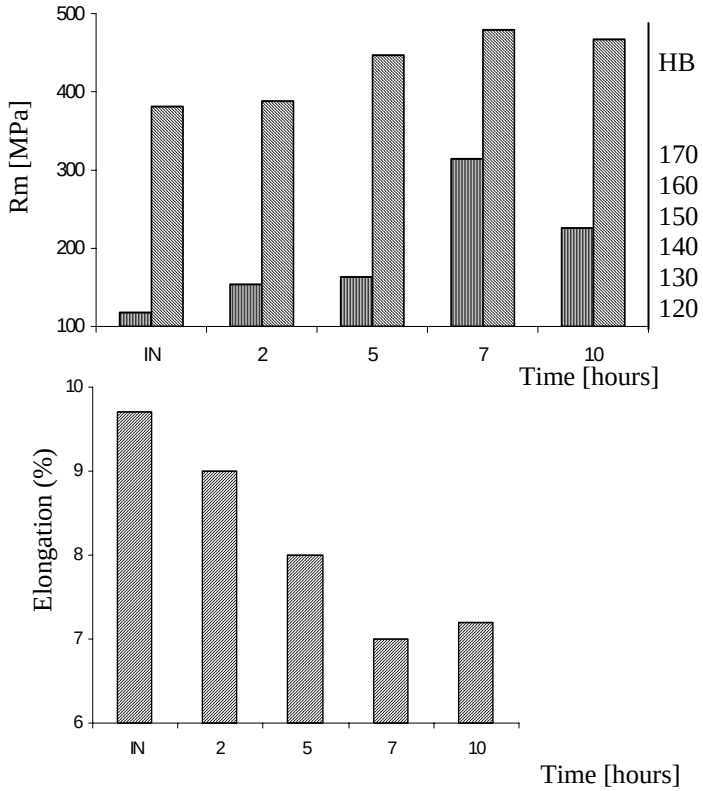

Fig.5 *Variation of the mechanical characteristics to the ageing time.*

From figure 5, could be seen that the strength and hardness grow up, once with ageing time increase (up to 7 hours), after which a hight decrease is recorded. The extension lowers with the ageing time increase.

Comparing the gotten results of the both a) and b) ways could be seen that in case of the plastic deformation, between the two ageings, the hardnesses are much higher than those in case of the hot deformation, followed by the artificial ageing.
In figure 6 the comparatively hardness values are showen, in case of the various thermal and thermomechanical treatment conditions are carried out.

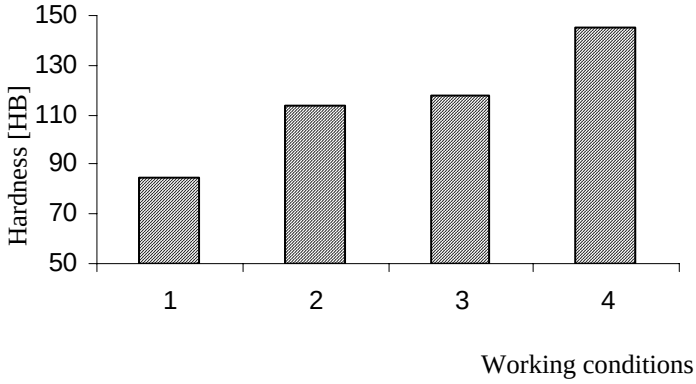

Fig.6 *Hardness variation against to the carried out treatment conditions*
QIS – quenching in solution ; PD – plastic deformation; AA – artificial ageing;
NA – natural ageing
1) QIS + AA; 2) QIS + PD + AA; 3) QIS + PD + NA; 4) QIS + NA + PD + AA

Variation way of the mechanical characteristics during these treatments, could be explained, in fact that, during quenching in solution, a partly dissolution of the secondary gases take place in the base solid solution.

By heat (artificial) ageing, a precipitation of the secondary phases take place, that is characterized by a certain scattering degree and range, which is determining a hardening of the alloys[2]. If the process is combined with a cold rolling, a cold strengthening is carried out, due to plastic deformation, which is determining a suplimentary hardening of the alloy. In figure 7 the gotten microstructure of the thermomechanical b) way treatment are shown.

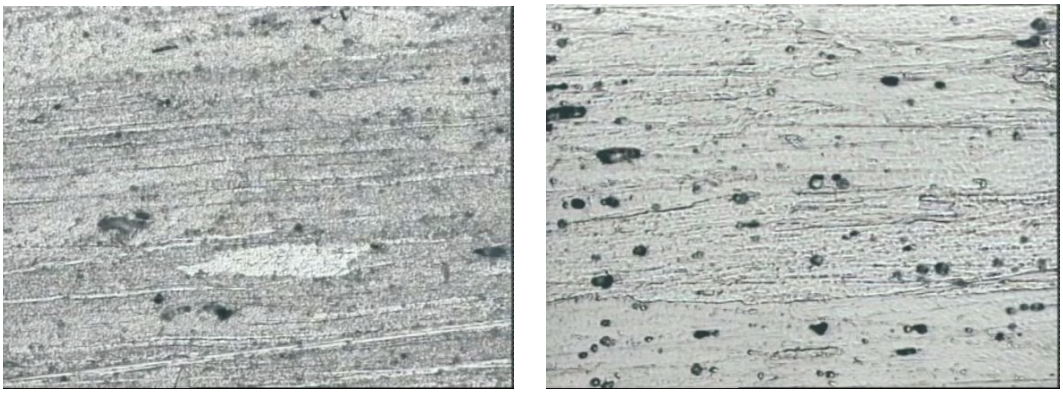

a ***b***

Fig.7 *Microstructures of the plastic deformation between two artificial ageing ageing time: a)-2 hours; b)-7 hours*

Could be seen that, once with the increase of the holding time at heat (artificial) ageing, the precipitate quantity of the secondary phase increases too. It explains the hardness variation with a growth up to a certain time (7 hours), after which the hardness lowers, once with the continuosly time increase. There is a holding time, when the precipitates is optimum recorded, from grain-size and scatering point of view.

Over this time, the precipitates coalescence process begin, which is determining a diminution of the strenght characteristics. [3]

4. Conclusions

The laboratory experiments carried out on Al-Mg-Zn-Cu type alloys resulted the following conclusions:

- the hot plastic deformation combined to a quenching in solution and heat (artificial) ageing lead to the sensitive hardness growth;
- cold plastic deformation, between two heat (artificial) ageing determines a more increased growth of the mechanical characteristics (hardness and mechanical strength);
- Al-Mg-Zn-Cu type alloys are sensitive to thermomechanical treatments, resulting high strength characteristics with acceptable plasticity for such materials.

References

[1] Cazimirovici E. ,Laminarea aliajelor speciale Ed. BREN 1998
[2] Dulamita T., Florian E., Tratamente termice si termochimice EDP – Bucuresti 1982
[3] Popescu N, Tratamente termice neconventionale ET – Bucuresti 1990

KINETICS OF NITROSO R-SALT SORPTION ON AMBERLITE IRA 402 RESIN

Eugen RADULESCU[1], Gheorghe CANTEMIR[2], Olga MITOSERIU[2],Constantin STANCIU[2]

[1]S.C. CET S.A. Braila
[2]"Dunarea de Jos" University of Galati
e-mail: cantemir.gheorghe@ugal.ro

ABSTRACT

The sorption of nitroso R salt from aqueous solution by ion exchange resins, such as AMBERLITE IRA 402 (Cl^- form) , is described. The experimental data have been analyzed by using the sorption kinetics for a first-order and pseudo-first order kinetic reaction models. The sorption rate constants according to these kinetic models have been calculated.

Keywords: Nitroso R-Salt, Chelating Resin, Ion-Exchange Kinetics, Sorption Rate Constant

1.Introduction

In the last years, the selective and quantitative retention of metal ions has been involving a great number of chelating sorbents.This studied sorbents are including inorganic materials (silicagel, kieselgur, controlled-pore glass) and organics (cellulose, dextran, polymeric resins, fibrous materials, foamed plastics) [1-4].

The chelating resin posses functional groups chemically bound (grafted groups) to an organic matrix and these active goups can form chelates with metal ions. However, only a few types of chelating resins are produced commercially and the use of resins such as these is limitated by the difficulty of synthesis and their high cost.

The above mentioned disadvantages can be eliminated by preparing a complexing resin (ion exchanger modified with chelating reagent), by ion-exchange sorption of a chelating reagent on a conventional ion exchanger [5,6]. All these applications imply a knowledge of kinetic properties of a given system.

The present study deals with the sorption kinetics of nitroso-R salt from aqueous solutions on strongly basic anion-exchanger AMBERLITE IRA 402.

The kinetics of nitroso R-salt sorption has been caried out to understand the behavior of this ion-exchange resin. So that, to quantify the changes in the sorption of nitroso R-salt with time, an appropiate kinetic model is required.

For this purpose two models were tested: first and pseudo-first order kinetic models [8,9].

2. Experimental

2.1. Reagents

All solutions were prepared with demineralized water (electrolytic conductivity $\gamma = 0{,}70...1{,}20 \mu S / cm$ and pH=5.7- 6.2) and all chemichals were of analytical-reagent grade.

The chloride form of a commercially available strongly basic anion exchange resin AMBERLITE IRA 402 type 1 (Rohm and Haas,France) was used for preparing the chelating resin. The physical properties and specifications for strongly basic anion-exchang resin AMBERLITE IRA 402-Cl are presented in table 1.

Nitroso R-salt (NRS), (disodium 3-hydroxy-4-nitroso-2,7-naphthalenedisulfonat), produced by Fluka AG Switzerland Germany, was used as a chelating reagent for the preparation of the modified resin.

Standard working solutions were freshly prepared by the appropiate dilution of $5 \cdot 10^{-3}$ M NRS stock solution with demineralized water.

Table 1. *Physical properties and specifications for strongly basic anion- exchange resin AMBERLITE IRA 402.*

Polymer matrix structure	Polystyrene cross-linked with divinylbenzene-gel
Physical form and appearance	Clear golden spherical beads
Functional groups	Type 1 ; $-N^+(CH_3)_3$
Ionic form (as shipped)	Cl^- form
Shipping Weight	610-680 g/l (Cl^- form)
Screen size:(U.S.Standard Screen)	16-50 mesh wet
Mean diameter (μm)	620-770
Uniformity coefficient	1.6
Specific gravity (moist Cl^- form)	1.063-1.093
Moisture retention (Cl^- form)	50-56 %
Swelling ($Cl^- \rightarrow OH^-$)	30%
Exchange capacity (Cl^- form)	3.70 meq/g
Operating temperature (Cl^- form)	max. 60 ^{0}C
pH range stability (OH^- form)	0-13

2.2. Apparatus

A UV-VIS Specord 205 (Analytik Jena AG, Germany) double-beam spectrophotometer equipped with two pairs of 1 cm path length glass cuvettes was used for the absorbance measurements.

An AG-3 (ITM, Romania) magnetic stirrer with top hot plate and speed control was used for this experiments.

2.3. Methods and analysis

Prior to use, the resin was backwashed and rinsed with water as reported previously [7]. The resin was conditioned by consecutive treatments with 2M NaOH (250 ml solution/100 ml of resin) and 2 M HCl (250 ml solution/100 ml of resin) to remove organic and inorganic impurities and then was rinsed with demineralized water till Cl^- elimination, and air-dried at constant weight (96 hours).

2.3.1. Kinetic curves of the sorption of NRS on Amberlite IRA 402-Cl

Weighed amounts (1.0 g) of air-dried anion-exchange resin in chloride form were swallen and equilibrated with 500 ml of NRS solution with different initial C_0 concentrations, in a 500-ml glass-stoppered flask. Then, the mixtures were stirred for a predetermined period by a magnetic stirrer.

The amount of NRS was determined at adequate time intervals by spectrophotometrically measurement at 420 nm according to Lambert-Beer low.

This was done by extracting 2.5 ml of solution at each adequate time interval.

3. Results and Discussion

The kinetics of sorption describing the solute retention rate, which in turn governs the residence time of the sorption reaction, is an important characteristic which defines sorption effciency.

In this paper, the calculation of rate constants starts from the assumption that the overall ion-exchange process can be assimilated to a pseudo-first order reaction. This approximation is acceptable because the order of this above-mentioned reaction is slightly over 1 for most ion-exchange systems [8].The ion-exchange sorption of NRS on Amberlite IRA 402 resin was previosly analysed [5, 6].

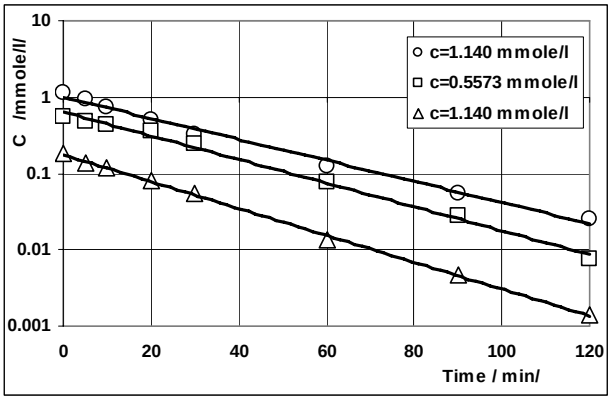

Fig.1.*The NRS concentration C of the external solution vs. time for different initial concentrations. Batch method: m/v=1 g/500 ml; stirring time* τ *= 2 h; t = 25* ^{0}*C. Semi-logarithmic graph.*

The effect of time on NRS concentration C of the external solution, is shown in fig.1. The semi-logarithmic plot C = f (t) shows that the C varies linearly. From the point of view of formal kinetics, it suggests that the ion-exchange reaction could follow a first order reaction.

3.1. First order sorption kinetic model

The sorption of nitroso R salt from liquid phase to solid may be considered as a reversible reaction with an equilibrium state being established between two phases. A simple first-order reaction model [8-10] was used to correlate the rates of reaction, which can be expressed as:

$$A \underset{k_2}{\overset{k_1}{\rightleftharpoons}} B$$

where k_1 is the forward reaction rate constant and k_2 is the backward reaction rate constant. If a is the initial concentration of NRS and x is the amount of NRS transferred from liquid phase to solid phase at any time t (expressed as concentration consumed in reaction), the rate can be expressed as:

$$\frac{dx}{dt} = \frac{-d(a-x)}{dt} = k(a-x) \qquad (1)$$

where C= a-x is the concentration of external solution at any time t and k is the overall reaction rate constant. Since k_1 and k_2 are the rate constants for the forward and reverse process (sorption and desorption), the rate can be expressed as:

$$\frac{dx}{dt} = k_1(a-x) - k_2 x \qquad (2)$$

If x_e represents the concentration of NRS sorbed at equilibrium, then $k_1(a-x_e) - k_2 x_e = 0$, because under these conditions:

$$\frac{dx}{dt} = 0 \quad \text{or} \quad K = \frac{x_e}{a-x_e} = \frac{k_1}{k_2} \qquad (3)$$

where K is the equilibrium constant. Now under equilibrium conditions, the rate becomes:

$$\frac{dx}{dt} = [k_1(a-x) - k_2 x] - [k_1(a-x_e) - k_2 x_e] \qquad (4)$$

The above equation is in the form dx/dt = k(a–x). Therefore,

$$(k_1 + k_2)t = \ln \frac{x_e}{x_e - x} \qquad (5)$$

$$\ln(1 - f_t) = -(k_1 + k_2)t = -kt \qquad (6)$$

where k is the overall rate constant and $ft = x/x_e$ is the fractional attainment of equilibrium of nitroso R salt. This was calculated by considering nitroso R-salt sorption on the resin in a given time range (2-3 hrs).

In the present study a concentration of nitroso R-salt in the range 0.1860 - 1.140 mmole/l was examined. Using the kinetic equations, the overall rate constant, the forward and backward rate constants were calculated.

As can be seen in fig.2, plotting ln (1– f_t) vs. t, a straight line passing through the orrigin is obtained.

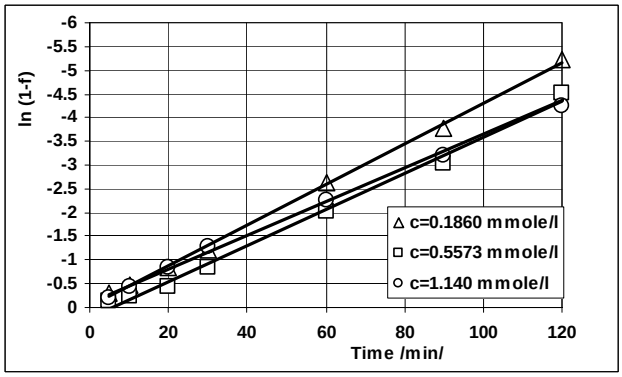

***Fig.2**.First order kinetic plot for NRS sorption on Amberlite IRA 402.*

The overall rate constant k for a given concentration of NRS was calculated considering the slope of the straight line, and by using eq. (6) the equilibrium constant K and forward rate constants k_1 were calculated and are shown in table 2.

***Table 2.** The first order reversible reaction parameters for NRS sorption on Amberlite IRA 402.*

Initial concentration, a (mmole/l)	Kinetic equation	Overall rate constant $k \cdot 10^{-3}$ (min^{-1})	Sorption rate constant $k_1 \cdot 10^{-3}$ (min^{-1})	Equilibrium constant K	Half time life $t_{1/2}$ (min)
0.1860	ln (1-f) = - 0.0427t-0.0291 R^2= 0.9985	42.70	42.61	464	16.26
0.5573	ln (1-f) = - 0.0380t-0.216 R^2= 0.9933	38.0	37.89	347.31	18.29
1.140	ln (1-f) = -0.0356t-0.0869 R^2= 0.9986	35.60	35.31	125.66	19.62

From table 2, it can be seen that the forward rate constants for the sorption of NRS are much higher than the backward rate constants, namely the desorption process.

The increasing of initial concentration of NRS (a) leads to the decreasing of the overall and forward rate constant, and to the increasing of the half time life $t_{1/2}$. The equilibrium constant, $K=k_1/k_2$, decreases with the increasing of a.

3.2. Pseudo-first order sorption kinetic model

The sorption kinetics may be described by a pseudo-first order reaction (Lagergren's first order rate equation has been called pseudo-first order since 1998 [9] .

The differential equation is as follows:

$$\frac{dq_t}{dt} = k'(q_e - q_t) \qquad (7)$$

By integrating eq. (7) for boundary conditions t=0 to t=t and q*t*=0 to q*t*=q*t*, gives:

$$\log(\frac{q_e - q_t}{q_e}) = -\frac{k't}{2.303} \qquad (8)$$

which is the integrated rate law for a pseudo-first order (Lagergren kinetic rate equation), where q*e* is the amount of nitroso R-salt sorbed at equilibrium (mmole/g of resin), q*t* is the amount of nitroso R-salt sorbed at time t (mmole/g of resin) and k` is the equilibrium rate constant of pseudo-first sorption. In order to obtain the rate constants, the straight line plots of log (q*e*–q*t*) vs. t for different concentrations of NRS have been analysed.

The rate constants, k` , were calculated from the slope of these plots (Figure 3). Linear fits were observed for all initial concentrations, indicating that sorption reaction can be approximated to pseudo-first order kinetics. Constants k` have been calculated and summarized in table 3.

From table 3, it can be seen that the pseudo-first order rate constants k` for the sorption of NRS decreased with the increasing of initial NRS concentration .

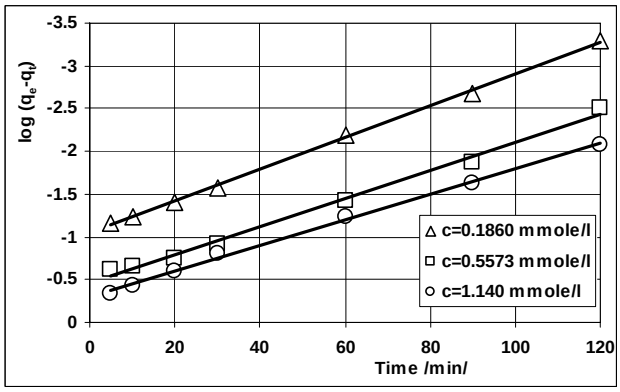

Fig.3.*Pseudo-first order kinetic plot for NRS sorption on Amberlite IRA 402.*

Table 3. *The pseudo-first order reaction parameters for NRS sorption on Amberlite IRA 402.*

Initial concentration, a (mmole/l)	Kinetic equation	Pseudo-first rate constant k` (min^{-1})
0.1860	log (qe-qt) = - 0.0186t-1,0446 (R^2= 0.9987)	$42.70 \cdot 10^{-3}$
0.5573	log (qe-qt) = - 0.0164t-0.4645 (R^2= 0.9938)	$37.77 \cdot 10^{-3}$
1.140	log (qe-qt) = -0.154t-0.2856 (R^2= 0.9984)	$35.46 \cdot 10^{-3}$

The values of the sorption rate constants k and k`, evaluated for the two kinetic models are practically identical and have the same size order as those in literature.

The ion-exchange process can be regarded as a mass transfer. Generally, the sorption rate is controlled either by a film-diffusion mechanism or particle diffusion mechanism.

The slower step controls the overall ion-exchange rate. In order to see which of these two processes is rate-determining a further analysis is necessary.

The NRS was initially sorbed by the exterior surface of resin.When the sorption of the exterior surface reached the saturation level, the NRS ions passed through the resin via the network and were sorbed by the interior surfaces.

When the NRS ions diffused into the pores of the resin, the diffusion resistance increased which in turn caused the diffusion rate to decrease.

The NRS functional groups of chelating resin have larger dimensions than the functional groups as classical exchanger and can hinder the diffusion of NRS ions into the center of the sorbent particle.

This could explain the decrease of sorption rate constans whereas the initial NRS concentration of the external solution increases.

4. Conclusions

In this paper it has been shown that Amberlite IRA 402 sorbent material can be used for the retention of Nitroso R-Salt from aqueous solutions. Kinetically, the sorption process was featured by applying two different models. Testing the system for the first and pseudo-first order kinetic equations, it was possible to determine the sorption rate constants.

Also, these results indicated that the first and pseudo-first order kinetic reaction models provided a good corellation of the experimental data for all initial concentrations.

References

[1]. Kil Sang Lee., Woon Lee and Dai Woon Lee., *Anal.Chem*., 50, pp.255-258, (1978).

[2]. Bilba, D., Bejan, D and Tofan, L.,*Croatica Chem.Acta*., 71(1), pp.155-178, (1998) .

[3]. Ryszard Kocjan., *Chem.Anal.(Warsav),* 41, pp.501-519, (1996).

[4]. Won,Lee.,Si-Eun Lee.,Mi-Kyoung Kim.,Chang-Heon Lee and Young-Sang Kim.,*Bull.Korean Chem.Soc.,vol.23, no.8,pp.1067-1072*, (2002).

[5]. Radulescu, E., Mitoseriu, O., Nedeff, V., Stanciu, C., Oproteh.National Conference:Optimizarea proiect`rii constructive]i tehnologice [n construc\ia de ma]ini., University of Bacau., 17-19 nov.Bacau, (2005).

[6]. Mitoseriu, O., Radulescu, E., Nedeff, V., Stanciu, C., Cantemir, G., Oproteh. National Conference: Optimizarea proiect`rii constructive]i tehnologice [n construc\ia de ma]ini., University of Bacau., 17-19 nov.Bacau, (2005).

[7]. **Radulescu, E., Mitoseriu, O., Cantemir, G., Stanciu, C.,** National Conference:Cercetarea stiintifica in conditiile integrarii europene.,University of Galati, may 28-29, Braila, (2004).

[8]. **Strambeanu, N. M.,**Teza de doctorat.,Univ.Politehnica Timisoara., (1988).

[9]..**Ho, Y.S. and McKay, G.,** Process Safety and Environmental Protection., vol. 76B, no. 2, p. 183-191, (1998); **Ho, Y.S. and McKay, G.,** Canadian Journal of Chemical Engineering.,vol. 76, no. 4, p. 822-827, (1998); **Ho, Y.S. ,** Scientometrics, vol. 59, no. 1, p. 171-177, (2004).

[10]. **Sternberg, S., Landauer, H., Mateescu, C., Geana, D., Visan,T.,**Chimie fizica.,Ed.Didactica si Pedagogica, Bucuresti,.p.386-387 and 424-425, (1981).

MANUSCRISELE, CĂRŢILE ŞI REVISTELE PENTRU SCHIMB, PRECUM ŞI ORICE CORESPONDENŢE SE VOR TRIMITE PE ADRESA:

MANUSCRIPTS, REVIEWS AND BOOKS FOR EXCHANGE COOPERATION, AS WELL AS ANY CORRESPONDANCE WILL BE MAILED TO:

LES MANUSCRIPTS, LES REVUES ET LES LIVRES POUR L'ECHANGE, TOUT AUSSI QUE LA CORRESPONDANCE SERONT ENVOYES A L'ADRESSE:

MANUSCKRIPTEN, ZIETSCHRITFTEN UND BUCHER FUR AUSTAUCH SOWIE DIE KORRESPONDENZ SID AN FOLGENDE ANSCHRIFT ZU SEDEN:

UNIVERSITATEA "DUNĂREA DE JOS" DIN GALAŢI
REDACŢIA ANALELOR
Str. Domnească nr. 47 – 800036 Galaţi, ROMÂNIA
E-mail: marian.bordei@ugal.ro

Revistă bianuală acreditată CNCSIS

Editată sub egida
Facultăţii de
METALURGIE ŞI ŞTIINŢA MATERIALELOR
şi a Centrului de Cercetare
CALITATEA MATERIALELOR ŞI A MEDIULUI

Annual subscription (2 issues per year) accredited CNCSIS

Edited under the care of
Faculty of
METALLURGY AND MATERIALS SCIENCE
and Research Center
QUALITY OF MATERIALS AND ENVIRONMENT

Data editării: 15.11.2005
Tiraj: 200 exemplare
Tiparul executat la
Fundaţia "Universităţii Dunărea de Jos"
din Galaţi, editură acreditată CNCSIS
Str. Domnească nr. 47. Galati 800036 Romania

Edited date: 15.11.2005
Issues number: 200
Printed by
"Dunărea de Jos" University Fundation
accredited CNCSIS
47 Domnească Street, 800036 Galati, Romania